Aalto University
School of Chemical
Engineering

Laura Aarnos

BURST DETECTION METHODS FOR HUMAN PLURIPOTENT STEM CELL-DERIVED NEURONAL NETWORKS

Master's Programme in Life Science Technologies
Major in Biosystems and Biomaterials Engineering

Master's thesis for the degree of Master of Science in Technology
submitted for inspection, Espoo, 29 July, 2019.

Supervisor Professor Alexander Frey

Instructors MSc Tanja Hyvärinen
PhD Laura Ylä-Outinen

Author Laura Aarnos

Title of thesis Burst detection methods for human pluripotent stem cell-derived neuronal networks

Degree Programme Life Science Technologies

Major Biosystems and Biomaterials Engineering

Thesis supervisor Professor Alexander Frey

Thesis instructors MSc Tanja Hyvärinen, PhD Laura Ylä-Outinen

Date 29.07.2019 **Number of pages** 75+18 **Language** English

A burst is a set of subsequent action potentials that are fired at a high frequency. Although bursts are a fundamental part of electrical activity of neuronal networks *in vitro*, no standardized method exists for burst detection. Visual identification of bursts is a widely accepted method, but it is not objective nor time-efficient. Therefore, various algorithms have been developed for burst detection. Burst detection algorithms are typically developed and verified only on one specific type of data. This can be problematic because the bursting activity is highly variable between different cell types. Consequently, the applicability of the algorithms is restricted to a narrow range of activity types. Especially applicability to human neuronal networks is questionable because the algorithms are often developed on rodent neuronal networks, which display distinct activity patterns in comparison to human networks. The aim of this thesis was to produce a test data set, which would well represent bursting and non-bursting activity observed in human pluripotent stem cell (hPSC)-derived neuronal networks, and to identify a single algorithm with optimal parameters that would successfully detect the bursts in this test data set. As rodent neuronal networks are also widely used in neuroscience, the algorithm was desired to function also on activity derived from rodent cultures. To achieve these goals, hESCs were differentiated into functional neuronal networks and cultured on microelectrode array (MEA). Primary rat cortical neurons were similarly cultured on MEA. Electrical activity of the developing networks was recorded twice a week until synchronized bursting emerged. At this point, pharmacological assays were performed in order to record modulated activity. On the MEA recordings, distinct activity patterns were identified, and short recordings representative of the distinct patterns were included to the test data set. The performance of four contemporary burst detection algorithms was evaluated on the test data set. The evaluation was based on visual identification of bursts from the raw MEA signal. For each algorithm, a performance score was determined and sensitivity and specificity were computed. The evaluation was performed in two runs using either 3 or 5 as minimum number of spikes required for a burst. Other algorithm parameters were set to default values suggested by the original authors. The optimization possibilities were not encouraging for other algorithms but logISI, which also provided the highest performance and the most balanced sensitivity and specificity values. Parameters of logISI were optimized for the test data set, which significantly improved its performance. As a result, logISI displayed good or excellent performance on the test data obtained from human and rat neuronal networks during spontaneous and pharmacologically modulated activity. Based on these results, logISI could have the potential to become a standard burst detection algorithm in the field.

Keywords burst detection, microelectrode array, MEA, hPSC-derived neuronal networks

Tekijä Laura Aarnos

Työn nimi Bursti-tunnistusmenetelmät ihmisperäisistä monikykyisistä kantasoluista erilaistetuille hermosoluverkostoille

Koulutusohjelma Life Science Technologies

Pääaine Biosystems and Biomaterials Engineering

Työn valvoja Professori Alexander Frey

Työn ohjaajat MSc Tanja Hyvärinen, PhD Laura Ylä-Outinen

Päivämäärä 29.07.2019 **Sivumäärä** 75+18 **Kieli** Englanti

Bursti (engl. *burst*) on peräkkäisten korkealla taajuudella esiintyvien toimintapotentiaalien ryhmä. Vaikka burstit ovat olennainen osa maljalla kasvatettujen hermosoluverkostojen sähköistä aktiivisuutta, ei niiden tunnistukseen ole standardimenetelmää. Visuaalinen bursti-tunnistus on laajasti hyväksytty menetelmä, mutta se ei ole objektiivinen eikä ajallisesti tehokas. Tästä syystä bursti-tunnistukseen on kehitetty useita algoritmeja. Tyypillisesti nämä algoritmit on kehitetty ja niiden toiminta on varmennettu vain tietyn tyyppisellä datalla. Tämä voi olla ongelmallista, koska bursti-aktiivisuus eri solutyyppien välillä on vaihtelevaa. Näin ollen algoritmien soveltaminen on rajoitettu vain pieneen osaan aktiivisuustyyppejä. Erityisesti algoritmien soveltaminen ihmisperäisiin hermosoluverkostoihin on kyseenalaista, sillä algoritmit on usein kehitetty jyrsijäperäisillä hermosoluverkostoilla, joiden aktiivisuustyypit eroavat ihmisperäisisten hermosoluverkostojen aktiivisuustyypeistä. Tämän työn tavoitteena oli kerätä testiaineisto, joka sisältäisi monikykyisistä ihmisen kantasoluista erilaistetuissa hermosoluverkostoissa havaittavat burstaavat ja ei-burstaavat aktiviisuustyypit, sekä löytää tällä testiaineistolla toimiva algoritmi ja optimaaliset arvot sen muuttujille. Koska jyrsijäperäiset hermosoluverkostot ovat neurotieteissä paljon käytettyjä, valitun algoritmin haluttiin toimivan myös niistä peräisin olevalla aineistolla. Tavoitteen saavuttamiseksi ihmisperäisistä alkion kantasoluista erilaistettiin toiminnallisia hermosoluverkostoja, joita viljeltiin mikroelektrodihilan (engl. *microelectrode array*, MEA) päällä. Rotan eristettyjä aivokuoren hermosoluja viljeltiin samoin MEA:lla. Hermosoluverkostojen sähköistä aktiivisuutta mitattiin niiden kehityksen aikana kahdesti viikossa, kunnes havaittiin synkronista bursti-aktiivisuutta. Synkronisen bursti-aktiivisuuden ilmaannuttua suoritettiin farmakologiset testit ja mitattiin näin muunneltua aktiivisuutta. Saaduista MEA-mittauksista etsittiin erilaisia aktiivisuustyyppejä, joista muodostettiin testiaineisto. Neljän nykyaikaisen algoritmin toimintaa arvioitiin tässä testiaineistossa. Arviointi tehtiin vertailemalla algoritmien tuloksia raakasignaalista tehdyn visuaalisen bursti-tunnistuksen tuloksiin. Jokaisen algoritmin suoritus pisteytettiin ja niiden herkkyys ja tarkkuus laskettiin. Suoritusta arvioitiin kahdesti siten, että burstin vähimmäispiikkimäärä asetettiin ensin kolmeen ja sitten viiteen. Muiden muuttujien arvot asetettiin algoritmien kehittäjien alkuperäisten suositusten mukaisesti. Optimointi-mahdollisuudet olivat lupaavat vain logISI-algoritmille, joka myös suoriutui parhaiten ja jonka herkkyys ja tarkkuus olivat parhaassa tasapainossa. LogISI:n muuttujat optimoitiin testiaineistolle, mikä huomattavasti paransi sen suoritusta kyseisessä aineistossa. Optimoidulla logISI:llä saatiin joko hyvä tai erinomainen tulos koko testiaineistolla, joka oli saatu mittaamalla spontaania ja farmakologisesti muunneltua aktiivisuutta sekä ihmisperäisistä kantasoluista erilaistetuista että rotan aivokuoresta eristetyistä hermosolu-verkostoista. Näiden tulosten perusteella logISI on potentiaalinen vaihtoehto bursti-tunnistuksen standardimetodiksi.

Avainsanat bursti-tunnistus, mikroelektrodihila, MEA, ihmisperäisistä monikykyisistä kantasoluista erilaistetut hermosoluverkostot

Acknowledgements

This thesis work was conducted in Neuro Group, Faculty of Medicine and Health Technology, Tampere University. I would like to express my gratitude to my instructors Tanja Hyvärinen and Laura Ylä-Outinen who have taught me a lot about being a researcher. Their guidance was invaluable for this work. I would also like to give my thanks to Susanna Narkilahti for providing me with the opportunity to work with the group. I enjoyed this time very much.

From Aalto University, I would like to thank my supervisor Alexander Frey whose feedback made my thesis a better piece and who has shaped my engineer-mindset during my years in Aalto University. With the completion of this thesis, I will graduate. The past years have been filled with hard work but also with constant happiness. I would like to thank my family and friends for all the support and joy that they have given me along this journey.

Espoo, July 29th 2019

Laura Aarnos

Table of contents

SYMBOLS AND ABBREVIATIONS

1. INTRODUCTION 1

2. BACKGROUND 3

2.1. Neurons in vivo 3

2.1.1. Neuronal networks 3

2.1.2. Electrophysiology of neurons 4

2.1.3. Glial cells 6

2.2. Human pluripotent stem cell-derived neurons 7

2.2.1. Neuronal differentiation of human pluripotent stem cells 7

2.2.2. Applications of human pluripotent stem cell-derived neurons 9

2.2.3. Advantages of human pluripotent stem-cell derived neurons 10

2.3. Human and rodent cell models *in vitro* 10

2.4. Measurement techniques for electrical activity of neurons 11

2.5. Microelectrode array technology 12

2.5.1. Microelectrode array devices 13

2.5.2. Origin of microelectrode array signal 14

2.5.3. Analysis of microelectrode array signal 17

2.6. Bursts 17

2.7. Burst detection algorithms 19

2.7.1. General principles of burst detection algorithms 19

2.7.2. Comparison of burst detection algorithms 21

2.7.3. Principles of MaxInterval, Poisson surprise, logISI and Cumulative moving average methods 22

3. MATERIALS AND METHODS 26

3.1. Ethical issues 26

3.2. Human stem cell culture and cortical neuronal differentiation 26

3.2.1. Human embryonic stem cell culture 26

3.2.2. Cortical neuronal differentiation 26

3.3. Primary rat cortical neuronal culture 28

3.4. Microscopy and immunocytochemistry 28

3.4.1. Phase-contrast microscopy 28

3.4.2. Immunocytochemical staining 28
3.5. Microelectrode array recordings 29
3.6. Microelectrode array data analysis 30
3.7. Performance analysis of burst detection algorithms 30
3.7.1. Data selection 30
3.7.2. Visual burst detection 31
3.7.3. Burst detection algorithms 31
3.7.4. Evaluation criteria for the algorithm performance 32
3.8. Statistics 33
4. RESULTS 34
4.1. Neuronal differentiation and synaptogenesis 34
4.1.1. Human pluripotent stem cell-derived neuronal networks 34
4.1.2. Primary rat neuronal networks 34
4.2. Electrophysiological properties of neuronal networks 36
4.2.1. Development of spontaneous activity 36
4.2.2. Pharmacophysiology of neuronal networks 36
4.3. Data selection 38
4.4. Performance of burst detection algorithms 41
4.4.1. Algorithm performance with default parameter values 41
4.4.2. Effects of increased minimum number of spikes 43
4.4.3. Computation of burst features 46
4.4.4. Identification of the most promising algorithm 48
4.5. Optimization of logISI algorithm 48
4.5.1. Optimization of void threshold 49
4.5.2. Optimization of intra-burst peak time window 50
4.5.3. Optimization of default maximum inter-spike interval 51
4.5.4. Combining optimized parameters 53
5. DISCUSSION 55
5.1. Properties of the differentiated neuronal networks 55
5.2. Evaluation of methods assessing burst detection performance 56
5.3. Variation of bursting activity and assembly of test data set 57
5.4. Comparative analysis of algorithm performances 58
5.4.1. Performance of logISI method 59

5.4.2. Performance of Cumulative moving average method 60
5.4.3. Performance of MaxInterval method 62
5.4.4. Performance of Poisson surprise method 63

5.5. Significance of minimum number of spikes in a burst 63

5.6. Significance of spike detection performance 64

5.7. Effects of logISI parameter optimization 65

5.8. Future prospects 66

REFERENCES 69

APPENDICES

Appendix 1: Additional data on statistical tests

Appendix 2: Additional data on test data set

Appendix 3: Burst detection results on test data set

Appendix 4: LogISI optimization results on test data set

Symbols and abbreviations

Symbols

α	α-factor
f	spike frequency
n	number of spikes
N	total number of bins
p	probability
S	Poisson surprise statistic
T	time interval

Abbreviations

AA	ascorbic acid
ALS	amyotrophic lateral sclerosis
AMPA	α-amino-3-hydroxy-5-methyl-4-isoxazole propionate
BDNF	brain-derived neurotrophic factor
begISI	maximum beginning inter-spike interval in a burst
BMP	bone morphogenetic protein
BSA	bovine serum albumin
CMA	Cumulative moving average
CNQX	6-cyano-7-nitroquinoxaline-2,3-dione
CNS	central nervous system
DAPI	4',6-Diamidino-2-Phenylindole, Dihydrochloride
D-AP5	D-(-)-2-amino-5-phosphonopentanoic acid

db-cAMP	dibutyryl cyclic adenosine monophosphate
DMEM	Dulbecco's modified Eagle's medium
DMSO	dimethyl sulfoxide
DPBS	Dulbecco's phosphate-buffered saline
EAP	extracellular action potential
EB	embryoid body
ECM	extracellular matrix
ECoG	electrocorticography
EEG	electroencephalography
endISI	maximum ending inter-spike interval in a burst
EPSP	excitatory postsynaptic potential
FGF	fibroblast growth factor
FIMEA	Finnish Medicines Agency
fMRI	magnetic resonance imaging
GABA	γ-aminobutyric acid
GDNF	glial-derived neurotrophic factor
hESC	human embryonic stem cell
hiPSC	human induced pluripotent stem cell
hPSC	human pluripotent stem cell
HSMM	hidden semi-Markov model
IBI	inter-burst interval
ICM	inner cell mass
iPSC	induced pluripotent stem cell

IPSP	inhibitory postsynaptic potential
ISI	inter-spike interval
ISIth	inter-spike interval threshold
KA	kainic acid
LFP	local field potential
LN521	recombinant human laminin-521
MAP2	microtubule-associated protein 2
maxISI	maximum inter-spike interval in a burst
MI	MaxInterval
minDur	minimum duration of a burst
minIBI	minimum inter-burst interval
minSpikes	minimum number of spikes in a burst
MEA	microelectrode array
NDS	normal donkey serum
NMDA	*N*-methyl-D-aspartate
NMM	neural maintenance medium
NPC	neural progenitor cell
PB	phosphate buffer
PCA	principal component analysis
PDL	poly-D-lysine
PEI	poly-ethylene-imine
PET	positron emission tomography
PFA	paraformaldehyde

PNS	peripheral nervous system
PO	poly-L-ornithine
PS	Poisson surprise
PSP	postsynaptic potential
Q1	lower quartile
Q3	upper quartile
RC_f	relative change in spike frequency
RT	room temperature
SNR	signal-to-noise ratio
TGFβ	transforming growth factor β
TTX	tetrodotoxin

1. Introduction

Neurons of the brain are the cells responsible for the cognitive functions, such as thinking and learning. These functions require interaction between the neurons and, as such, the neurons form complex networks. In the neuronal networks, signals are transferred in the form of electrical impulses, called action potentials. A burst is a set of subsequent action potentials that are generated at a high frequency. *In vivo*, bursts have a significant role in brain function for being information carriers in the brain (Obien et al. 2015). Also neuronal networks *in vitro* display bursting activity. In these networks, bursts are considered to be an indicator of mature electrical activity (Weick 2016). Analysis of the bursting activity and changes in it has been used to study for example the impact of genetic variations and chemical manipulations (Cotterill et al. 2016; Weick 2016).

Even though burst analysis is a fundamental part when evaluating the development and properties of electrical activity, no standard method exists for burst detection. Bursts can be identified visually by a human observer, but this is not an objective nor efficient method. Consequently, various burst detection algorithms have been developed. Burst detection algorithms have typically been developed and verified on specific type of neuronal network or activity. Unfortunately, this can restrict their application on a wider range of data (Cotterill et al. 2016; Pasquale et al. 2010; Kapucu et al. 2012). Especially applicability to human neuronal networks, typically derived from human pluripotent stem cells (hPSCs), is questionable as majority of the burst detection methods have been developed on rat networks (Cotterill et al. 2016). Furthermore, many of the burst detection algorithms used on hPSC-derived networks are outdated because the recent progress in culture and neuronal differentiation methods has enhanced the development of electrical activity and bursting behavior of these networks.

There is utmost need for a standard contemporary burst detection method (Cotterill et al. 2016). The fact that many algorithms are developed for specific type of data is problematic because the bursting activity is widely variable (Wagenaar 2006; Heikkilä et al. 2009). The lack of a standard burst detection algorithm is a huge disadvantage for researchers because it prevents comparison of results between laboratories. It can even prevent comparison of results within a single laboratory if the method used is not suitable for neuronal networks derived from distinct cell lines. Standardization would be important also for the characterization of electrophysiological properties of hPSC-derived neuronal cells to be utilized in applications such as disease

modelling, pharmacological tests and regenerative medicine. A good, constant quality is a basic requirement in these applications and cannot be validated without a standardized method.

Recently, the performances of different burst detection algorithms have been evaluated on synthetic data and on biological data from spontaneously firing human induced pluripotent stem cell (hiPSC)-derived neuronal networks (Cotterill et al. 2016). No ideal burst detection algorithm has been found for hPSC-derived neuronal networks but use of different algorithms, and even different parameters within a single algorithm, are still recommended for different types of activity (Cotterill et al. 2016). This is not practical, however, as use of different algorithms and parameters requires an investigation of the activity types prior to burst detection. A single experiment can include various activity types due to different states of maturation or modulation of electrical activity. Moreover, use of different algorithms prevents the comparison of results. Further evaluation and comparison of algorithm performances is needed on a wider range of biological data to find a single algorithm that could be utilized for all activity types observed on hPSC-derived neuronal networks.

The aims of this thesis were to assemble a test data set, which would well represent the variety of bursting and non-bursting activity on hPSC-derived neuronal networks, and to identify the most promising algorithm with optimal parameters that could be applied for the wide range of electrical activity types included in the test data set. As rodent neurons are still widely used in the neuroscience, it was additionally desirable that the algorithm would similarly function on rodent neuronal networks. To achieve the goals, functional neuronal networks were derived from hPSCs and embryonic rat cortical neurons. Spontaneous electrical activity of developing networks was recorded to identify different activity types present during the network development. Additionally, responses to pharmacological reagents were recorded on bursting neuronal networks, and different activity patterns were identified amongst this modulated activity. Based on this information, a data set was assembled for performance analysis of four promising burst detection algorithms. The four algorithms included MaxInterval (MI) (Nex Technologies 2014), Poisson surprise (PS) (Legendy, Salcman 1985), logISI (Pasquale et al. 2010) and Cumulative moving average (CMA) (Kapucu et al. 2012) methods. The algorithm with the highest performance was chosen for further analysis and parameter optimization to enhance its performance and to achieve a high, or at least satisfactory, performance on all identified activity types.

2. Background

2.1. Neurons in vivo

Neurons are cells specific to the nervous system of the body. The nervous system receives information about the changes within the body and about the changes in the environment outside of the body. The brain, which is a part of the central nervous system (CNS), is the site of cognitive functions, such as thinking, memorizing and learning. Thus, all the information received by the nervous system is processed in the brain. Based on the results of the information processing, the brain generates an appropriate response, which ultimately alters the functions of the body, e.g. the function of muscles and glands. In other words, the system receives an input, processes the information, and generates an output. The function of the nervous system translates well to the function of a single neuron, which handles information in a similar manner.

2.1.1. Neuronal networks

In an adult human brain, there are approximately 85 billion neurons (Bear et al. 2015). Neurons have many different subtypes, which are distinguishable by their localization in the brain, morphology, connectivity, electrophysiological properties and protein expression, e.g. neurotransmitter expression (Mertens et al. 2016). Nevertheless, all types of neurons share certain morphological and functional characteristics (Bear et al. 2015). A neuron consists of a soma, an axon, and one or, more often, multiple dendrites. A soma is the body of a neuron that contains the nucleus and most of the cell organelles. An axon is a process of a neuron, which carries information in a form of an electrical impulse to other neurons or to a target cell in the peripheral nervous system (PNS). The electrical impulse is called an action potential. A dendrite is also a process of a neuron, but it carries information received from other neurons to the soma of the cell. The neurons form connections to each other to enable information transfer from one to another. As a single neuron can have multiple connections, together the neurons construct a complex network of connections. These connections are called synapses. In the human brain, there are more than 10^{14} synaptic connections (Eroglu, Barres 2010). Typically, the synapses are established between the axon of the presynaptic neuron, and the dendrite or the soma of the postsynaptic neuron.

2.1.2. Electrophysiology of neurons

The cell membrane potential is an important feature for the information transfer within a neuron. The membrane potential is defined as the electrical potential difference across the cell membrane. At rest, this potential difference is approximately -65 mV (Bear et al. 2015). If the resting state is disturbed, the membrane potential changes. Ions crossing the cell membrane *via* ion pumps or open ion channels alter the membrane potential (Bear et al. 2015). When positive ions cross the membrane from the extracellular space to the cytosol, the potential changes to the positive direction and the membrane is said to depolarize. On the contrary, when positive ions cross the membrane from the cytosol to the extracellular space, the potential becomes more negative and the membrane is said to polarize. Polarization can also result from an influx of negative Cl^- ions from the extracellular space to the cytosol. If the polarization takes the membrane potential below the resting potential, the process is called hyperpolarization (Bear et al. 2015). The main reason for the opening of ion channels and, consequently, for the membrane potential changes are signals from other neurons.

A neuron can simultaneously receive multiple signals, inputs, from other neurons *via* synapses (Figure 1). The inputs are mediated by neurotransmitters, such as glutamate or γ-aminobutyric acid (GABA) (Bear et al. 2015). The neurotransmitters are released from the axon terminal of the presynaptic neuron, when an action potential reaches the terminal. The neurotransmitters cross the synaptic cleft and bind to their specific receptor at the cell membrane of the postsynaptic neuron. As such, the information is transferred in a chemical form across the synapse. The input can be either excitatory or inhibitory. Glutamate is an excitatory neurotransmitter, the receptors of which include α-amino-3-hydroxy-5-methyl-4-isoxazole propionate (AMPA) receptors, *N*-methyl-D-aspartate (NMDA) receptors and kainate receptors, whereas GABA is an inhibitory neurotransmitter that binds to $GABA_A$ and $GABA_B$ receptors (Bear et al. 2015). The binding of the neurotransmitter or a signaling cascade initiated by the binding leads to a change in ion channel function, which in turn causes a change in the ion fluxes. As a result, the membrane potential changes. An excitatory input causes the membrane to depolarize as the channels permeable to Na^+ and Ca^{2+} are opened (Bear et al. 2015). An inhibitory input causes the membrane to polarize or hyperpolarize due to the opening of Cl^- channels (Bear et al. 2015). The resulting potentials are called excitatory postsynaptic potential (EPSP) and inhibitory postsynaptic potential (IPSP), respectively.

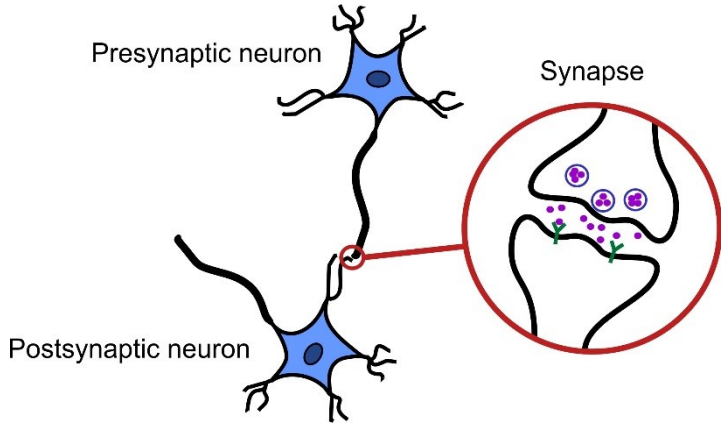

Figure 1. Illustration of a chemical synapse. A synapse typically forms between the axon of a presynaptic neuron and the dendrite of a postsynaptic neuron. Information is transferred across the synapse by neurotransmitters (purple). Neurotransmitters are released into the synaptic cleft from the vesicles (blue) located in the axon terminal in a response to an arrival of an action potential. The neurotransmitters diffuse across the synaptic cleft and bind to the receptors (green) of the postsynaptic neuron.

On some occasions, the information between two neurons is not transferred in a chemical form across a synapse but is transferred *via* gap junctions. A gap junction between two neurons can also be called an electrical synapse. Through the gap junctions, ions can be transferred to both directions unlike in chemical synapses (Bear et al. 2015). The ion transfer generates a postsynaptic potential (PSP) in the ion-receiving neuron. Electrical synapses are rare in comparison to chemical synapses but are common particularly during development (Bear et al. 2015).

The effects of multiple inputs are superimposed. The summation is both spatial and temporal. This means that the inputs are superimposed from different dendrites and that a higher input frequency leads to a larger effect. The summation applies to both excitatory and inhibitory inputs, which signifies that the number of inputs does not necessarily correlate to the scale of depolarization as there are polarizing inputs involved as well (Bear et al. 2015). If the resulting superimposed depolarization at the proximal end of the axon, called the axon hillock, exceeds a threshold potential, an action potential is generated, or fired, as an output (Bear et al. 2015). A single, weak input might not be enough to generate an action potential but due to summation multiple weak inputs together can result in depolarization that exceeds the threshold.

When generating an action potential, the local Na^+ channels of the cell membrane open resulting in an influx of Na^+ ions and depolarization of the membrane. The membrane potential typically reaches approximately 40 mV (Bear et al. 2015). The depolarization causes the nearby, more distal voltage-gated Na^+ channels to open

and, in this way, the action potential proceeds all the way to the axon terminal, where it causes the release of the neurotransmitters enabling them to bind the receptor of the connected neuron (Bear et al. 2015). Right after the depolarization, the local Na^+ channels close and K^+ channels open (Bear et al. 2015). As K^+ ions flow out, the membrane repolarizes, meaning that the resting potential is recovered. Additionally, Na^+ ions are actively pumped out of the cell, and this contributes to the repolarization (Bear et al. 2015). Before returning to the resting potential, the membrane potential dives slightly below it (Bear et al. 2015). This sink is referred to as afterhyperpolarization (Bear et al. 2015). As a result, the action potential can be seen as a sharp, positive spike followed by a small, negative sink.

2.1.3. Glial cells

Even though the neurons are the most important cells regarding the information transfer and other cognitive functions of the brain, they could not function without other cells supporting them. These supporting cells are glial cells. In the brain, the number of glial cells is approximately equal to the number of neurons (Bear et al. 2015). The three types of glial cells are astrocytes, oligodendrocytes, and microglia, and each type supports neurons in different ways. Astrocytes are especially important to the electrical activity as they regulate the formation, maturation, and pruning of synapses (Clarke, Barres 2013). Astrocytes also maintain the homeostasis of the brain and have a role in the function of the blood-brain barrier (Abbott et al. 2006). Oligodendrocytes wrap around the axons of the neurons forming a myelin sheath. Almost the whole axon is insulated and protected by myelin. Only small periodical areas between the sheaths, called the nodes of Ranvier, are exposed and allow transmembrane ion current. Owing to the myelin, the action potential propagation is saltatory, which allows very rapid information transfer (Bear et al. 2015). The axons of the neurons are myelinated only in the inner parts of the brain, which are accordingly referred to as white matter. On the brain cortex, the axons are not myelinated, and that part of the brain is called gray matter. Finally, microglia are responsible for the immune defenses of the brain. They are phagocytic and mediate the inflammation response. They also appear to be involved in remodeling of synaptic connections (Bear et al. 2015). In fact, microglia are resident macrophages of the neural tissue and are not of neuroectodermal origin like neurons and other glial cells. Microglia are derived from primitive macrophages of the yolk sac (Ginhoux et al. 2010).

2.2. Human pluripotent stem cell-derived neurons

Stem cells are cells that have a potential to differentiate to other cell types and a capacity for self-renewal. Different stem cells have different levels of differentiation potential and of self-renewal capacity. Pluripotent stem cells can differentiate to any cell type except trophoblasts of the placenta. In other words, pluripotent stem cells can produce cells from all the three germ layers: endoderm, mesoderm and ectoderm. They also have the highest self-renewal capacity. hPSCs include human embryonic stem cells (hESCs) and hiPSCs (Figure 2). hESCs are derived from the inner cell mass (ICM) of a blastocyst 5-6 days after fertilization. hiPSCs are derived from somatic cells, such as fibroblasts, by introduction of a few defined transcription factors which induce conversion to pluripotent state (Takahashi et al. 2007). hPSCs provide an inexhaustible source for different cell types including neurons.

2.2.1. Neuronal differentiation of human pluripotent stem cells

hPSCs differentiate into neurons due to specific environmental cues. Differentiation is defined by changes in gene expression and its regulation. When a stem cell differentiates into a neuron, specific genes are activated or permanently silenced. Environmental cues mediate these changes by stimulating or inhibiting specific signaling pathways. The signaling pathways involved in neuronal differentiation are similar *in vivo* and *in vitro* (Vieira et al. 2018). *In vivo,* the activity of each pathway is naturally controlled by the environmental cues. *In vitro,* the stimulation or inhibition of a specific pathway is initiated artificially. This involves timed introduction and retrieval of combinations of mitogens and morphogens, which mimic the environmental cues *in vivo* (Mertens et al. 2016). For example, Noggin and a small molecule called SB431542 are added to inhibit bone morphogenetic protein (BMP) and transforming growth factor β (TGFβ) pathways, respectively (Chambers et al. 2009). Inhibition of these pathways trigger conversion from pluripotent state to neural lineage commitment (Chambers et al. 2009). In contrast, fibroblast growth factor 2 (FGF2) is frequently used to stimulate FGF pathway, which promotes the proliferation of neural progenitor cells (NPCs) while also allowing neuronal differentiation (Vieira et al. 2018; Shi et al. 2012). Besides soluble signaling molecules, components of neural extracellular matrix (ECM), such as laminin, can be utilized in the culture system to promote neuronal differentiation (Vieira et al. 2018). There are various protocols for neuronal differentiation that differ in respect to the choice of inducer molecules. Additionally, distinct protocols can utilize either a 2D or 3D platform. In a 2D platform, the cells can be cultured in aggregates called embryoid bodies (EBs) or in an adherent culture system (Mertens et al. 2016). In 3D platform,

the cells are cultured on a 3D scaffold that aims to mimic the mechanical and chemical properties of neural ECM (Vieira et al. 2018).

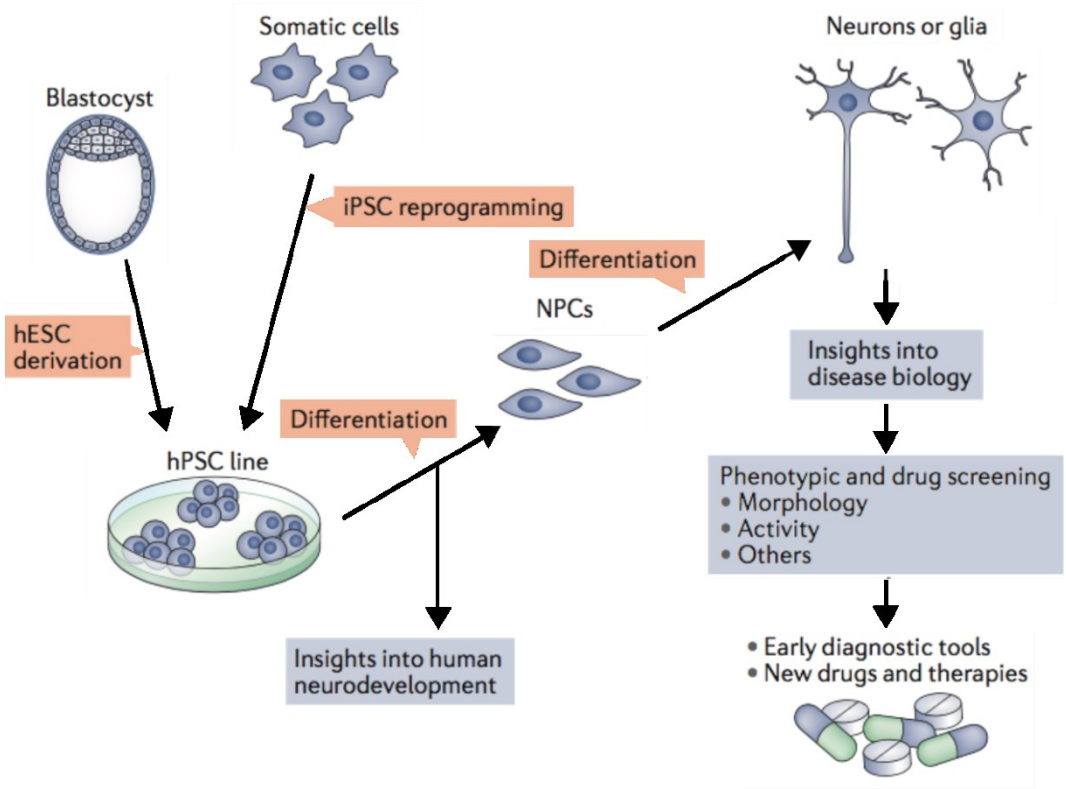

Figure 2. Generation of neurons and glial cells from hPSCs. Neurons and glial cells can be differentiated from hPSCs, which include hESCs and hiPSCs. hESCs are derived from the ICM of a blastocyst whereas hiPSCs are reprogrammed from somatic cells. The differentiation process of hPSCs into neurons or glial cells often includes an interphase of NPCs. The study of the differentiation provides insights to human neurodevelopment. Neurons and glial cells derived from hPSCs are utilized to model neurological diseases. The disease models can be further applied in phenotypic and drug screening, which provide ways to develop novel tools for early diagnostics as well as novel treatments. The figure is modified from Mertens et al. (Mertens et al. 2016).

The first step of the neuronal differentiation is initiating neural commitment and regionalization, which results in the generation of NPCs (Mertens et al. 2016). Commitment refers to the reduction of differentiation potential to neural lineage. Regionalization refers to the specification of the positional identity to a certain region along the anterior-posterior axis and the dorsal-ventral axis of the developing CNS (Mertens et al. 2016). Different subtypes of NPCs differ in respect of differentiation potential and positional identity (Mertens et al. 2016) and, thus, the generation of NPCs already guides the final composition of the fully differentiated neurons. The NPCs are further differentiated into neurons by alterations to the cocktail of the mitogens and morphogens together with extended maturation time (Mertens et al. 2016). Altogether, the generation of functional neurons from hPSCs takes typically 5

weeks or more (Weick 2016). The desired end-product of differentiation is a mature neuron that mimics the morphology, electrophysiology and other properties of a neuron *in vivo*. These properties are evaluated with a combination of light or electron microscopy, immunostaining, fluorescence microscopy, gene expression, patch clamp technique, calcium imaging, and microelectrode array (MEA) technology (Obien et al. 2015). Light and electron microscopy display the morphology of the neuron. Immunostaining and fluorescence microscopy aim to demonstrate the presence of molecules specific for mature neurons and synapses, whereas patch clamp, calcium imaging and MEA provide data of the electrophysiological events of a neuronal culture. A wide spectrum of different neuronal subtypes has been generated from hPSCs, including excitatory cortical neurons, cortical interneurons and motor neurons (Mertens et al. 2016). Protocols to enrich astrocyte and oligodendrocyte differentiation from hPSCs have also been developed (Mertens et al. 2016). Nevertheless, a co-culture of neurons and astrocytes is often desired as astrocytes have a crucial role in the development of functional neuronal networks (Fukushima et al. 2016; Odawara et al. 2016).

2.2.2. Applications of human pluripotent stem cell-derived neurons

hPSC-derived neurons have many applications. The neurons and their differentiation are studied to gain basic knowledge about human neural development and function (Mertens et al. 2016). Moreover, hPSC-derived neurons can be applied within drug discovery and neurotoxicology assays (Ylä-Outinen et al. 2010; Odawara et al. 2016). They are also widely used to model neurological and neurodegenerative diseases such as amyotrophic lateral sclerosis (ALS) (Di Giorgio et al. 2008), Parkinson's disease (Monti et al. 2016) and schizophrenia (Brennand et al. 2011). Some of the diseases affect specific subtypes of neurons and, therefore, good characterization methods are needed to analyze the fate of the generated neurons (Weick 2016). Once a disease model has been established, it can be applied for drug discovery and development of novel diagnostic tools that exploit the distinguishable properties of the disease cell phenotype (Weick 2016; Mertens et al. 2016). Furthermore, both hPSC-derived neurons and NPCs are of great interest in regenerative medicine. Although the brain hosts neural stem cells, the regenerative capacity of adult human neural tissue is poor (Gage 2000). hPSC-derived neurons and glial cells could potentially be used to replace damaged cells or activate endogenous cells to repair the damage (Gage 2000).

2.2.3. Advantages of human pluripotent stem-cell derived neurons

Besides hPSCs, there are other sources of human neurons. Adult and fetal brain host neural stem cells, which are multipotent. Multipotent stem cells can give rise to several specific cell types. Neural stem cells have the potential to differentiate into neurons, astrocytes and oligodendrocytes. Adult neural stem cells are found for example in the subventricular zone and the hippocampus whereas fetal neural stem cells are more abundant and found in several more structures of the developing brain (Gage 2000). The advantage of the neural stem cells is that they have naturally developed *in vivo*. The availability of neural stem cells for research is, however, very limited. Their derivation is an invasive process, which is why they cannot be harvested freely from the human brain. Neuronal tumors are yet another source of neurons (Biedler et al. 1978). Cancer cell lines are immortal but have limited use outside of cancer research due to their pathophysiological state (Ylä-Outinen et al. 2010). In conclusion, hPSCs are a superior source of neurons as they possess healthy physiology and provide unlimited material for research due to their accessibility and capacity for self-renewal.

Direct conversion is a method that converts somatic cells into neurons or NPCs without first converting them all the way to the pluripotent state. Direct conversion is induced by overexpression of cell type-specific transcription factors (Mertens et al. 2016; Pang et al. 2011). Direct conversion shares a major advantage of hiPSCs as the neurons derived by these methods are specific to the donor. This is highly useful when setting up disease models as the hiPSC-derived neurons and directly converted neurons originating from patients naturally possess their mutations or genetic instabilities underlying the emergence of disease. Unlike hiPSCs, direct conversion also conserves transcriptomic and functional signatures of ageing, which could provide additional information when studying late-on-set diseases (Mertens et al. 2016). Only hPSCs can be used to study the full course of CNS development though, because the direct conversion skips most developmental steps. Consequently, hPSCs are often a better option when modelling diseases that involve neurodevelopmental defects (Mertens et al. 2016). In further comparison to hPSCs, major disadvantages of direct conversion are limited expansion capacity and lower competence for synaptogenesis (Zhang et al. 2013; Mertens et al. 2016; Weick 2016).

2.3. Human and rodent cell models *in vitro*

Many ground-breaking discoveries in biology and biotechnology have first been described on rodent cell models. For example, induced pluripotent stem cell (iPSC)

technology and the direct conversion method were first demonstrated with mice fibroblasts (Takahashi, Yamanaka 2006; Vierbuchen et al. 2010). Rodent cells are popular because they are well-characterized, cheap, and easy to produce. Rodent models are also required in pre-clinical studies in drug discovery. Although rodent models are the golden standard in the field, their use has raised ethical concerns. Furthermore, translatability of the results from rodent studies to human physiology is dubious. Alternative methods for rodent models are actively investigated.

Rodent neural stem cells and neurons are harvested from prenatal, postnatal or adult brain of a rodent. Currently, they are widely used for research in neuroscience, more so than hPSC-derived NPCs and neurons. Therefore, many of the methods used to characterize stem cell-derived neurons and glial cells are mostly developed on rodent cell models. These methods include antibodies used in immunostaining (Mertens et al. 2016) as well as burst detection methods for MEA data analysis (Cotterill et al. 2016). However, significant species differences raise a major concern for the generalization of rodent-based discoveries to human cell physiology, diseases, and drug development (Fukushima et al. 2016). The species differences make it impossible to satisfyingly predict human drug responses on rodent models (Cummings 2018). Due to this, numerous drugs fail in clinical trials. hPSC-derived cells provide a human-based platform to study cell physiology and pathology as well as to screen drugs and study toxicological effects. Naturally, rodent cells cannot be applied in clinical applications either whereas hPSC-derived cells have wide potential in this area.

2.4. Measurement techniques for electrical activity of neurons

As described in the previous chapters, the electrophysiological events of neuronal networks comprise all ion currents across the cell membrane. This electrical activity can be measured with different techniques. MEA technology, intracellular recording techniques, and optical methods are used to measure the electrical activity of neurons *in vitro* and *in vivo* (Obien et al. 2015; Homma et al. 2009). MEA and intracellular recording techniques record potential changes with electrodes whereas optical methods utilize for example dyes to visualize electrical activity-related events in different ways. All these techniques record real-time activity.

MEA records extracellular field potentials generated by electrical activity of the neurons. The major advantage of MEAs is allowing simultaneous, non-invasive, and long-term recordings of neuronal populations (Spira, Hai 2013; Odawara et al. 2016). A disadvantage of MEAs is that they attenuate and temporally filter electrical signals

(Spira, Hai 2013). As various events from multiple neurons contribute to the MEA signal, the interpretation of the whole signal can be challenging. Often only information about action potentials is extracted and analyzed whereas other electrical activity is excluded from the scope of study. In comparison, intracellular recording performed by sharp or patch electrodes provide precise and accurate information about all the electrophysiological events of a neuron (Spira, Hai 2013). However, intracellular methods are invasive and only individual neurons can be measured. Therefore, these methods are not suitable for population-level or long-term studies. Optical methods utilizing fluorescent calcium indicators or genetic markers are similarly used at cellular resolution (Obien et al. 2015). Calcium imaging with fluorescent calcium indicators is an especially common method. An indicator binding to Ca^{2+} ion results in a fluorescent signal. Arrival of an action potential to the axon terminal causes Ca^{2+} ion channels to open, which leads to influx of Ca^{2+} ions (Bear et al. 2015). Increased Ca^{2+} concentration stimulates the release of neurotransmitters into the synaptic cleft (Bear et al. 2015). Thus, synaptic events are indicated by Ca^{2+} changes, which are detectable with calcium imaging. Similar to MEA technology, calcium imaging can be used to record the activity of neuronal networks. However, the temporal resolution is not as accurate as that of electrical potential recording techniques (Homma et al. 2009). Similar to MEA signal, multiple factors can affect the optical signal making the analysis more challenging (Obien et al. 2015).

Besides MEA, intracellular recording technologies, and optical methods, there are other methods to measure electrical activity of neuronal networks. Magnetic resonance imaging (fMRI), electroencephalography (EEG), electrocorticography (ECoG), positron emission tomography (PET), and magnetoencephalography are utilized to measure neural populations in macroscale, such as large regions of the brain (Spira, Hai 2013; Obien et al. 2015).

2.5. Microelectrode array technology

MEA technology is applied to monitor, record, and stimulate electrical activity of neurons both *in vitro* and *in vivo*. As mentioned in the previous chapter, electrical activity of the neurons generates extracellular field potentials, which are recorded by the electrodes of a MEA device. The multiplicity of electrodes makes it possible to study the neurons at a population level. *In vitro* MEAs can include up to 10,000 electrodes and *in vivo* over a hundred electrodes (Spira, Hai 2013). MEA recordings are used to study neuronal circuit-connectivity, physiology and pathology (Spira, Hai 2013; Buzsáki et al. 2012). The possibility of electrical stimulation can help research that aims to develop implants, control limbs, and treat disorders *via* stimulation

(Obien et al. 2015; Ghane-Motlagh, Sawan 2013). MEAs are also exploited in pharmacological tests and diagnostics (Obien et al. 2015). Similar to neurons, the electrical activity of cardiomyocytes has been studied with MEAs (Navarrete et al. 2013; Ryynänen, Kujala et al. 2011).

It is notable that the information obtained by MEAs is limited and cannot actually reveal what mechanism triggers the observed firing (Spira, Hai 2013). Nevertheless, the electrical activity patterns and features of distinct neuronal populations can be studied and compared. The activity patterns are spatially and temporally variable in the brain. Both *in vivo* and *in vitro*, distinct neuronal subtypes, e.g. GABAergic and glutamatergic neurons, have their own characteristic activity patterns and the pattern recorded by MEA is a combination of these individual patterns, an average activity pattern (Gelfman et al. 2018). Some drugs, such as certain anti-psychotics, can selectively target neuronal subtypes but their effect can be undetectable if the change in the average activity is not notable (Gelfman et al. 2018). Besides chemical stimulation, factors altering the electrical activity include electrical stimulation, mutations and maturation state of neuronal networks.

2.5.1. Microelectrode array devices

The first electrophysiological studies with MEAs were made in 1970s (Thomas Jr. et al. 1972; Pine 1980). Since then, many different MEA devices have been developed. The devices can differ in design, materials and fabrication techniques. Regarding *in vitro* experiments, the electrodes can be divided into two types. The most commonly used type is a substrate-integrated planar electrode (Figure 3). The electrode diameters vary between 5 and 50 μm (Obien et al. 2015). The other type is a 3D structured electrode such as a silicon nanowire (Robinson et al. 2013) and an Au mushroom (Hai et al. 2009). The 3D structured electrodes have been developed in hopes of decreasing the attenuation of the signal. This aim is pursued by the small electrodes being engulfed by the neurons (Spira, Hai 2013). Also, some designs have used electroporation to enable intracellular recording with these electrodes (Spira, Hai 2013).

For the materials, the most important aspect is their biocompatibility (Toivanen et al. 2017; Obien et al. 2015). The electrodes are typically made with metallic conductors but there are also non-metallic electrodes combined with field-effect transistor-based transducers (Obien et al. 2015). For the electrode fabrication, a major focus is obtaining a low impedance in order to achieve a higher signal-to-noise ratio (SNR) (Obien et al. 2015; Ghane-Motlagh, Sawan 2013). The objective is to have a SNR of 5:1 or higher (Obien et al. 2015). It is notable that the requirements for SNR limit the

reduction of electrode surface area. This is because the smaller the surface area the higher its impedance and, consecutively, the lower the SNR (Obien et al. 2015; Spira, Hai 2013). The limitation to the reduction of electrode surface area restricts the electrode density and spatial resolution of a MEA (Obien et al. 2015).

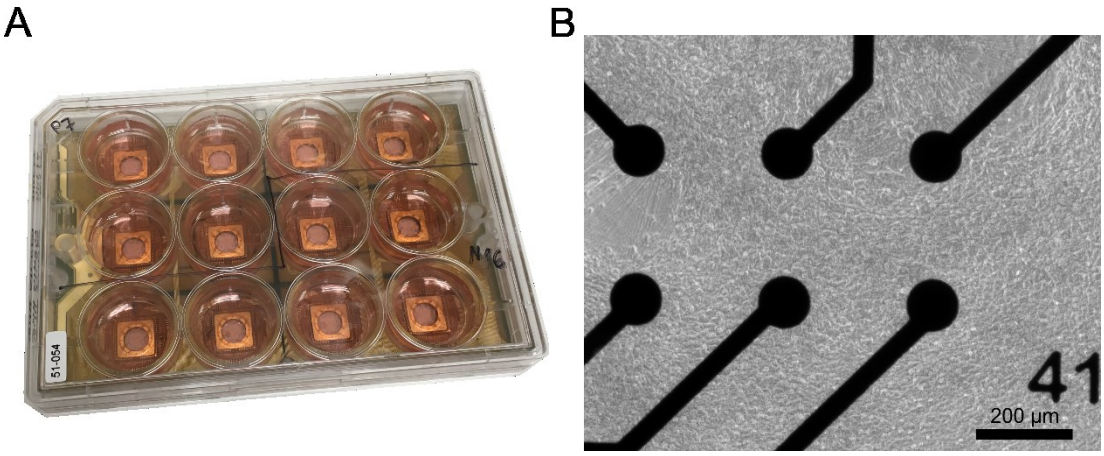

Figure 3. A) A 12-well MEA plate with cell culture. The electrodes are located within the circular area inside a square at them bottom of each well. The plate in the image is a commercial product from Axion BioSystems (Atlanta, GA, USA). B) A phase-contrast microscope image of hPSC-derived neurons on MEA. The black dots are substrate-integrated electrodes, which are in contact with the cell culture. The black lines connected to the electrodes are conductive wires. Cells can be seen around the electrodes. There are cells also on top of the electrodes but this cannot be seen in a phase-contrast microscope image. Neuronal processes are visible for example in the vicinity of the upper-leftmost electrode.

2.5.2. Origin of microelectrode array signal

As mentioned earlier, MEAs measure the extracellular field potentials generated by the electrical activity of the neurons. The potentials are measured at a sub-millisecond time scale (Buzsáki et al. 2012). Electrical activity of neurons comprises all transmembrane currents, but for the extracellular field potential the most significant events are action potentials, EPSPs, and IPSPs. Electrical synapses do not directly contribute to the extracellular field potential but can affect the generation of transmembrane currents (Buzsáki et al. 2012). Extracellular signals caused by action potentials range between 500 to 1000 Hz (Spira, Hai 2013). These high frequency signals are called extracellular action potentials (EAPs). The low frequency signal below 500 Hz is called a local field potential (LFP) and it is caused by joined activity of various electrophysiological events. PSPs are the main component of LFP (Buzsáki et al. 2012). Other contributors include membrane oscillations, glial potentials, and any ion fluxes through voltage- and ligand-gated channels. PSPs cause extracellular signals of 100 Hz, membrane oscillations cause extracellular signals between 1 and 50 Hz (Spira, Hai 2013), and slow glial potentials cause signals of < 0.1 Hz (Einevoll et

al. 2013; Buzsáki et al. 2012). The LFP signals are more difficult to interpret than EAPs due to the multitude of potential sources (Einevoll et al. 2013). Consequently, analysis of EAPs is more common than analysis of LFPs.

A single EAP is considered to present a putative action potential (Obien et al. 2015). An EAP can be detected from a distance of ∼100 μm, and its duration is < 2 ms (Obien et al. 2015). In MEA data analysis, an EAP is often called a spike referring to the shape of an EAP (Figure 4A). A typical spike form is a mirror image of an intracellular action potential. Accordingly, a spike in a MEA recording actually consists of two spikes. A sharp negative spike of high amplitude is followed by a more curved positive spike of low amplitude (Obien et al. 2015). The negative spike is caused by influx of Na^+ and is sharp due to the rapidness of the influx, whereas the curved positive spike results from the slow efflux of K^+ (Obien et al. 2015).

It is important to understand, that the extracellular field potential measured by the electrode is a superposition of separate transmembrane currents of the neurons in the proximity of the electrode. The effect of an individual transmembrane current on the detected potential depends on its magnitude, sign and distance from the electrode (Obien et al. 2015) (Figure 4B). Temporal synchrony and favorable spatial alignment of neurons strengthen the signal from these neurons (Obien et al. 2015). Additionally, there are multiple noise sources in MEA system that contribute to and modify the signal (Figure 5). Relevant noise sources at the interface of metal and culture medium include thermal noise and hum from the power lines (Obien et al. 2015). Noise from the device itself arises from amplification and digitalization of the signal (Obien et al. 2015). Biological noise comprises signals from those electrophysiological events that are not of interest. Consequently, LFP is also considered biological noise when investigating only action potentials (Obien et al. 2015). Overall, the biophysics related to the extracellular field potential measurements are well understood (Buzsáki et al. 2012).

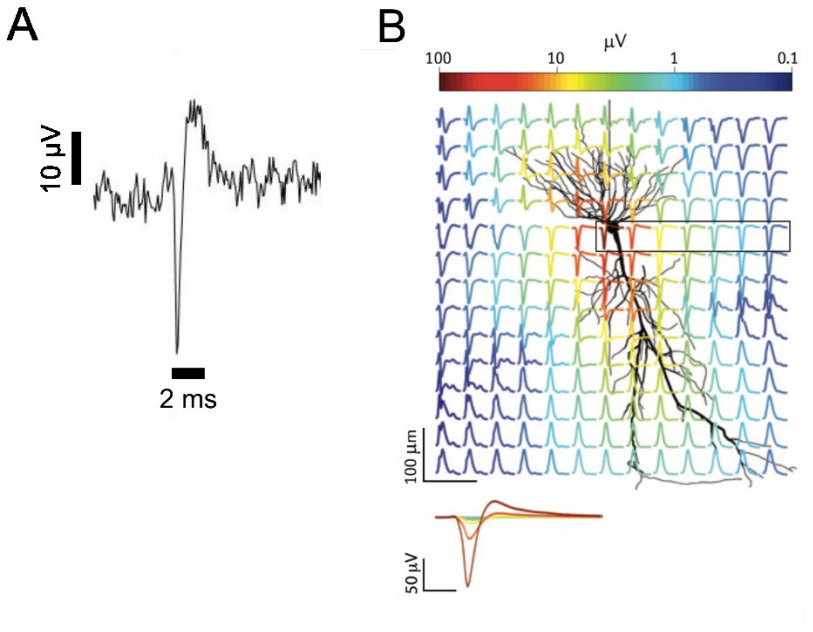

Figure 4. A) A single spike with a typical waveform in raw MEA signal. The spike in fact consists of two spikes as a sharp negative spike is followed by a more curved positive spike. B) The location of an electrophysiological event in respect to the recording electrode affects the sign, shape and magnitude of the recorded extracellular field potential. The amplitude of a spike decreases rapidly with increasing distance as seen in the lower figure. In the upper figure, the magnitudes of the spikes are normalized, and the color indicates the voltage range. Figure B has been modified from Buzsaki et al. (Buzsáki et al. 2012).

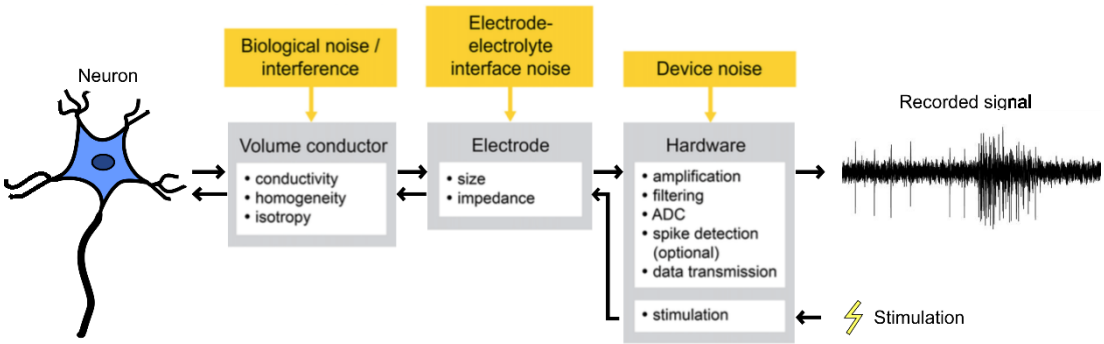

Figure 5. A diagram of a MEA system and its noise sources. MEA system is used to record and stimulate the electrical activity of a neuron. The properties of the volume conductor, e.g. culture medium, and the electrode affect the signal transmission. The hardware processes the recorded signal and generates the stimuli. The noise contributing to the signal and modifying the signal arises from biological sources, the electrode-electrolyte interface, and the device. The figure has been modified from Obien et al. (Obien et al. 2015).

2.5.3. Analysis of microelectrode array signal

MEA signal processing requires high computational power due to a great amount of data. The signal processing comprises of filtering the raw MEA data, spike detection, and spike sorting (Obien et al. 2015). The objective of the filtering is to achieve a higher SNR and also to decrease the occurrence of false positives in spike detection (Obien et al. 2015). Typically, a band-pass filter with a band of 300-3000 Hz is applied (Obien et al. 2015) and the rest of the signal is discarded. Spike detection is the process of extracting spikes from the signal. The most common and perhaps simplest method is to set a threshold for the amplitude of a spike. Typically, the threshold is set as a multiple of the baseline noise level (Obien et al. 2015). Less common spike detection methods include two-point procedure and template-matching (Obien et al. 2015) Finally, spike sorting is the process of assigning spikes to groups according to their shapes (Obien et al. 2015). Spike sorting can utilize different methods, such as principal component analysis (PCA) or wavelet transform (Obien et al. 2015). It should be noted that the filtering can alter the shape of a spike (Obien et al. 2015) and, therefore, the filtered signal should not be used for spike sorting. The spike timing information obtained in spike detection can be exploited to retrieve the shapes of the detected spikes from the original raw signal (Obien et al. 2015).

From the spike timing information, different features such as spike frequency can be calculated to describe and evaluate the electrical activity of the subject neuronal population. Spike timing information is also utilized in burst detection (Pasquale et al. 2010; Legendy, Salcman 1985; Kapucu et al. 2012). Bursts and burst detection algorithms are discussed in the following chapters. Spiking and bursting features, including total counts, are considered to constitute the foundation for the evaluation of electrical activity of a neuronal population (Kapucu et al. 2012). Additional and more complex activity features can be calculated to describe the network synchronization. The network synchronization features include network spikes, network bursts, cross-correlation and entropy (Gelfman et al. 2018).

2.6. Bursts

A burst is a set of subsequent spikes that are fired in close temporal proximity of each other. In other words, the burst spikes are fired at a relatively high frequency. Often a quiet period is observed after a burst (Obien et al. 2015). *In vivo,* spontaneous bursting is observed during development and bursts are associated with synapse formation and long-term potentiation (Kirwan et al. 2015; Cotterill et al. 2016). Postnatally, bursting generally does not occur spontaneously (Kirwan et al. 2015).

Bursts are considered to be information carriers of the brain, and are related to neural processes, such as motor pattern generation (Obien et al. 2015). *In vitro,* spontaneous bursting has been shown to increase during the development of synapses in cultured neuronal networks (Muramoto et al. 1993). Synchronized bursting is considered mature activity (Weick 2016). Bursts are preceded by simple spiking (Weick 2016; Heikkilä et al. 2009) and, provided with prolonged maturation time, followed by more complex activity patterns (Kirwan et al. 2015).

Bursts are a prominent component of the electrical activity patterns *in vitro*. Yet, there is no formal, global definition for a burst. Despite this, bursts are rather easily identified from a spike train by human eye. Bursts stand out as the spike frequency within a burst is typically higher than the overall spike frequency of the spike train. When trying to describe the essence of a burst more precisely, different parameters have been used. These parameters include maximum inter-spike interval within a burst (maxISI), minimum number of spikes in a burst (minSpikes), minimum duration of a burst (minDur), and minimum inter-burst interval (minIBI) (Figure 6). Still, use of parameters to define a burst is challenging due to the variability of bursting activity. Variability is displayed in neuronal networks derived from primary rat cortical neurons (Wagenaar et al. 2006) and even more so in networks derived from hPSCs (Kapucu et al. 2012; Heikkilä et al. 2009). Furthermore, the inter-spike intervals (ISIs) within a single burst vary as well. The spikes at the core of the burst have typically short ISIs whereas the spikes at the boundaries of a burst, also called burst-related spikes, have higher ISIs (Kapucu et al. 2012; Pasquale et al. 2010).

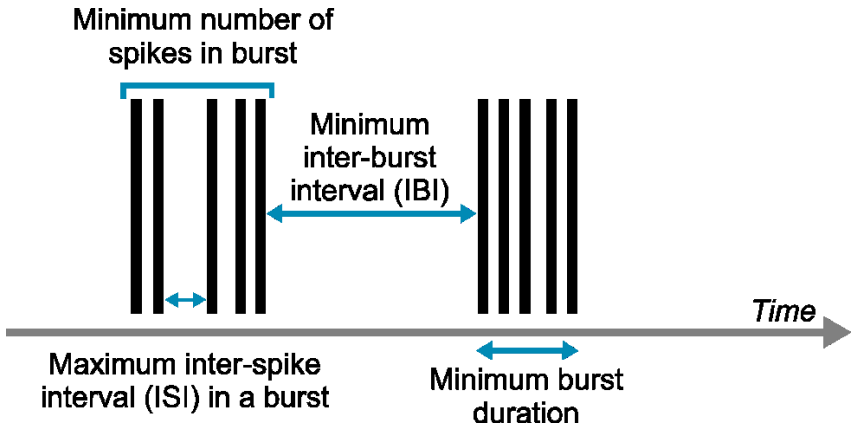

Figure 6. Parameters used to determine a burst *in vitro*. These parameters include maximum inter-spike interval in a burst (maxISI), minimum number of spikes in burst (minSpikes), minimum burst duration (minDur), and minimum inter-burst interval (minIBI). MaxISI in a burst is used to determine, which spikes could be included in a burst. MinSpikes and minDur set additional requirements for a burst. MinIBI is used to define, when two bursts should be detected as one.

Identification and characterization of bursting activity are crucial for the evaluation of neuronal network activity *in vitro* (Cotterill et al. 2016; Kapucu et al. 2012). The bursting activity has been described to emerge 1-2 months after the onset of neurogenesis on hPSC-derived neuronal networks (Kirwan et al. 2015; Heikkilä et al. 2009). On neuronal networks derived from primary rat neurons, the activity develops approximately after one week *in vitro* (Charlesworth et al. 2015). Burst features, such as burst duration or intra-burst ISI, have been reported to vary according to the maturation state of the networks (Heikkilä et al. 2009; Charlesworth et al. 2015). Analysis of bursting activity has been used in assessment of neuronal network development and maturation, impact of genetic variations, and influence of chemical manipulations (Cotterill et al. 2016; Weick 2016). As the subtypes of neurons differ in respect to electrical activity patterns, characterization of these patterns using burst features could also be used to identify subtypes in a culture (Mertens et al. 2016).

2.7. Burst detection algorithms

Although the analysis of bursting activity is a fundamental part when evaluating the neuronal network activity *in vitro*, there is no standard method or algorithm for bursts detection (Cotterill et al. 2016). The lack of a standard method could be partly due to the lack of a formal definition of a burst. Typically, burst detection algorithms have been developed and verified on an ad hoc basis for a certain type of data (Cotterill et al. 2016). This can be problematic because the bursting activity is widely variable. While a standardized burst detection algorithm is non-existent, visual identification of bursts is still used as a widely accepted method for burst detection despite the fact that it is not an objective nor an optimal method.

2.7.1. General principles of burst detection algorithms

Majority of burst detection algorithms utilize spike timing information to calculate bursts. These algorithms can typically be divided into three categories based on their mode of function (Cotterill et al. 2016). Two of these modes of function are based on use of parameters that define a burst, such as maxISI or a minSpikes. The algorithm can either use predefined, fixed parameters that are constant for all spike trains (Nex Technologies 2014; Chiappalone et al. 2005), or it can use parameters that are individually adjusted according to the properties of each spike train, such as distribution of ISIs (Pasquale et al. 2010; Kapucu et al. 2012). The adjustments to parameters are computed within the algorithm. The third mode of function is drastically different as it is surprise-based. The algorithm does not rely on burst-defining parameters but calculates a surprise statistic for a set of spikes (Legendy,

Salcman 1985). If the surprise statistic is above a predefined threshold, the spike set is considered a burst. More precisely, the algorithm searches for deviations from an assumed underlying spike frequency distribution (Cotterill et al. 2016).

Each of these modes of function have their advantages and disadvantages. Algorithms using predefined parameters are very consistent as identical parameters are used for all spike trains. However, the variability of bursting activity is a challenge for them (Pasquale et al. 2010; Kapucu et al. 2012). Burst features such as spike frequency in burst are variable (Pasquale et al. 2010) and can also be very different between cultures derived from different species. To solve this issue, self-adaptable methods have been developed (Pasquale et al. 2010; Kapucu et al. 2012). Adjusting the parameters individually for each spike train can allow detection of a wider variety of bursts. However, these methods are not as consistent. A spike set of a specific spike frequency can be detected as individual spikes or as a burst depending on the mean spike frequency or other properties of the spike train. This is often desirable but can also cause problems in some types of data. Nevertheless, self-adapting methods are typically deterministic as the same bursts are detected on repeated runs on the same data (Cotterill et al. 2016). Use of parameters, whether pre-defined or adjusted, could be considered artificial or excessively restricting though, especially when there is no formal definition for a burst. Although surprise-based methods might also utilize some parameters, they rely more strongly on statistics for burst detection. Assuming that the activity follows a fixed statistical distribution, however, can be considered erroneous as the bursting and even non-bursting activity is very variable and thus the underlying distributions are also variable. There is no consensus on a single statistical distribution that would best represent the whole of the variety of spiking and bursting activity (Cotterill et al. 2016). A similarly erroneous idea encountered in parameter-based and surprise-based algorithms alike is to presume a limit for the maximum proportion of spikes in a spike train that can be included in bursts (Cotterill et al. 2016; Hennig et al. 2011; Gourévitch, Eggermont 2007). This restricts the application of the algorithm to specific type of data because in some spike trains practically all spikes can be located within bursts.

Many of the burst detection algorithms are more or less variations of each other (Cotterill et al. 2016). Nevertheless, other modes of function exist along the three modes described above. One interesting example is utilizing hidden semi-Markov model (HSMM) (Tokdar et al. 2010), which is a statistical model for stochastic processes and is also used to find genes from DNA sequences. A nucleotide in a DNA sequence can be located either in or out of a gene and similarly a spike in a spike train can be located either in or out of a burst. The performance of HSMM method is, however, not deterministic in burst detection (Cotterill et al. 2016). Another example

is to use channel synchrony to detect bursts (Wagenaar et al. 2006). This method only allows detection of bursts after the emergence of synchronicity however.

2.7.2. Comparison of burst detection algorithms

When evaluating and comparing the performance of burst detection algorithms, visually identified bursts have been used as a standard (Cotterill et al. 2016; Pasquale et al. 2010). Due to the lack of a formal burst definition and a standard burst detection method, there are no better alternatives for the evaluation of algorithm performance. Besides biological data burst detection algorithms have been tested on synthetic data (Cotterill et al. 2016). Synthetic bursts and parameters defining them are determined by the designer and thus also the synthetic bursts are a man-made standard. Use of synthetic data is an efficient way to validate algorithm function. Distinct synthetic spike trains with known activity and bursting properties can be designed to test specific aspects of the algorithm performance and a large data set can be constructed in a relatively short time (Cotterill et al. 2016). Nevertheless, designing synthetic spike trains that would well represent the biological activity patterns requires expert knowledge of the properties, such as an ISI distribution of a spike train or a typical intra-burst ISI, of distinct activity patterns.

In their study in 2016, Cotterill et al. (Cotterill et al. 2016) suggested a list of desired features for an ideal burst detection algorithm. These features included 1) good performance in different activity patterns, 2) deterministic behavior, 3) small number of adjustable parameters, 4) having no assumption of spike train distribution, and 5) reasonable computational time. Good performance in different activity patterns is a basic requirement. Deterministic behavior was required so that same bursts would be identically detected on repeated runs. A small number of adjustable parameters was preferred because this reduces variability of results introduced through parameter choice. Assumption of a distribution was deemed disadvantageous as it restricts applicability to a limited range of activity patterns. Reasonable computational time was desirable because MEA applications often produce great amounts of data.

Based on these evaluation criteria, Cotterill et al. (Cotterill et al. 2016) compared the performances of eight burst detection algorithms. The eight algorithms were selected as representatives of the major contemporary approaches to detect bursts. The performance of the algorithms was tested on synthetic data and biological data. The performance on biological data was evaluated based on the coherence between the algorithm results and the bursts detected by human eye. First, the algorithm performances were evaluated on synthetic data and MEA data from spontaneously

firing mouse retinal ganglion cells. Four most promising algorithms, namely MI, PS, logISI and CMA methods, were further tested using MEA data from spontaneously firing hiPSC-derived neuronal networks. Although no ideal algorithm was found, MI and logISI showed the most promise. Both had an overall high performance on different activity patterns. In regard to other four desirable features, MI possessed three and logISI all four of them. MI did not possess feature 3 as it has five adjustable parameters. Of the two algorithms, MI was reported to have a better average correspondence to visually identified bursts on hiPSC-derived neuronal networks. Consequently, MI was recommended as a first choice when selecting a burst detection algorithm. LogISI, PS and CMA were recommended in case that appropriate parameters for MI could not be determined. LogISI was suggested to be used when the lengths of intra-burst ISIs were clearly distinct from the lengths of inter-burst intervals (IBIs). PS and CMA were recommended if there was no such distinction. All in all, utilization of multiple burst detection methods and comparison of their results was considered to be the most robust approach.

2.7.3. Principles of MaxInterval, Poisson surprise, logISI and Cumulative moving average methods

The four burst detection algorithms that provided highest performance in the comparative study by Cotterill et al. (Cotterill et al. 2016) were MI, PS, logISI and CMA. In this chapter, principles of these algorithms are explained in detail.

MaxInterval. MaxInterval (MI) method was developed by Nex Technologies in 2014 (Nex Technologies 2014). The method utilizes ISIs of a spike train to detect bursts. A burst is determined by five predefined parameters: maximum beginning ISI (begISI), maximum ending ISI (endISI), minIBI, minSpikes, and minDur. A burst must fulfill all five conditions. First, the algorithm scans a spike train until an ISI ≤ begISI is found. This marks the beginning of a burst. Each following ISI < endISI is included in the burst. If an ISI ≥ endISI is encountered, the burst is ended. After going through all ISIs, the bursts with a distance smaller than minIBI are merged. Finally, the bursts, for which duration is smaller than minDur or a spike number is smaller than minSpikes, are discarded.

Poisson surprise. Poisson surprise (PS) method was introduced by Legendy et al. already in 1985 (Legendy, Salcman 1985). It was developed on *in vivo* data recorded from cat striate cortex. PS is a statistic method, which evaluates the probability of a burst being a chance occurrence. Thus, it is a surprise-based method. PS assumes that the baseline spike frequency in a spike train follows a Poisson distribution with spike frequency *f*, which is set equal to the mean spike frequency over the spike train. First,

the algorithm scans a spike train for three sequential spikes with ISIs that are both smaller than $ISI_{mean}/2$. The found three spikes are considered as an initial burst. The following spikes are added to the initial burst until an ISI > $2*ISI_{mean}$ is found. Next, a Poisson surprise statistic *S* is calculated for bursts containing different number of spikes starting from three spikes and terminating to the total number of spikes within the initial burst. The Poisson surprise statistic is defined as

$$S = -\log(p)$$

where *p* is the probability of *n* or more spikes randomly occurring in a time interval of length *T* in the underlying Poisson distribution. The *p* is defined by Poisson formula as

$$p = \mathrm{e}^{-\mathrm{fT}} \sum_{i=n}^{\infty} (fT)^i / i!$$

where *f* is the mean spike frequency in a spike train, *T* is a length of a time interval, and *n* is a number of spikes occurring in this time interval.

S is calculated for every possible sequential set of spikes. The burst with the highest surprise is selected, and if the surprise and the number of spikes in the burst are both greater than the respective threshold values, the burst is added to the burst list.

LogISI. LogISI method was developed by Pasquale et al. in 2010 on rat cortical neuronal networks (Pasquale et al. 2010). The algorithm was based on earlier methods, which utilize two predefined parameters for burst detection, namely maxISI and minSpikes (Chiappalone et al. 2005; Turnbull et al. 2005). LogISI algorithm combined this methodology with a method developed by Selinger et al. (Selinger et al. 2007), which resulted in a self-adaptable method. The algorithm utilizes log-adjusted ISI histogram to compute ISI threshold (ISIth) for intra-burst ISI and detects bursts based on this threshold. First, the algorithm computes a histogram of log-adjusted ISIs of a spike train. Peaks in the histogram are detected. If the value of a point is higher than both of its neighbors, it is considered a peak. Minimum distance of two peaks has to be more than two points. A peak corresponding to the maximum frequency within a defined time window is found and selected to represent the most probable ISI intra-burst ISI. Typically, the cutoff for the time window is 100 ms, which is an empirical value determined by the authors. The intra-burst peak is paired with all the following peaks, the minimum between each peak pair is found, and a void parameter is calculated for each pair. The void parameter describes the level of separation of a peak pair. The void parameter is defined as

$$void = 1 - \frac{g(minimum)}{\sqrt{g(peak_1)g(peak_2)}}$$

where *g(x)* is the distribution of $x = \log(ISI)$. When *g(minimum)* = 0, the void parameter is 1 and the peaks are well separated. When $g(minimum) = \sqrt{g(peak_1)g(peak_2)}$, the void parameter is 0 and the peaks are not separated.

Next, the algorithm checks whether any of the calculated void parameters exceeds the threshold, which is typically set to 0.70, an empirical value determined by the author. If a void parameter greater than the threshold is found, the ISI corresponding to the minimum between the peak pair is chosen as the ISIth.

Finally, the algorithm uses the ISIth to define bursts in the spike train. There are three possible paths for burst detection and the selection of a path depends on the calculated value of ISIth. Path 1 is selected if ISIth is smaller than 100 ms. In this case, subsequent spikes with ISI < ISIth are assigned into a burst.

Path 2 is selected if ISIth is greater than 100 ms. Here, more steps are needed for burst detection. Besides the calculated ISIth, a predefined default maxISI is used. First, the subsequent spikes with ISI < maxISI are assigned into a burst. After finding all the bursts with this condition, the spikes at the boundaries with ISI < ISIth are added to the bursts. Additionally, the algorithm merges bursts if the time between them is smaller than ISIth.

Path 3 is selected if the algorithm fails to find a void parameter or if the derived ISIth is higher than acceptable (> 1 s). In this case, the predefined default maxISI is used to detect bursts. The subsequent spikes with ISI < maxISI are assigned into a burst. This backup strategy is not very elegant but is necessary to provide some tolerable burst detection with challenging data and in case of failure of the more precise algorithm. If even an intra-burst peak is not found, the spike train is considered non-bursting and burst detection is not performed.

Cumulative moving average. Cumulative moving average (CMA) method was developed by Kapucu et al. in 2012 on developing hESC-derived neuronal networks (Kapucu et al. 2012). The algorithm utilizes CMA of an ISI histogram to determine separate ISIths for burst cores and burst-related spikes. CMA of an ISI histogram presents the cumulative average spike count up to a particular ISI. It highlights long-term trends while suppressing short-term fluctuations. Majority of the intra-burst ISIs are expected to be located at the proximity of the maximum value of the CMA, CMA_m. To find this maximum, CMA is calculated for each bin of the ISI histogram. CMA of *I*th ISI bin is defined as

$$CMA_I = \frac{1}{I}\sum_{i=1}^{I} n_i$$

where n_i is the number of spikes in the *i*th ISI bin. CMA_m is reached at the *m*th ISI bin, which is calculated as

$$m = \underset{k=1,\ldots,N}{\arg\max} \left(\frac{1}{k}\sum_{i=1}^{k} n_i\right)$$

where *N* is the total number of ISI bins and n_i is the number of spikes in the *i*th ISI bin.

Next, skewness of the ISI distribution is calculated to determine factors α_1 and α_2. The skewness intervals and corresponding α-factors were empirically determined by the authors. The longer the tail of the distribution is, the further intra-burst ISIs can be expected to be from the peak value of the histogram. Therefore, large skewness results in larger ISIths. The ISI bin which is located after *m*th ISI bin and for which the value of CMA curve is closest to $\alpha_1 * CMA_m$ is identified, and the mid time point of this ISI bin is set as ISIth for burst cores, ISI_1. Similarly, $\alpha_2 * CMA_m$ is applied to find ISIth for burst-related spikes, ISI_2. Now, subsequent spikes with ISI < ISI_1 are defined as burst cores. Burst-related spikes with an ISI < ISI_2 are added to the burst. Also, two bursts are merged if the time between them is less than ISI_2.

3. Materials and Methods

3.1. Ethical issues

The hESCs used in this work were derived at BioMediTech, Tampere University, Finland. BioMediTech has received approval from the Finnish Medicines Agency (FIMEA) for use of human embryos in research (Dnro 1426/32/300/05). Supportive statements for the derivation, culture and differentiation of hESCs (R05116) have been received from the regional ethics committee of Pirkanmaa Hospital District.

The experiments using primary rat cortical neurons were carried out according to institutional guidelines (University of Helsinki internal license number: KEK17-016).

3.2. Human stem cell culture and cortical neuronal differentiation

3.2.1. Human embryonic stem cell culture

hESC line Regea 08/023 (feeder-free passage 6) was used to produce human neuronal networks. The hESC line has been characterized earlier (Skottman 2010). To maintain the hESC line, hESCs were cultured on top of human foreskin fibroblast feeder cell layer in Dulbecco's modified Eagle's medium (DMEM, Thermo Fisher Scientific), which contained 20% KnockOut Serum Replacement (Thermo Fisher Scientific). This maintenance protocol has been described previously by Rajala et al. (Rajala et al. 2007). To expand the hESCs before neuronal differentiation, the hESCs were transferred to a feeder-free system where they were cultured on recombinant human laminin-521 (LN521, Biolamina, Sweden) in E8 medium (Thermo Fisher Scientific). The expansion culture has been described previously by Hongisto et al. (Hongisto et al. 2017). The pluripotency of the hESC line was monitored regularly. The hESCs were stained for pluripotency markers Nanog, Oct-3/4, SSEA-4, TRA-1-81 and TRA-1-60, and the capacity to produce different germ layers was examined in EB assay by staining for α-smooth muscle actin, α-fetoprotein and Nestin.

3.2.2. Cortical neuronal differentiation

hESCs were detached using TrypLE Select (Thermo Fisher Scientific). The detached cells were plated at density of $5x10^5$ cells/cm^2 on plates coated with poly-L-ornithine (PO, Sigma-Aldrich) and LN521 in E8 medium, which contained 10 μM ROCK Inhibitor (Y-27632, Sigma-Aldrich). After 24 hours, medium was changed to plain E8 medium.

The next day, neuronal differentiation was started. The following cortical neuronal differentiation was performed with a protocol modified from Shi et al. (Shi et al. 2012). The protocol included periods of induction, proliferation and final maturation. For each stage, a distinct medium was used. In these mediums, neural maintenance medium (NMM) was used as a basal medium. NMM consisted of 1:1 DMEM/F12 with Glutamax and Neurobasal, 0.5% N2, 1% B27 with Retinoic Acid, 0.5 mM GlutaMAX, 0.5% NEEA, 50 µM 2-mercaptoethanol (all from Thermo Fisher Scientific), 2.5 µg/ml Insulin (Sigma-Aldrich) and 0.1% penicillin/streptomycin (Thermo Fisher Scientific). During the following cultures, the cells were passaged using StemPro Accutase (Thermo Fisher Scientific), and 10 µM ROCK Inhibitor was added to the medium when plating and removed after 24 hours. Otherwise, the medium was changed every day during neural induction period and every two to three days during proliferation and final maturation periods. At all times, 100% of the medium was changed. The cells were kept at 37 °C in 5 % CO_2 atmosphere and 95 % humidity.

During a 12-day neural induction, NMM supplemented with 100 nM LDN193189 and 10 µM SB431542 (both from Sigma-Aldrich). On day 12, the cells were passaged and plated at density of $2.6x10^5$ cells/cm^2 on plates coated with PO and LN521. After 24 hours, the neural proliferation was started and the medium was switched to NMM supplemented with 20 ng/ml fibroblast growth factor-2 (FGF2, Thermo Fisher Scientific). Cells were passaged on day 17. On day 21, the cells used in this work were cryopreserved in the neural proliferation medium containing 10% dimethyl sulfoxide (DMSO, Sigma-Aldrich) and 10 µM ROCK Inhibitor. The cells were thawed and plated at density of $3.1x10^5$ cells/cm^2 on plates coated with PO and LN521. The cells were passaged on day 25 and plated at density of $2.6x10^5$ cells/cm^2 on plates coated with PO and LN521. On day 26, the final maturation was started and the medium was switched to NMM, which was supplemented with 20 ng/ml brain-derived neurotrophic factor (BDNF, R&D Systems), 10 ng/ml glial-derived neurotrophic factor (GDNF, R&D Systems), 500 µM dibutyryl cyclic adenosine monophosphate (db-cAMP, Sigma-Aldrich) and 200 µM ascorbic acid (AA, Sigma-Aldrich). On day 32, the cells were plated for experiments on ⌀ 13 mm glass coverslips, which were placed on 24-well plate, or on CytoView MEA 48-well plate. The coverslips were coated with PO and LN521, and the cells were plated at density of $5.4x10^4$ cells/cm^2. The MEA plate was coated with poly-ethylene-imine (PEI) and LN521, and the cells were plated at $1x10^6$ cells/cm^2.

3.3. Primary rat cortical neuronal culture

Cortex tissue was harvested from Wistar rat embryos on embryonic day 17-18 as described earlier by Sahu et al. (Sahu et al. 2019). The cells were plated on ⌀ 13 mm glass coverslips, which were placed on 24-well plate, or on CytoView MEA 48-well plate. Both the coverslips and the MEA plate were coated with poly-D-lysine (PDL, Sigma-Aldrich). The cells were plated at density of $7.53x10^4$ cells/cm^2 on the coverslips and at $2.9x10^5$ cells/cm^2 on the MEA plate. The culture medium consisted of Neurobasal, 2% B27, 2 mM GlutaMAX, and 1% penicillin/streptomycin (all from Thermo Fisher Scientific). 50% of the medium was changed every two to three days until the day before pharmacological assays.

3.4. Microscopy and immunocytochemistry

3.4.1. Phase-contrast microscopy

During culturing, the cells were imaged with phase-contrast microscope to evaluate the morphology of the cells and to monitor the adherence of cells. Imaging was performed once a week using either Nikon Eclipse Ti with Nikon digital sight DS-Fi2 camera and NIS-Elements F 4.30.00 64-bit software (Nikon, Tokyo, Japan) or Zeiss Axion Observer.A1 with Axiocam 506 color camera and ZEN2 software (blue edition) (Carl Zeiss, Jena, Germany).

3.4.2. Immunocytochemical staining

Human neuronal cultures on the coverslips were fixed four weeks after final plating (61 days after the onset of neurogenesis) and rat neuronal cultures on the coverslips after three weeks (22 days) *in vitro*. The protocol has been described earlier (Lappalainen et al. 2010). The cells were washed with Dulbecco's phosphate-buffered saline (DPBS, Lonza), after which they were fixed in 4% paraformaldehyde (PFA, Sigma-Aldrich) for 15 minutes at room temperature (RT). The cells were again washed with DPBS. The fixed cells were stored at 4 °C in DPBS until stainings. For stainings, the cells were first incubated in a blocking solution containing 10 % normal donkey serum (NDS, Biowest), 0.1 % Triton-X Sigma-Aldrich and 1% bovine serum albumin (BSA, Sigma-Aldrich) in DPBS for 45 minutes. The cells were washed with primary solution containing 1% NDS, 0.1 % Triton-X and 1 % BSA in DPBS. Next, the cells were incubated with primary antibodies in the primary solution at 4 °C overnight. The primary antibodies comprised β_{III}-tubulin (chicken, 1:100, Abcam: ab107216),

microtubule-associated protein 2 (MAP2, rabbit, 1:100, Millipore: AB5622), PSD95 (mouse, 1:50, Abcam: ab2723), S100β (mouse, 1:100, Abcam: ab11178), and synaptophysin (rabbit, 1:100, Abcam: ab32127). On the following day, the cells were washed twice with secondary solution consisting of 1% BSA in DPBS. The cells were then incubated with secondary antibodies in the secondary solution for one hour at RT. The secondary antibodies comprised of Alexa Fluor 488 (1:200), Alexa Fluor 568 (1:200) or Alexa Fluor 647 (1:200) dyes (all from Thermo Fisher Scientific). Next, the cells were incubated with 4',6-Diamidino-2-Phenylindole, Dihydrochloride (DAPI, 1:1000, Thermo Fisher Scientific) in DPBS for five minutes. The cells were washed first with DPBS and then with phosphate buffer (PB). After drying, the cells were mounted with ProLong™ Gold Antifade Mountant with DAPI (Invitrogen) and stored at 4 °C until imaging. The cells were imaged using Olympus IX51 microscope with Olympus DP30BW camera (Olympus Corporation, Hamburg, Germany) and LSM780 Laser Scanning Confocal Microscope with Quasar spectral GaAsP detector (Carl Zeiss, Jena, Germany).

3.5. Microelectrode array recordings

MEA data was recorded with Axion Maestro system that is controlled by AxIS Software (Axion Biosystems, Atlanta, GA, USA). The sampling rate used in all MEA recordings was 12.5 kHz. Temperature was set to 37°C for all recordings. For pharmacological assays, also 5% CO_2 atmosphere was set due to a long recording time.

Ten-minute recordings of the spontaneous electrical activity of the cell cultures were recorded twice a week until cultures were used for pharmacological assays. The pharmacological assays for the human culture were performed after four weeks on MEA (61 days after the onset of neurogenesis). For the rat culture, the pharmacological assays were performed after three weeks (22 days) on MEA. Day prior to the assays, 100% of the medium was removed and an identical amount of fresh medium was added to each well. In the pharmacological assays, electrical activity patterns were altered by treatment with reagents including GABAergic agonist GABA (10 μM, Sigma-Aldrich), AMPA/kainate receptor antagonist 6-cyano-7-nitroquinoxaline-2,3-dione (CNQX, 50 μM, Abcam), NMDA receptor antagonist D-(-)-2-amino-5-phosphonopentanoic acid (D-AP5, 50 μM, Sigma-Aldrich), $GABA_A$ antagonist gabazine, also known as SR95531 (30 μM, Sigma-Aldrich), and kainate receptor agonist kainic acid (KA, 5 μM, Sigma-Aldrich). All neuromodulators were added into distinct wells in identical amount of final maturation medium. On control wells, an identical amount of final maturation medium was added without any

reagent. On human culture, four wells were treated by each reagent and four wells were used as control. On rat culture, seven wells were treated by each agent and six wells were used as control. Additionally, sodium channel blocker tetrodotoxin (TTX, 1 μM, Tocris) was used to validate the biological origin of the activity. TTX was added to two wells of each treatment and at least to two control wells. Before the addition of the neuromodulators, the baseline activity was recorded for 30 minutes. The electrical activity influenced by the neuromodulators was similarly recorded for 30 minutes. The activity affected by TTX was recorded for 10 minutes.

The data selected for burst detection analysis were re-recorded from the recordings described above.

3.6. Microelectrode array data analysis

Spike detection was performed with an in-house Matlab script (The MathWorks Inc., Natick, MA, United States, version 2018a) based on amplitude thresholding (Kapucu et al. 2012; Quiroga et al. 2004). To allow detection of significant transitions observed during the development of the spontaneous activity, inactive electrodes were excluded from the spontaneous activity data. An electrode was considered inactive if its spike frequency was < 0.17 Hz (10 spikes per minute). The same condition was applied for the baseline recordings of the pharmacological assays but not for the recordings of neuromodulator-induced activity. Only the electrodes that were considered active in the baseline recordings were included in the analysis of pharmacological data.

No conditions were set for the spike frequency on data selected for burst detection analysis.

3.7. Performance analysis of burst detection algorithms

3.7.1. Data selection

The data selection was conducted so that the data set represented all activity patterns observed in spontaneous activity and pharmacological assays. No synthetic data was used in this work as a recent study of Cotterill et al. (Cotterill et al. 2016) had analyzed the performance of burst detection algorithms on synthetic data.

3.7.2. Visual burst detection

Bursts were visually observed from the raw MEA signal. A custom-made Matlab script was used to generate a plot that allowed zooming of the raw signal. The timing of the bursts was recorded at the scale of 10 ms. During visual burst identification, a burst was required to include at least five spikes. The bursts were given identity of either a definite burst or a possible burst. When doubting whether a spike set was a possible burst or not a burst at all, the ISIs within the spike set were inspected and approximately 100 ms was considered as an acceptable ISI in this kind of a possible burst.

3.7.3. Burst detection algorithms

The performance of four algorithms was investigated. The four algorithms chosen for the analysis had shown most promise in a study conducted by Cotterill et al. (Cotterill et al. 2016). The analysis was performed with a custom-made R script (The R Foundation for Statistical Computing, Vienna, Austria, version 3.5.1). Especially the R package meaRtools (Gelfman et al. 2018) was applied in the script. The burst detection algorithms were accessed from a publicly available source at https://github.com/ellesec/burstanalysis, where they had been loaded by Cotterill et al. (Cotterill et al. 2016). A single modification was made to the code of the CMA method to fix an erroneous calculation of mean ISI in burst.

For the initial performance analysis, minSpikes was set to 3 for all the algorithms. Rest of the parameter values were set according to the original values used by the authors with a single exception (Table 1). For PS, the threshold for surprise statistic was set to ~4.6 to allow comparison with the results of the study by Cotterill et al. (Cotterill et al. 2016). The surprise thresholds used by Legendy et al. were 10 and 20 (Legendy, Salcman 1985). The threshold used in this work is lower than the originals and, therefore, the result will include more bursts than it would using the original thresholds.

Table 1. Default parameter values for initial burst detection analysis. The pre-defined parameters and their values are presented for each of the four algorithms included in the performance analysis. The parameter values for the initial performance analysis were set according to the original authors except for the minimum surprise statistic used in PS algorithm.

Algorithm	Parameter	Value
MaxInterval	Maximum beginning ISI	0.17 s
	Maximum ending ISI	0.3 s
	Minimum IBI	0.2 s
	Minimum number of spikes	3
	Minimum burst duration	0.01 s
Poisson surprise	Minimum surprise statistic	-ln(0.01) ~4.6
	Maximum beginning ISI	ISImean/2
	Maximum ending ISI	ISImean*2
	Minimum number of spikes	3
LogISI	Maximum cutoff for time window	0.1 s
	Minimum void	0.70
	Default maximum ISI	0.1 s
	Minimum number of spikes	3
Cumulative moving average	Minimum number of spikes	3
	$\alpha 1$ and $\alpha 2$	1.0 and 0.5 if skew < 1
		0.7 and 0.5 if 1 ≤ skew < 4
		0.5 and 0.3 if 4 ≤ skew < 9
		0.3 and 0.1 if 9 ≤ skew

3.7.4. Evaluation criteria for the algorithm performance

Each algorithm was given a score based on two aspects of its performance. First, the result of each algorithm was compared with the result of the visual inspection. Second, the result of each algorithm was compared with the results of other algorithms. The scoring criteria was as follows:

0) *Failure*: Many bursts are missed, or many false bursts are detected.
1) *Satisfactory performance*: Majority of bursts are detected but not necessarily reasonably timed. False bursts are not excessive.
2) *Good performance*: Majority of bursts are detected and reasonably timed. False bursts are rare.
3) *Excellent performance*: All or nearly all bursts are detected and reasonably timed. Very few false bursts are detected, or none.

To allow revelation of subtle differences between algorithms performances, the average level of algorithm performances was used to adjust the accepted level of excess or scarcity of false bursts as well as the accuracy requirements for the timing of bursts separately for each spike train.

For quantitative and objective evaluation, sensitivity and specificity were calculated for each algorithm for each spike train. The calculations were based on the visually observed identities of spikes. A time period of 10 ms was added to both ends of a burst to compensate for the limited accuracy of visual observation. If a spike was located within a definite burst in the visual inspection, it was considered a burst spike. If a spike was outside of bursts in the visual inspection, it was considered an individual spike. If a spike was located within a possible burst in the visual inspection, it was excluded from the calculations because both identities were accepted for this spike. The sensitivity states the probability of the algorithm detecting true burst spikes. The sensitivity was calculated as

$$sensitivity = \frac{true\ burst\ spikes}{true\ burst\ spikes + false\ individual\ spikes}$$

If no bursts were observed in a spike train, sensitivity could not be calculated. The specificity describes the probability of the algorithm avoiding detection of false burst spikes. Specificity was calculated as

$$specificity = \frac{true\ individual\ spikes}{true\ individual\ spikes + false\ burst\ spikes}$$

3.8. Statistics

The effect of pharmacological reagents on spike frequency was investigated by testing whether the relative change in spike frequency (RC_f) was different on an electrode under the influence and on an uninfluenced electrode. RC_f for a single electrode was calculated as

$$RC_f = \frac{f(influence)}{f(baseline)} * 100$$

where *f(influence)* is spike frequency after addition of reagent or normal medium and *f(baseline)* is spike frequency of the baseline recording. Normal distribution was tested with Shapiro-Wilk's test. As the data of most test groups did not follow normal distribution, the difference was tested for using Kruskal-Wallis' test. Multiple comparisons were performed using Steel with control. Significance level was set to 0.05. Median, lower (Q1) and upper quartiles (Q3) were shown as descriptive statistics. Statistical analyses were performed using JMP (SAS Institute Inc., Cary, NC, USA, version 13.1.0).

4. Results

4.1. Neuronal differentiation and synaptogenesis

Immunocytochemical staining showed that both the hPSC-derived and primary rat cortical neuronal networks included neurons and astrocytes (Figure 7A). In both cultures, the neurons and astrocytes developed an appropriate morphology similar to their counterparts *in vivo.*

4.1.1. Human pluripotent stem cell-derived neuronal networks

The hPSC-derived neuronal cells attached well in the final plating. During the culture, some aggregation was observed but the cells did not form detached aggregates. The behavior was similar on glass slips and on MEA plate. The neurons had a compact soma and thin long processes, which assembled in cable-like formations (Figure 7A). Majority of the astrocytes were star-shaped with a less compact soma and short processes. Both the presynaptic synaptophysin and the postsynaptic PSD95 were present in the neurons and were co-localized suggestive of structural synapses (Figure 7B). The synapse formation indicates that the neurons developed electrophysiological functionality.

4.1.2. Primary rat neuronal networks

The primary rat cortical neurons attached well when plated. There was no notable aggregation during culture. The behavior was similar on glass slips and on MEA plate. The neurons had a compact soma and thin long processes, which in some neurons included a single process thicker than the others (Figure 7A). These thicker processes could be axons. The astrocytes were star-shaped and had a less compact soma and short processes, which were thicker and more numerous than the processes of neurons. The morphology of individual rat cells was more apparent than that of individual human cells as there was no aggregation in rat neuronal culture. Staining for synapses revealed a presence and a co-localization of synaptophysin and PSD95 (Figure 7B) indicating structural synapses. Staining for PSD95 was more abundant in rat neuronal culture in comparison to human neuronal culture.

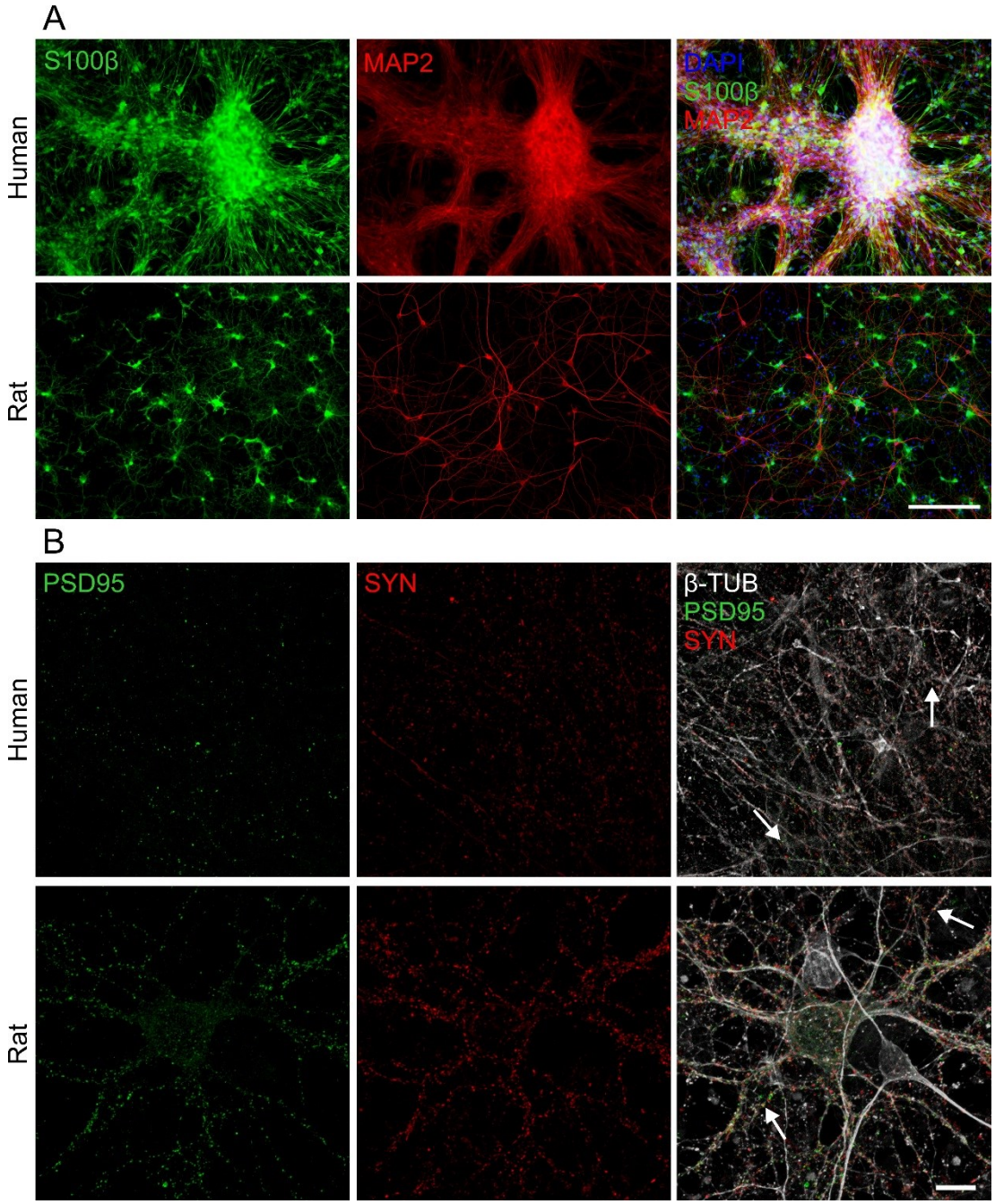

Figure 7. Morphology and synaptogenesis in human neuronal networks on day 61 and rat neuronal networks on day 22. A) The presence of astrocytes and neurons was confirmed by staining of astrocyte marker S100β (green) and neuron marker MAP2 (red), respectively. DAPI (blue) was stained to show the location of nuclei. Scale bar is 200 µm. B) The synaptogenesis of the neurons was confirmed by staining of the presynaptic marker synaptophysin (red) and the postsynaptic marker PSD95 (green). β-tubulin (white) was stained to elucidate the localization of synaptic markers on the neuronal processes. Synaptophysin and PSD95 were co-localized in both cultures, which is pointed out by arrows at two sites in the images of both human and rat networks. Scale bar is 10 µm.

4.2. Electrophysiological properties of neuronal networks

4.2.1. Development of spontaneous activity

In human neuronal networks, the spike frequency varied during the four weeks on MEA (Figure 8A). The activity was highest between time points of 14 and 21 days. The median spike frequency reached its peak value 1.35 Hz on day 21 but the increase to this point was not continuous. Afterwards, the median spike frequency decreased. The proportion of active electrodes over the plate increased continuously during the recordings. The proportion was 67.2% in the last recording of the spontaneous activity on day 28.

In rat neuronal networks, first activity was observed after 7 days on MEA (Figure 8A). There was a substantial increase in median spike frequency on day 10, after which the median decreased slightly until there was another great increase on day 21. Highest median spike frequency was 6.60 Hz on day 21. The proportion of active electrodes increased continuously until it reached 98.6% on day 17 on MEA. The proportion decreased to 85.0% on day 21.

4.2.2. Pharmacophysiology of neuronal networks

The relative changes in spike frequencies are presented per electrode in percentages for each reagent in Figure 8B. The median RC_f (Q1, Q3) on control electrodes was 102.45% (90.76, 112.52) on human culture and 93.12% (76.19, 104.68) on rat culture. GABAergic antagonist gabazine increased the spike frequency to 147.05% (112.41, 190.41; $p < 0.01$) in human neuronal culture but no statistically significant effect was observed in rat culture for which the median RC_f was 105.82% (68.38, 174.49; $p = 0.57$). GABAergic agonist GABA decreased the spike frequency to 43.73% (25.25, 65.99; $p < 0.01$) in human culture and to 0.00% (0.00, 0.04; $p < 0.01$) in rat culture. Interestingly, KA also decreased the spike frequency despite of being a glutamatergic agonist. The spike frequencies decreased to 38.67% (10.07, 84.43; $p < 0.01$) and 0.86% (0.04, 24.23; $p < 0.01$) on human and rat cultures, respectively. Glutamatergic antagonists CNQX and D-AP5 also decreased the spike frequency in both cultures. The decrease due to CNQX was to 27.97% (6.81., 40.84; $p < 0.01$) on human culture and to 9.96% (2.48, 49.18; $p < 0.01$) on rat culture. Corresponding decreases due to D-AP5 were 27.34% (15.03, 49.53; $p < 0.01$) and 6.02% (1.08, 17.73; $p < 0.01$). All median decreases were greater in rat culture than in human culture. TTX silenced all activity in both cultures. The number of electrodes included in each test group (N) in statistical analysis are reported in Appendix 1, Table A1.

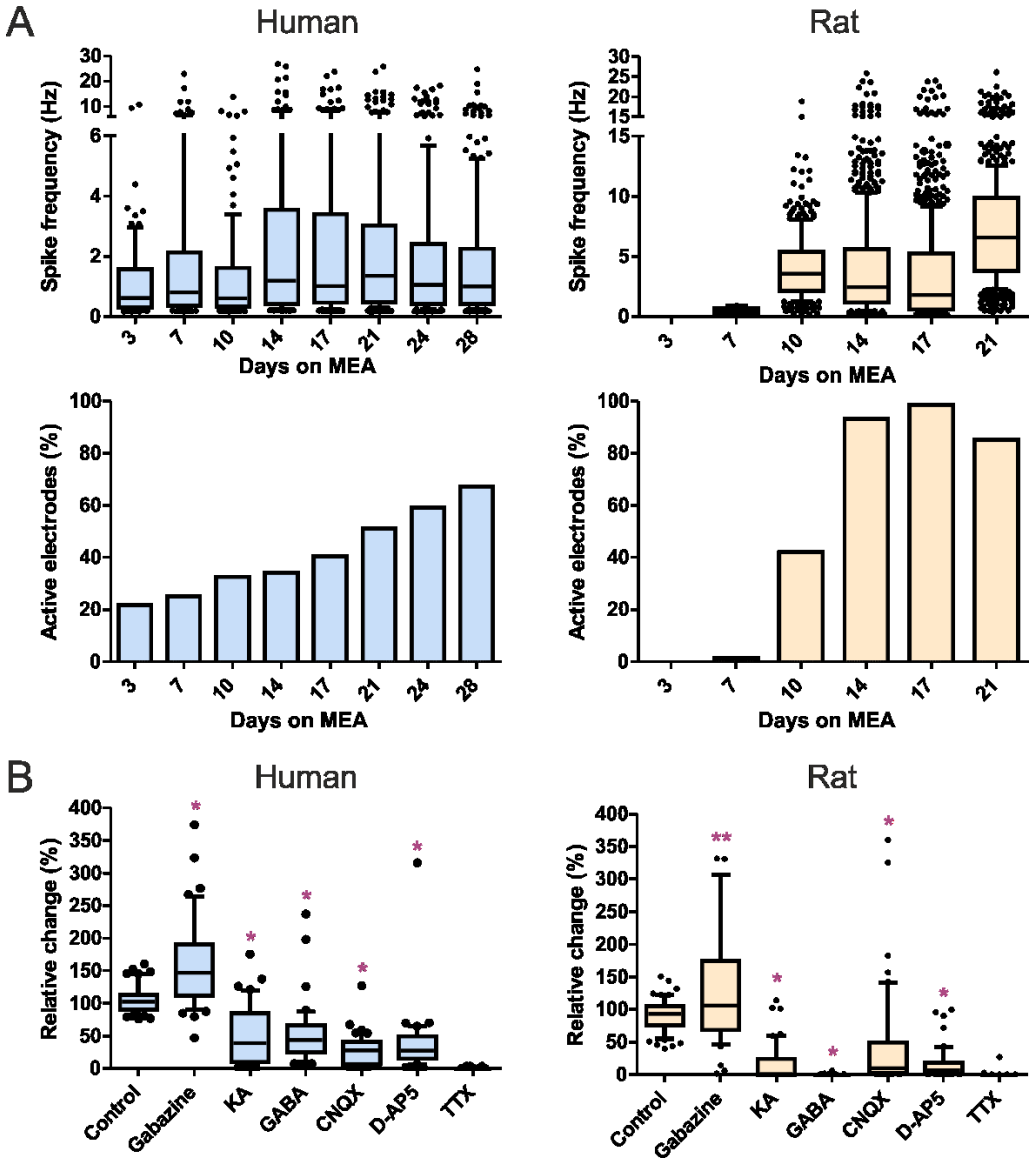

Figure 8. Electrical activity and pharmacophysiology of human and rat neuronal networks. A) The upper figures display spike frequencies of individual electrodes for active electrodes (spike frequency > 0.17 Hz) at different time points on MEA. The lower figures display the proportion of active electrodes on corresponding time points. Median is marked with a black line, the box reaches from Q1 to Q3, and the whiskers cover 80% of the data points. B) Neuromodulators influenced the spike frequency of human and rat neuronal networks. The relative change is shown per electrode as a percentage of the influenced activity of the baseline activity. The analysis included electrodes, which were active (spike frequency > 0.17Hz) during the baseline recording prior neuromodulator addition. The number of electrodes included in each test group (N) in statistical analysis are reported in Appendix 1, Table A1. Median is marked with a black line, the box reaches from Q1 to Q3, and the whiskers cover 80% of the data points. The y-axis of the plot displaying rat data has been cut to allow reasonable resolution of the effect. Three data points are located outside of the plot. *p < 0.01, **p = 0.57.

4.3. Data selection

The aim of the data selection was to produce a data set, which represented the various activity patterns identified during the development of spontaneous firing and in the pharmacological responses in both human and rat neuronal cultures. Regarding bursting activity, these patterns could be classified into four categories (cat.):

I) Non-bursting activity of low spike frequency
II) Non-bursting activity of high spike frequency
III) Bursting activity with noise
IV) Bursting activity with well-separated bursts

It should be remarked that even though occasional short bursts could be observed in Categories I and II, the activity cannot be called bursting due to the scarcity of bursts. It should also be noted that here, discussing burst detection, the noise mentioned in Category III refers to individual spikes outside of bursts.

The development of spontaneous activity followed along these categories over time. First, the spike trains displayed a low spike frequency. The spike frequency increased with time. Later, the bursting activity emerged. On some electrodes, the number of spikes outside of bursts decreased over time resulting in well-separated bursts. On few electrodes, however, well-separated bursts were observed very early. In human cultures, two types of bursts were observed: short bursts and long bursts, also called super bursts. In the raw MEA signal, the short bursts visually resembled blocks and the super bursts roughly resembled the shape of a hemisphere. In rat culture, only short bursts were observed.

The effects of neuromodulators to the spike frequency was presented in Chapter 4.2.1. The inhibiting modulators GABA, D-AP5 and CNQX resulted in low spike frequency patterns, generally without bursting activity (Cat. I). KA decreased spike frequency in both cultures. KA dispersed the bursts, which resulted in a high frequency pattern without bursting activity (Cat. II). The effect was especially distinct in human culture. Gabazine increased the spike frequency in both cultures. It was more remarkable, however, that gabazine concentrated the spikes into bursts. In other words, the number of spikes outside of bursts was decreased resulting in well-separated bursts (Cat IV). TTX eliminated all activity.

Overall, 14 two-minute spike trains of different activity patterns were selected for the burst detection analysis. Eight spike trains were from human culture and six spike trains from rat culture. Each category of activity patterns was represented in the

spike trains from both cultures. Additionally, the spike trains from human culture included both short and super bursts. Effect of each neuromodulator was also represented but not from both human and rat cultures. Only spike trains displaying the effect of gabazine were included from both cultures. Detailed information of the selected spike trains as well as their categories are collected in Table 4.3.1. Raw MEA signals, detected spikes and ISI distributions of four spike trains representing each category are shown in Figure 9. Same information for all selected spike trains is presented in Appendix 2, Figure A1.

Table 2. Spike trains selected for the burst detection analysis. The spike trains are ordered by category, which is displayed in the first column. The source organism and days on MEA are shown in the second and third column, respectively. A detailed description of the activity pattern is given in the fourth column. Spike count and spike frequency (Hz) are presented in the fifth and sixth column, respectively.

Category	Culture	Days on MEA	Description	Spike count	Spike frequency (Hz)
I	Human	29	D-AP5-inhibited activity	123	1.0
I	Human	29	GABA-inhibited activity	224	1.9
I	Rat	10	Immature, low frequency activity	113	0.9
I	Rat	22	CNQX-inhibited activity	279	2.3
II	Human	29	KA-induced high frequency activity	1360	11.3
II	Rat	10	Immature, high frequency activity	620	5.2
III	Human	14	Short bursts with noise	826	6.9
III	Human	28	Super bursts with noise	2288	19.1
III	Rat	17	Short bursts with noise	2442	20.4
IV	Human	7	Short bursts without noise	465	3.9
IV	Human	29	Gabazine-induced super bursts	462	3.9
IV	Rat	17	Short bursts without noise	2474	20.6
IV	Rat	22	Gabazine-induced short bursts	782	6.5
-	Human	29	TTX-inhibited activity	0	0.0

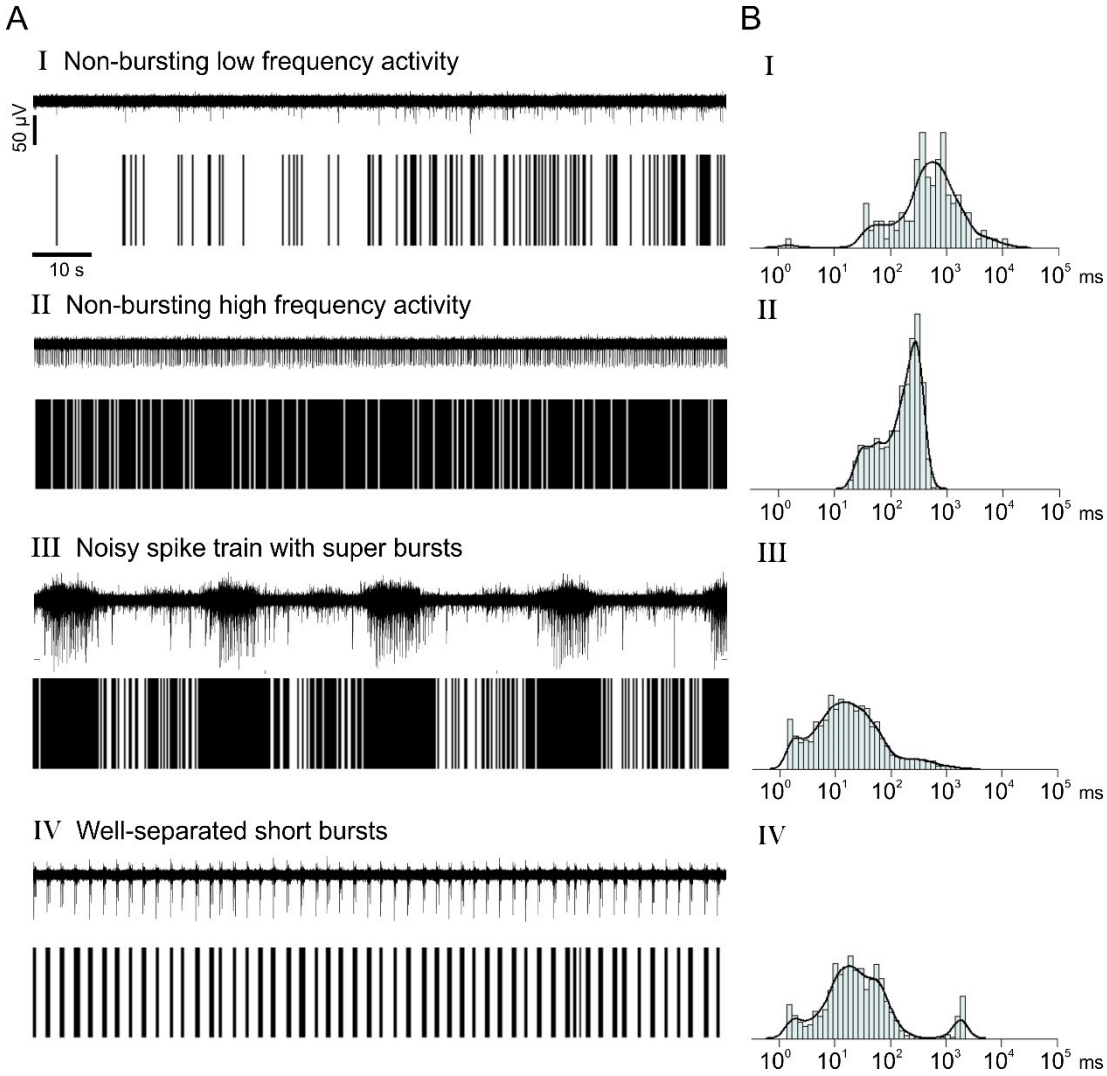

Figure 9. Raw MEA signals, detected spikes, and ISI distributions of four spike train representing activity pattern Categories I-IV. A) The activity patterns are visible from both the raw MEA signals and from the detected spikes. In Categories I and II, no bursts are present. The spikes appear at a low frequency in Category I and at a high frequency in Category II. In Categories III and IV, bursts are visible. In Category III, spikes can be seen between the bursts. The bursting activity pattern is referred as noisy as the identification of bursts can be challenging due to the spikes outside of bursts. In Category IV, no spikes appear outside of bursts. The bursts are well separated and easy to identify. Length of the raw MEA signal in the image is two minutes. Detected spikes are presented in the same time scale as the raw signal. B) The ISI distributions are presented as log-adjusted histograms. Kernel density estimate is displayed as a black line on top of the histograms. It is notable that majority of ISIs are above 100 ms in the non-bursting activity patterns and below 100 ms in the bursting activity patterns. The good separation of bursts in Category IV is apparent in the ISI distribution as the distribution is clearly divided into two parts. The part which is mostly located below 100 ms represents the ISIs within bursts, and the part mostly located above 1000 ms represents the IBIs.

4.4. Performance of burst detection algorithms

4.4.1. Algorithm performance with default parameter values

The initial burst detection was carried out using the default parameter values presented in Materials and Methods (Table 1). The overall performance of each algorithm is described below and illustrated for each activity pattern category in Figure 10A. Performance on all spike trains is illustrated in Appendix 3, Figure A2. The performance scores of each algorithm are presented for individual spike trains as well as for the overall performance in Table 3. The sensitivities and specificities for individual spike trains and their mean values are similarly presented in Table 4.

MI detected many false bursts in low frequency non-bursting activity (Cat. I). Some of these bursts were quite long (Appendix 3, Figure A2). On high frequency non-bursting activity (Cat. II), MI failed completely. It created a series of long bursts and placed most of the spikes into bursts (Figure 10A and B). The behavior was similar on noisy bursting activity (Cat. III) displaying rat bursts. MI was unable to distinguish bursts from mere high frequency activity. In noisy bursting activity (Cat. III) from human culture, MI detected many false bursts. Moreover, MI unnecessarily extended and, consequently, merged bursts. Nevertheless, the super bursts were detected well in both spike trains with and without noise, although few super bursts were split into two parts. The performance of MI was excellent also with the rest of the well-separated bursts (Cat. IV). Yet, its tendency to extend and merge bursts was apparent also on these spike trains.

Similar to MI, PS detected many false bursts in low frequency non-bursting activity (Cat. I), and some of the bursts were quite long (Appendix 3, Figure A2). On the contrary, PS outperformed on high frequency non-bursting activity (Cat. II). It detected no bursts in high frequency activity from rat culture (Figure 10A and B) and detected only very short bursts in KA-treated activity. In noisy bursting activity (Cat. III), PS typically detected only the core of the burst leaving out many spikes that should have been included. Additionally, PS missed many bursts in the noisy activity displaying human short bursts. The performance was very similar on activity displaying well-separated bursts (Cat. IV). The bursts were detected but not all burst spikes were included and, in the activity displaying human short bursts, many bursts were missed.

LogISI performed very well on low frequency non-bursting activity (Cat. I). The number of false bursts was small (Figure 10A and B). The performance was similar on high frequency non-bursting activity (Cat. II) from rat culture. However, logISI failed

on KA-treated activity as it found many false short bursts (Appendix 3, Figure A2). On noisy bursting activity (Cat. III), logISI performed very well although three issues emerged. First, some false bursts were detected. Second, only the cores of some short bursts were detected, which shortened the bursts. Third, many visually observed bursts were detected as multiple shorter bursts. In other words, logISI tended to split bursts into parts. Well-separated bursts (Cat. IV) were detected excellently, similar to MI. Some super bursts were split into parts. Contrary to its behavior on noisy bursting activity (Cat. III), logISI tended to extend and merge bursts on activity displaying well-separated human short bursts (of Cat. IV).

CMA detected many false bursts in most low frequency non-bursting activity (Cat. I). These bursts were typically short but on D-AP5-inhibited activity the bursts were quite long (Figure 10A and B). On high frequency non-bursting activity (Cat. II), CMA failed entirely. It detected many short and long bursts in KA-treated activity and included all the spikes into a single burst on un-treated high frequency activity (Appendix 3, Figure A2). The latter behavior was similar to the behavior of MI. On noisy bursting activity (Cat. III), CMA performed very well but had two of the same issues as logISI: some false bursts, and many split bursts. Well-separated bursts (Cat. IV) were detected excellently by CMA, as they were by MI and logISI. In fact, CMA outperformed other algorithms on human gabazine-treated activity displaying super bursts. The detection of short bursts was not as flawless though, as they were often split into parts.

There were two general issues that were not specific for any algorithm. The first issue was a presence of few bursts, which were visually confirmed but missed by the algorithms. It was noted that within the time frame of the visually observed burst the spike detection algorithm had recognized a fewer number of spikes than the human eye. The issue was left unsolved as it was not dependent on the performance of burst detection algorithms. The second issue was the opposite of the first issue. All the algorithms detected a great number of extremely short bursts, which were considered to be false bursts according to the visual observation. Due to their great numbers, the extremely short bursts had a tremendous effect on burst features derived from the detected bursts, such as burst duration or number of spikes in a burst. For example, on the noisy spike trains displaying super bursts, the median number of spikes in bursts was 5.0 or less for MI, PS and logISI and 9.5 for CMA (Figure 10B). To dispose of the insignificant findings, burst detection was conducted again with a single change in the parameter values: minSpikes was increased from 3 to 5.

4.4.2. Effects of increased minimum number of spikes

The increase of minSpikes enhanced the overall performance of all algorithms (Tables 3 and 4). The cause of this was a decreased number of false bursts (Figure 10Ca). Especially the performance on non-bursting low frequency activity (Cat. I) from rat culture was improved. On similar activity from human culture, only the performances of MI and logISI were considered to have improved.

Not all of the newly excluded bursts were false though. MI, logISI and CMA ended up missing some bursts that they had previously correctly detected (Figure 10Ca). This negative effect was observed on short bursts, but rarely. The effect was partly due to poor spike detection (Figure 10Cb). Furthermore, the bursts that had been split into parts, mostly by logISI and CMA, now lost the smallest of these parts. Still, the positive effect of the minSpikes increase was greater as the specificity of each algorithm increased or maintained its value on every spike train with a single exception – the specificity of PS on noisy spike train displaying rat bursts decreased by 0.01.

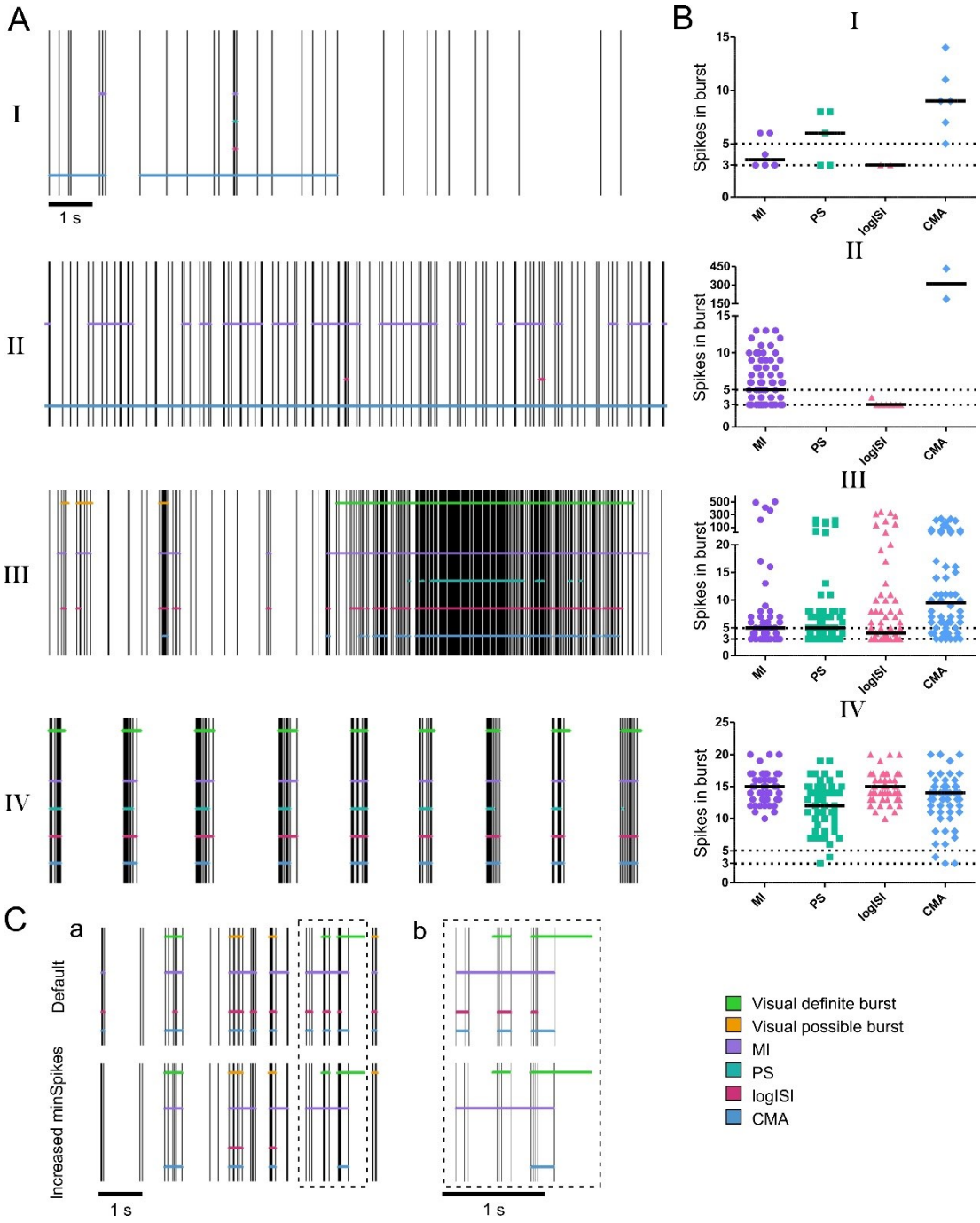

Figure 10. Performance of algorithms in different activity patterns and the effect of minSpikes selection. A) The performance of the algorithms in activity pattern Categories I-IV using default parameters. In D-AP5-inhibited low frequency activity (Cat. I), all algorithms detected false bursts. CMA detected few very long bursts. In untreated high frequency activity (Cat. II), PS outperformed the other algorithms as it detected no false bursts. LogISI found few short bursts. MI and CMA were unable to distinguish between mere high frequency activity and bursting activity. In noisy spike train with human super bursts (Cat. III), MI timed the super bursts well but also detected many false bursts. PS shortened the super bursts. LogISI and CMA split super bursts into multiple shorter bursts and detected short false bursts. In gabazine-treated well-separated rat bursts (Cat. IV), all algorithms timed the bursts excellently except for PS, which shortened the bursts. B) Number of spikes in a burst on the spike trains named in A. Detection of extremely short false

bursts consisting of only few spikes was a common issue of the algorithms. In non-bursting activity patterns (Cat. I and II) all the detected bursts were false. Each data point represents number of spikes in a single detected burst. The median is marked with a black line. C) Effect of minSpikes selection. Increase of minSpikes (from 3 to 5) decreased the number of detected false bursts but additionally some bursts, which were previously correctly detected, were now excluded (a). Some of the incorrectly excluded bursts were lost due to poor spike detection. Not all spikes, which were visually identified and included in bursts, were detected by the spike detection algorithm (b). In A and C, vertical lines represent spikes. Horizontal lines represent visually identified bursts and algorithms results. Detection method is indicated by color and location as shown in bottom right corner of the panel. Definite and possible visual bursts are drawn at the same level, and the results of each algorithm are drawn at their own level.

Table 3. Performance scores of algorithms using default parameters or increased minSpikes. The only difference between the analysis runs was the value of minSpikes. Default parameters used the value of 3 whereas the increased minSpikes used the value of 5. Performance of all algorithms was improved. 0 = failure, 1 = satisfactory, 2 = good and 3 = excellent. In the data column, h = human and r = rat.

		Default parameters				Increased minSpikes			
Category	**Data**	**MI**	**PS**	**LogISI**	**CMA**	**MI**	**PS**	**LogISI**	**CMA**
I	D-AP5-inhibited activity (h)	0	0	2	0	2	0	3	0
I	GABA-inhibited activity (h)	0	0	3	0	0	0	3	2
I	Immature, low frequency activity (r)	0	0	0	0	3	3	3	3
I	CNQX-inhibited activity (r)	0	0	3	3	3	3	3	3
II	KA-sinduced high frequency activity (h)	0	1	0	0	0	1	0	0
II	Immature, high frequency activity (r)	0	3	2	0	0	3	3	0
III	Short bursts with noise (h)	0	0	1	1	0	0	1	2
III	Super bursts with noise (h)	1	0	1	2	1	0	2	2
III	Short bursts with noise (r)	0	2	3	2	0	2	2	2
IV	Short bursts without noise (h)	2	0	2	2	1	0	1	1
IV	Gabazine-induced super bursts (h)	2	1	2	3	2	1	2	3
IV	Short bursts without noise (r)	2	2	3	3	3	2	3	3
IV	Gabazine-induced short bursts (r)	3	1	3	2	3	1	3	2
	Total score	10	10	25	18	18	16	29	23

Table 4. Sensitivities and specificities of algorithms using default parameters or increased minSpikes. The only difference between the analysis runs was the value of minSpikes. Default parameters used minSpikes of 3 whereas the increased minSpikes used 5. Specificity of all algorithms was essentially improved whereas the sensitivity was either maintained or slightly decreased. SE = sensitivity, SP = specificity. In the data column, h = human and r = rat.

		Default parameters								Increased minSpikes							
		MI		**PS**		**LogISI**		**CMA**		**MI**		**PS**		**LogISI**		**CMA**	
Category	**Data**	**SE**	**SP**	**SE**	**SP**	**SE**	**SP**	**SE**	**SP**	**SE**	**SP**	**SE**	**SP**	**SE**	**SP**	**SE**	**SP**
I	D-AP5-inhibited activity (h)	-	0.80	-	0.77	-	0.95	-	0.55	-	0.90	-	0.82	-	1.00	-	0.55
I	GABA-inhibited activity (h)	-	0.61	-	0.61	-	1.00	-	0.80	-	0.70	-	0.61	-	1.00	-	0.97
I	Immature, low frequency activity (r)	-	0.50	-	0.65	-	0.68	-	0.53	-	1.00	-	1.00	-	1.00	-	1.00
I	CNQX-inhibited activity (r)	-	0.52	-	0.72	-	1.00	-	1.00	-	1.00	-	1.00	-	1.00	-	1.00
II	KA-induced high frequency activity (h)	-	0.02	-	0.93	-	0.25	-	0.19	-	0.03	-	0.96	-	0.47	-	0.27
II	Immature, high frequency activity (r)	-	0.21	-	1.00	-	0.96	-	0.00	-	0.43	-	1.00	-	1.00	-	0.00
III	Short bursts with noise (h)	1.00	0.24	0.46	0.98	0.88	0.66	0.97	0.52	0.98	0.52	0.45	1.00	0.71	1.00	0.94	0.85
III	Super bursts with noise (h)	1.00	0.42	0.72	1.00	0.99	0.70	0.96	0.95	1.00	0.60	0.69	1.00	0.98	0.94	0.95	0.99
III	Short bursts with noise (r)	1.00	0.02	0.91	1.00	0.98	0.97	0.92	0.98	1.00	0.04	0.91	0.99	0.94	0.98	0.89	0.98
IV	Short bursts without noise (h)	0.99	0.82	0.70	1.00	0.99	0.50	0.98	0.89	0.96	0.82	0.69	1.00	0.92	0.61	0.89	0.93
IV	Gabazine-induced super bursts (h)	1.00	0.83	0.94	1.00	0.98	0.83	1.00	0.83	0.98	0.83	0.94	1.00	0.97	0.83	1.00	0.83
IV	Short bursts without noise (r)	1.00	0.02	0.96	0.25	1.00	0.13	1.00	0.14	1.00	0.08	0.96	0.25	1.00	0.15	1.00	0.14
IV	Gabazine-induced short bursts (r)	1.00	0.10	0.87	0.57	1.00	0.05	0.98	0.24	1.00	0.10	0.86	0.57	1.00	0.05	0.96	0.24
	Mean	1.00	0.39	0.79	0.81	0.97	0.67	0.97	0.59	0.99	0.54	0.79	0.86	0.93	0.77	0.95	0.67

4.4.3. Computation of burst features

Exclusion of extremely short bursts allowed derivation of more representative burst features. Four burst features were computed and examined to further evaluate the algorithm function after setting minSpikes to 5. These features included: burst count, percentage of spikes located in bursts, number of spikes in a burst and burst duration. For the examination, the spike trains representing Categories II and III were selected since these categories seemed to be the most challenging for the algorithms in general. The representative spike trains were the un-treated non-bursting high frequency spike train (Cat. II) and the noisy spike train displaying super bursts (Cat. III).

Extremely short bursts had been excluded but this did not equal exclusion of all false bursts. MI still detected over 40 false bursts on the non-bursting spike train (Figure 11). CMA detected two extremely long false bursts that included 100% of the spikes. As reported above, MI and CMA could not distinguish between bursts and mere high frequency activity. PS and logISI did not detect false bursts on this non-bursting spike train. On the bursting spike train, MI outperformed other algorithms in detection of super bursts. However, some false bursts remained and the specificity was low. Because of the short false bursts, the median number of spikes in a burst was lower than that of logISI and CMA despite the superior timing of the long super bursts. Nevertheless, the burst count of the other algorithms was higher because they split super bursts into shorter bursts. PS additionally shortened the bursts, which was visible in the burst duration and percentage of spikes within bursts when compared to other algorithms. Despite the split bursts, logISI and CMA had very high sensitivities and specificities. The splitting behavior was stronger with CMA, which was shown by its higher burst count in contrast to the similar percentage of spikes in bursts as well as by its shorter burst duration.

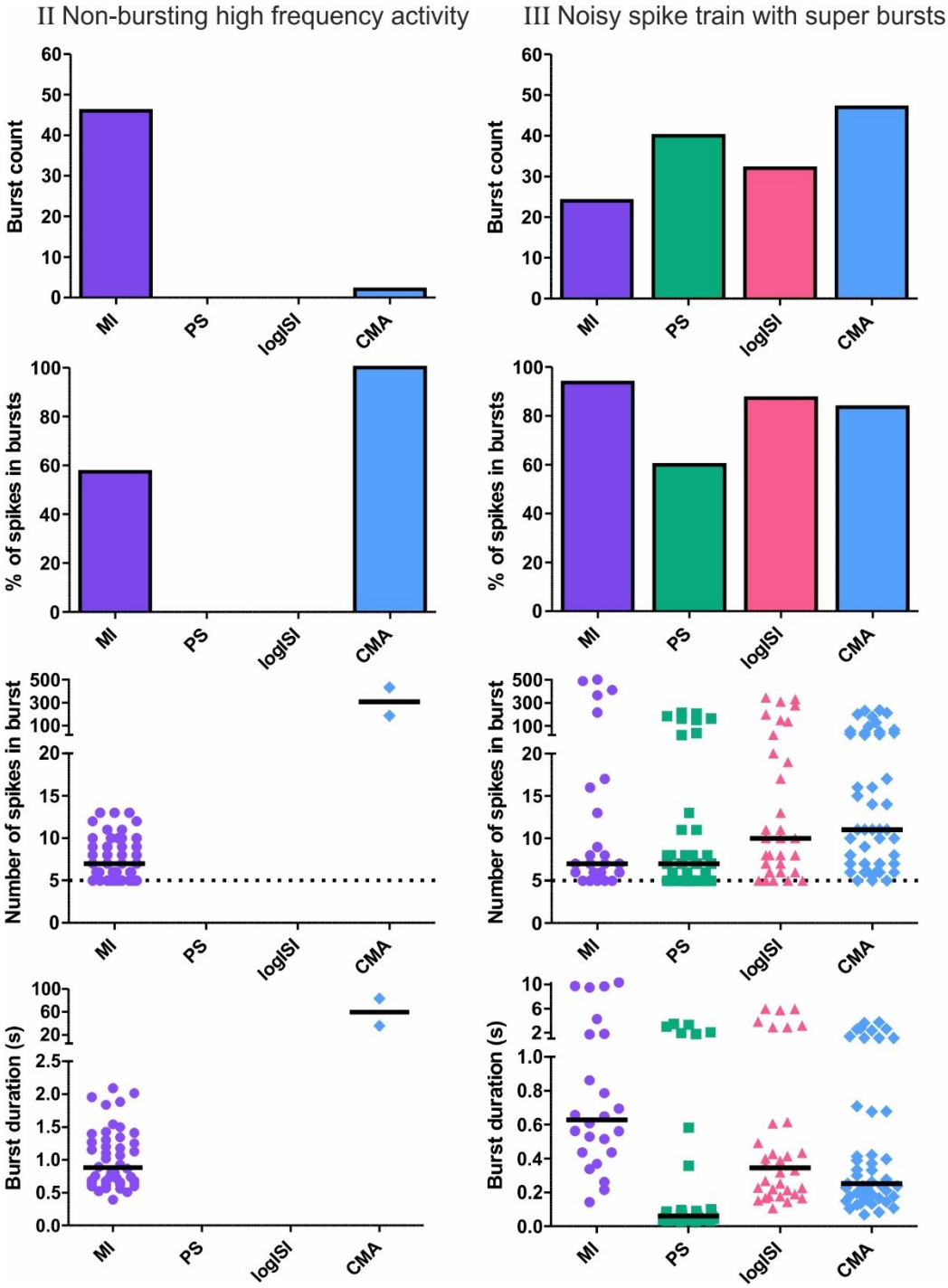

Figure 11. Computed burst features for two spike trains representing non-bursting high frequency activity (Cat. II) and noisy bursting activity (Cat. III). Burst count, percentage of spikes located in bursts, numbers of spikes in a burst and burst durations are presented for the un-treated non-bursting high frequency spike train (Cat. II) and for the noisy bursting spike train displaying super bursts (Cat. III). All the bursts detected on non-bursting high frequency spike train were false. For number of spikes in a burst and burst duration, each data point represents the corresponding feature of a single detected burst. Medians of these features are marked with black lines.

4.4.4. Identification of the most promising algorithm

The most promising algorithm was chosen based on the performance using the increased minSpikes. In the performance scores, the ranking from highest to lowest score was logISI (29 points), CMA (23 points), MI (18 points) and PS (10 points). The ranking in sensitivity was MI (0.99), CMA (0.95), logISI (0.93) and PS (0.79). Finally, the ranking in specificity was PS (0.86), logISI (0.77), CMA (0.67) and MI (0.54). When sensitivity and specificity were evaluated as a combination, logISI had the highest performance as its sensitivity was practically at a tie with CMA and its specificity was significantly higher than that of CMA. Moreover, the issues of logISI were not as grave as the issues of the other three algorithms. LogISI failed on one spike train only whereas the other three algorithms failed at least on three spike trains. Consequently, logISI was identified to be the most promising burst detection algorithm of the four.

4.5. Optimization of logISI algorithm

Setting minSpikes to 5 resolved the issue of false bursts for most spike trains. Only KA-treated activity (of Cat. II) still contained many false positives. On other spike trains, on the contrary, some bursts had been lost and thus further increase of minimum spikes was considered unprofitable. Remaining major issues of logISI algorithm included shortening, splitting and missing of bursts especially on noisy bursting activity (Cat. III). On well-separated human short bursts (of Cat. IV), extension and merging of bursts was deemed acceptable but the missed bursts, mostly missed only after the increase of minimum spikes, were regarded problematic.

Parameters for logISI algorithm include 1) minSpikes, 2) void threshold, 3) cutoff for the time window in which the intra-burst peak is to be found, and 4) default maxISI. MinSpikes was set to 5 according to the results of the previous chapter. The possibilities for void threshold and cutoff optimization were explored. The original void threshold 0.70 and cutoff 100 ms were empirical values determined by the author (Pasquale et al. 2010) and thus other values could be more suitable for the data used in this thesis. The effect of default maxISI was tested with values higher than the original value 100 ms to prevent logISI from shortening and splitting bursts.

4.5.1. Optimization of void threshold

Void parameters for all peak pairs were recorded to investigate possibilities for optimization. Nine spike trains had a void parameter above 0.70 and thus either path 1 or 2 was selected for them (Table 5). Path 3 that uses only default maxISI was selected for four spike trains: both non-bursting high frequency trains (Cat. II), and for both noisy bursting trains from human culture (of Cat. III). Three of these spike trains were considered problematic. Only on un-treated high frequency activity, logISI performed excellently. The highest void parameters for these spike trains were 0.60 for un-treated high frequency activity, 0.38 for noisy bursting activity displaying human short bursts, and 0.67 for noisy bursting activity displaying human super bursts. For KA-treated high frequency activity, there were no void parameters as there were no peaks subsequent to the intra-burst peak. According to the observed void parameters, the void threshold was first decreased to 0.60 and then further to 0.35. The resulting performance scores are presented in Table 6 and the sensitivities and specificities are displayed in Table 7.

Table 5. LogISI-computed values leading to path selection on each spike train. In the table, the intra-burst ISI represents the most probable ISI within a burst based on the computation by logISI. Out-of-burst ISI represents the lowest ISI, which logISI estimates to be outside of bursts with high probability. This probability is represented by the void parameter. Default threshold for void is 0.70, which is why no out-of-burst ISI is found when no void parameter exceeds the threshold. Used void parameter is reported if such a void was found. Otherwise, highest void is reported. ISIth is computed if a void above the threshold is found. The value of ISIth determines the path selected for a spike train. If ISIth is lower or higher than the default maxISI, here 100 ms, path 1 or path 2 are selected, respectively. If ISIth could not be calculated, path 3 is selected. It is notable that path 3 is chosen only for spike trains from Categories II and III. Path 3 covers the majority of the spike trains considered problematic for logISI burst detection. In the data column, h = human and r = rat.

Category	Data	Intra-burst ISI	Out-of-burst ISI	Used void or highest void	ISIth	Path
I	D-AP5-inhibited activity (h)	34	356	0.71	43	1
I	GABA-inhibited activity (h)	17	55	0.80	22	1
I	Unmatured, low frequency activity (r)	55	1512	0.93	367	2
I	CNQX-inhibited activity (r)	1	55	1.00	3	1
II	KA-induced high frequency activity (h)	92	-	-	-	3
II	Unmatured, high frequency activity (r)	28	-	0.60	-	3
III	Short bursts with noise (h)	22	-	0.38	-	3
III	Super bursts with noise (h)	11	-	0.67	-	3
III	Short bursts with noise (r)	2	92	0.72	36	1
IV	Short bursts without noise (h)	44	588	0.95	464	2
IV	Gabazine-induced super bursts (h)	10	281	0.80	176	2
IV	Short bursts without noise (r)	1	70	0.91	55	1
IV	Gabazine-induced short bursts (r)	17	1512	1.00	289	2

The decrease of void threshold to 0.60 improved the performance of logISI algorithm on noisy bursting activity displaying human super bursts due to reduced splitting of

super bursts (Figure 12A). The calculated ISIth was 143 ms. For non-bursting, un-treated high frequency activity, the calculated ISIth was 73 ms but the performance was unchanged, and no bursts were detected.

The decrease of void threshold to 0.35 slightly improved the algorithm performance on noisy bursting activity displaying human short bursts as less bursts were missed. Consequently, the sensitivity was increased. However, the bursts were unnecessarily extended and merged, which was seen as a decrease in specificity. A change in performance was also observed on well-separated rat bursts as the second highest void parameter for the spike train was 0.39 and was now above the threshold. The change was negative as some bursts were shortened and many entirely missed (Figure 12B). This led to a destructive decrease in sensitivity. The calculated ISIths for these human and rat spike trains were 229 and 35 ms, respectively.

4.5.2. Optimization of intra-burst peak time window

The cutoff for the time window, in which to find intra-burst peak, was originally set to 100 ms. This was an empirical value determined by the author. Examination of intra-burst peaks showed that they were successfully computed for all spike trains (Table 5). Thus, increasing the cutoff would have been unprofitable. Possibilities of cutoff decrease were explored. The intra-burst ISI of KA-treated activity (of Cat. II) was 92 ms, which was remarkably higher than those of other spike trains. KA-treated activity was also the only one without peaks subsequent to the intra-burst peak, which prevented computation of ISIth. KA-treated activity had a very high spike frequency, which explains the lack of subsequent peaks. However, there was a single preceding peak at 1 ms. It was theorized that decreasing the cutoff could allow computation of ISIth for KA activity. The second and third highest intra-burst ISIs were 55 and 44 ms. The corresponding intra-burst peaks did not have preceding peaks. Consequently, decreasing the cutoff below these intra-burst ISIs would have prevented the computation of ISIth for the corresponding spike trains. This was not a desirable consequence. Thus, the effect of decreased cutoff value was investigated for KA-treated activity only.

The cutoff was set to 75 ms as this was around the mean of the highest and second highest intra-burst ISIs. As a result, the peak corresponding to 1 ms was nominated the intra-burst peak and the peak corresponding to 92 ms was nominated the outer peak. The void parameter of the peak pair was 0.89. The corresponding ISIth was 2 ms and thus path 1 was selected. The algorithm performance was remarkably improved (Tables 6 and 7), as no bursts were detected on the KA-treated activity.

4.5.3. Optimization of default maximum inter-spike interval

Default maxISI parameter is used in paths 2 and 3 and, therefore, alteration of maxISI affects only spike trains for which path 2 or 3 is selected. In path 2, the bursts cores are detected using maxISI. In path 3, maxISI is applied for the whole burst. A major problem recognized in logISI performance was its tendency to shorten and split bursts. In search for a solution, maxISI was increased from the original value of 100 ms to 150, 200 and 250 ms. The threshold for the selection between paths 1 and 2 was also changed according to each maxISI. Key changes in algorithm performance due to maxISI alteration are illustrated in Figure 12C. The performance scores are presented in Table 6 and the sensitivities and specificities are presented in Table 7.

Overall, increase of maxISI to 150 ms had a positive effect. The increase improved the results in bursting activity (Cat. III and IV) from human culture. More short bursts were correctly detected, and parts of super bursts were merged together. Yet, some splitting remained. One false burst was observed on noisy bursting activity displaying super bursts. On non-bursting high frequency activity (Cat. II), the increase had a negative effect as more false bursts were detected, especially on KA-treated activity. On un-treated activity the effect was minor as only one false burst was detected.

Increase to 200 ms had both positive and negative effects. The most positive effect was observed on noisy bursting activity displaying super bursts (of Cat. III) as the splitting was reduced even more. On short human bursts (of Cat. III and IV), the number of correctly detected bursts was slightly higher in comparison to the performance using 150 ms. However, there were significant changes in performance on the noisy bursting spike train. Many bursts were extended, more often unnecessarily. One false burst was detected. As a result, the specificity decreased to an unacceptably low value. On non-bursting high frequency activity (Cat. II), the negative effect was more prominent than when using 150 ms. Even more false bursts were observed on both spike trains.

Increase to 250 ms gave poor results except for one positive effect. This positive effect was observed on noisy bursting activity displaying super bursts (of Cat. III) as splitting was again slightly reduced. An additional false burst emerged though. On noisy bursting activity displaying human short bursts (of Cat. III), bursts were excessively extended and merged and more false bursts were detected. The number of false bursts increased also on non-bursting high frequency activity (Cat. II). This resulted in a failure even on un-treated activity.

No increase affected logISI performance in gabazine-treated activity displaying well-separated bursts (of Cat. IV) nor in non-bursting, un-treated low frequency activity

(of Cat. I). Nevertheless, the path selection for the gabazine-treated human spike train was changed from 2 to 1 when maxISI was increased from 150 to 200 ms. This was because the ISIth of the spike train was between these two values, namely 176 ms. For other unaffected spike trains, path 2 was selected constantly.

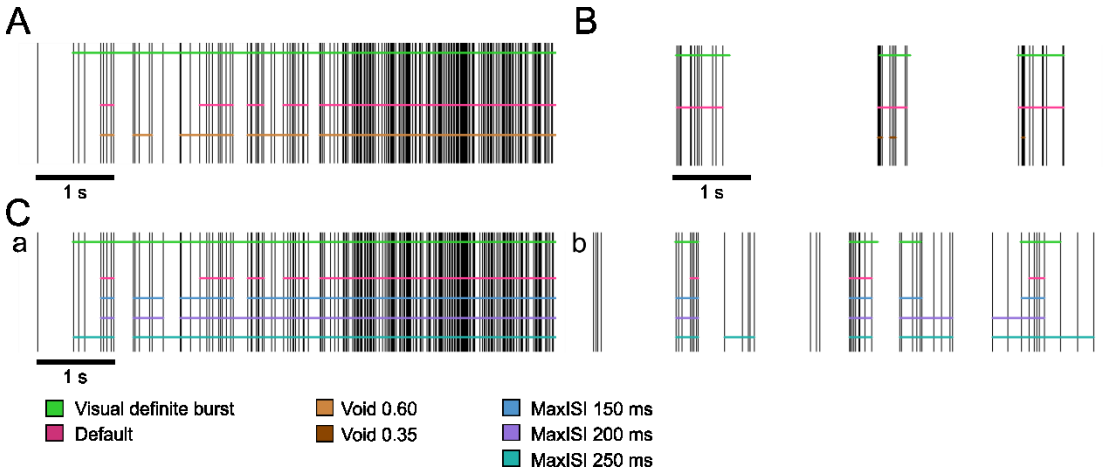

Figure 12. Effects of void threshold and default maxISI optimization. A) Using void threshold of 0.60, splitting was reduced on the noisy spike train displaying super bursts. B) Further decrease of void threshold to 0.35 had an extremely negative effect on gabazine-treated rat bursts. The bursts were significantly shortened and some were missed entirely. C) On the noisy spike train displaying super bursts (a), the higher the increase of maxISI was, the better was the performance as splitting was reduced. On the noisy spike train displaying human short bursts (b), the burst detection was most accurate using 150 ms. Using 200 ms, the bursts were unnecessarily extended. The extension was even more excessive using 250 ms and also false bursts were detected. In all parts, vertical lines represent spikes. Horizontal lines represent visually identified bursts and algorithm results with default or modified parameters.

Table 6. Performance scores using modified parameter values during the optimization of logISI performance. The scores of the affected individual spike trains are highlighted in blue even if no change in the performance was observed. 0 = failure, 1 = satisfactory, 2 = good and 3 = excellent. In the data column, h = human and r = rat.

Category	Data	Default	Void 0.60	Void 0.35	Cutoff 75 ms	MaxISI 150 ms	MaxISI 200 ms	MaxISI 250 ms
I	D-AP5-inhibited activity (h)	3	3	3	3	3	3	3
I	GABA-inhibited activity (h)	3	3	3	3	3	3	3
I	Immature, low frequency activity (r)	3	3	3	3	3	3	3
I	CNQX-inhibited activity (r)	3	3	3	3	3	3	3
II	KA-induced high frequency activity (h)	0	0	0	3	0	0	0
II	Immature, high frequency activity (r)	3	3	3	3	3	2	0
III	Short bursts with noise (h)	1	1	2	1	2	2	1
III	Super bursts with noise (h)	2	3	3	2	3	3	3
III	Short bursts with noise (r)	2	2	2	2	2	2	2
IV	Short bursts without noise (h)	1	1	1	1	2	2	2
IV	Gabazine-induced super bursts (h)	2	2	2	2	2	2	2
IV	Short bursts without noise (r)	3	3	3	3	3	3	3
IV	Gabazine-induced short bursts (r)	3	3	0	3	3	3	3
	Total score	29	30	28	32	32	31	28

Table 7. Sensitivities and specificities using modified parameter values during the optimization of logISI performance. The sensitivities and specificities of the affected spike trains are highlighted in blue even if no change in the performance was observed. On the bottom row, the relation of the mean to the default mean is shown. Sensitivity was increased by all modifications except when using void threshold of 0.35. Void threshold and cutoff modifications increased specificity. Specificity was decreased by increase of default maxISI. SE = sensitivity, SP = specificity. In the data column, h = human and r = rat.

		Default		Void 0.60		Void 0.35		Cutoff 75 ms		MaxISI 150 ms		MaxISI 200 ms		MaxISI 250 ms	
Category	Data	SE	SP	SE	SP	SE	SP	SE	SP	SE	SP	SE	SP	SE	SP
I	D-AP5-inhibited activity (h)	-	1.00	-	1.00	-	1.00	-	1.00	-	1.00	-	1.00	-	1.00
I	GABA-inhibited activity (h)	-	1.00	-	1.00	-	1.00	-	1.00	-	1.00	-	1.00	-	1.00
I	Immature, low frequency activity (r)	-	1.00	-	1.00	-	1.00	-	1.00	-	1.00	-	1.00	-	1.00
I	CNQX-inhibited activity (r)	-	1.00	-	1.00	-	1.00	-	1.00	-	1.00	-	1.00	-	1.00
II	KA-induced high frequency activity (h)	-	0.47	-	0.47	-	0.47	-	1.00	-	0.24	-	0.08	-	0.05
II	Immature, high frequency activity (r)	-	1.00	-	1.00	-	1.00	-	1.00	-	0.99	-	0.93	-	0.72
III	Short bursts with noise (h)	0.71	1.00	0.71	1.00	0.96	0.76	0.71	1.00	0.89	0.95	0.95	0.74	0.97	0.51
III	Super bursts with noise (h)	0.98	0.94	0.99	0.94	0.99	0.94	0.98	0.94	0.99	0.89	0.99	0.84	1.00	0.76
III	Short bursts with noise (r)	0.94	0.98	0.94	0.98	0.94	0.98	0.94	0.98	0.94	0.98	0.94	0.98	0.94	0.98
IV	Short bursts without noise (h)	0.92	0.61	0.92	0.61	0.92	0.61	0.92	0.61	0.96	0.61	0.97	0.61	0.98	0.50
IV	Gabazine-induced super bursts (h)	0.97	0.83	0.97	0.83	0.97	0.83	0.97	0.83	0.97	0.83	0.97	0.83	0.97	0.83
IV	Short bursts without noise (r)	1.00	0.15	1.00	0.15	1.00	0.15	1.00	0.15	1.00	0.15	1.00	0.15	1.00	0.15
IV	Gabazine-induced short bursts (r)	1.00	0.05	1.00	0.05	0.51	0.67	1.00	0.05	1.00	0.05	1.00	0.05	1.00	0.05
	Mean	0.93	0.77	0.93	0.77	0.90	0.80	0.93	0.81	0.96	0.74	0.97	0.71	0.98	0.66
	Relative to default			1.00	1.00	0.97	1.04	1.00	1.05	1.03	0.97	1.05	0.92	1.05	0.85

4.5.4. Combining optimized parameters

In the preceding chapters, parameters were optimized separately. The performance of logISI was most improved when 1) minSpikes was set to 5, 2) void threshold was set to 0.60, 3) cutoff for intra-burst peak time window was set to 75 ms, and 4) default maxISI was set to 150 ms. Next, the combined effects of the optimized parameters were examined. MinSpikes had already been set to 5 during the separate optimization of the other three parameters. The optimization effects of these three parameters overlapped on three spike trains, namely the KA-treated non-bursting high frequency spike train (of Cat. II), the un-treated non-bursting high frequency spike train (of Cat. II) and the noisy spike train displaying super bursts (of Cat. III). On both non-bursting high frequency spike trains, the effect of increased maxISI became non-existent since the path selection had become 1 due to either the optimal cutoff or the optimal void threshold. This was advantageous as it also resulted in the highest performance. On the spike train displaying super bursts, optimal void threshold and maxISI had earlier improved the performance due to reduced splitting of bursts. When the two optimal parameters were combined, the ISIth was computed to be 143 ms and, consequently, path 1 was selected. The path selection was different than when using either one of the optimal parameters separately, but all performances highly resembled each other. In conclusion, combined use of optimal parameters maintained the individual positive effects of each parameter. This resulted in the

highest performance score to this point (Table 8). The performance of optimized logISI algorithm is illustrated in Appendix 4, Figure A3.

Table 8. Performance scores, sensitivities and specificities using the default parameter values and the optimized parameter values. MinSpikes was set to 5 in both runs. In the default run, void threshold was set to 0.70, cutoff for intra-burst peak time window to 100 ms, and default maxISI to 100 ms. In the optimized run, void threshold was set to 0.60, cutoff to 75 ms, and default maxISI to 150 ms. The results are highlighted for spike trains, on which the effects of optimal cutoff, optimal void threshold or optimal maxISIs overlap. P = performance, SE = sensitivity, SP = specificity. In the performance scores, 0 = failure, 1 = satisfactory, 2 = good and 3 = excellent. In the data column, h = human and r = rat.

		Default			Optimized		
Category	**Data**	**P**	**SE**	**SP**	**P**	**SE**	**SP**
I	D-AP5-inhibited activity (h)	3	-	1.00	3	-	1.00
I	GABA-inhibited activity (h)	3	-	1.00	3	-	1.00
I	Immature, low frequency activity (r)	3	-	1.00	3	-	1.00
I	CNQX-inhibited activity (r)	3	-	1.00	3	-	1.00
II	KA-induced high frequency activity (h)	0	-	0.47	3	-	1.00
II	Immature, high frequency activity (r)	3	-	1.00	3	-	1.00
III	Short bursts with noise (h)	1	0.71	1.00	2	0.89	0.95
III	Super bursts with noise (h)	2	0.98	0.94	3	0.99	0.93
III	Short bursts with noise (r)	2	0.94	0.98	2	0.94	0.98
IV	Short bursts without noise (h)	1	0.92	0.61	2	0.96	0.61
IV	Gabazine-induced super bursts (h)	2	0.97	0.83	2	0.97	0.83
IV	Short bursts without noise (r)	3	1.00	0.15	3	1.00	0.15
IV	Gabazine-induced short bursts (r)	3	1.00	0.05	3	1.00	0.05
	Total score (P) or mean (SE, SP)	29	0.93	0.77	35	0.96	0.81

5. Discussion

The aim of this thesis was to assemble a test data set representing the variety of activity patterns observed in neuronal networks derived from hPSC and rat cortical neuronal cells, and to identify a single burst detection algorithm with optimal parameters that would successfully detect bursts in this test data set. As such, functional neuronal networks were derived from hPSCs and primary rat cortical neuronal cells and their electrical activity was recorded on MEA. Both spontaneous and pharmacologically modulated activity was recorded. A variety of activity patterns was identified in the recordings. A test data set representative of the identified activity patterns was assembled to evaluate the performances of four burst detection algorithms, namely MI (Nex Technologies 2014), logISI (Pasquale et al. 2010), PS (Legendy, Salcman 1985), and CMA (Kapucu et al. 2012). Of the four methods, logISI was identified as the highest-performing algorithm and was chosen for parameter optimization. Parameter optimization significantly improved the performance of logISI.

5.1. Properties of the differentiated neuronal networks

Neuronal networks derived from hPSCs and primary rat cortical neuronal cells obtained appropriate morphology and developed synapses and electrical activity. The activity of the hPSC-derived networks developed within the typical time line observed in earlier studies (Heikkilä et al. 2009; Lappalainen et al. 2010; Mertens et al. 2016). The effects of neuromodulators were in accordance with their known function except for the effect of KA and, on rat culture only, the effect of gabazine. KA decreased the spike frequency in both cultures despite of being a glutamatergic agonist. It is probable that the concentration of 5 µM was high enough to become excitotoxic for the cultures. In a previous study that used human HIP-009 neurons, 10-fold increases of KA concentration were shown to increase the spike frequency in a concentration-dependent manner between 0.001 and 1 µM but 10 µM KA decreased the spike frequency (Fukushima et al. 2016). However, 5 µM KA was shown to increase the spike frequency in another study using hiPSC-derived neurons (Odawara et al. 2016). The difference in results could be due to various reasons such as the age of the neuronal networks or the different origin of hPSCs. On rat culture, the effect of gabazine on spike frequency was not statistically significant. It is possible that degradation of connections had already begun on rat neuronal networks in certain wells as indicated by the decrease in proportion of active electrodes just prior the pharmacological assays. Setting a threshold for number of active electrodes per

well could allow exclusive selection of active networks for the analysis. In this study, the effect of neuromodulators was investigated per electrode and, accordingly, a threshold was set only for the spike frequency of a single electrode. Although there was no statistically significant difference in spike frequency, gabazine was observed to reduce the number of individual spikes outside of bursts on many electrodes both in human and rat cultures.

5.2. Evaluation of methods assessing burst detection performance

The performance of burst detection algorithms was evaluated by comparing the burst detection results to visually identified bursts. Bursts were visually identified from the raw MEA signal. This was occasionally challenging especially on noisy bursting activity patterns, which contained many individual spikes between the bursts. Additionally, some spikes of low amplitude might have been missed by human eye and, consequently, some bursts including these low-amplitude spikes could have been missed as well. This did not raise a concern in regard to performance analysis of burst detection algorithms as it was noticed that the spike detection algorithm missed even more spikes making it impossible for burst detection algorithms to correctly detect all bursts.

Visual burst identification is never objective as it is performed by a human observer. Yet, visual identification of bursts is an accepted method for burst detection, and comparison of algorithm results to visually identified bursts has been used to evaluate algorithm performance (Cotterill et al. 2016; Pasquale et al. 2010; Gourévitch, Eggermont 2007). Visual identification of bursts can be considered an adaptive technique. Human brain automatically looks for abnormalities in data. Thus, to the human eye, a spike set of a specific spike frequency might look tighter in a low frequency spike train and looser in a high frequency spike train. Consequently, a spike set of a specific spike frequency might be considered a burst in a low frequency environment but not in a high frequency environment when visually inspecting these spike trains. Visual identification adapts to each individual spike train similarly to self-adapting algorithms, such as logISI (Pasquale et al. 2010) and CMA (Kapucu et al. 2012).

The aims of this thesis did not include finding a definition for a burst. Yet, some defining restrictions had to be made to reach the aims of this thesis. A key question in this thesis was what events the burst detection algorithm should help the researcher to recognize from the data. In this work, only mature bursts apparent to the human eye were considered as essential findings. Because of this, the visually

identified bursts were given identity of either a definite burst or of a possible burst. The detection of definite bursts was a strong requirement for a burst detection algorithm, but the detection of possible bursts was not required. Visual identification of the possible bursts was still necessary as they should not be considered as false bursts either if detected by the algorithms. Classification of visually detected bursts into definite and possible bursts has not been used in this format elsewhere in the literature according to the knowledge of the author.

The performance of each algorithm was given a separate score for its performance on each of the spike trains included in the test data. This allowed evaluation of the algorithms also separate of each other and made their strengths and weaknesses visible in the scores. A ranking system, where the best algorithm receives 1 point, the second best receives 2 points etc., has been used for comparative performance analysis before (Cotterill et al. 2016) and would have been more straightforward, but it would have disabled examination of the algorithm performances independently. Sensitivity and specificity are widely used to evaluate methods in different fields. They have also been utilized to evaluate the performance of burst detection algorithms (Cotterill et al. 2016). However, there are two noteworthy points when discussing sensitivities and specificities. First, the sensitivity value does not reveal whether a burst has been detected as a whole or in parts. Only the performance score takes this into account. Second, on spike trains containing well-separated bursts the effect of a single erroneously classified individual spike is huge on specificity as there are very few individual spikes. This should be kept in mind when evaluating and comparing the specificity values for well-separated bursts (Cat. IV). Nevertheless, the conditions are same for all the algorithms and, thus, the ranking of specificities is informative.

5.3. Variation of bursting activity and assembly of test data set

The goal of the test data set was to represent the variety of bursting and non-bursting activity identified during neuronal network development and pharmacological assays. The data was derived from both human and rat neuronal networks. The main focus was on human neuronal networks on which burst detection algorithms have rarely been verified. Rat neuronal networks were included in the study because they are commonly used in the field. The bursting patterns were variable in both cultures but especially the burst duration varied more in the human culture. Similar observations have been made in earlier studies (Wagenaar et al. 2006; Heikkilä et al. 2009). Generally, human bursts also had longer intra-burst ISIs and a smaller number of spikes in a burst in comparison to rat bursts. The different types of bursting activity

identified in each culture were included to the data set. Additionally, at least one spike train was selected to represent the response to each pharmacological reagent. Naturally, the data set in this work was relatively small and for example duplicates of the most varying activity patterns, namely noisy bursting activity patterns (Cat. III), could have provided useful information to this work. On the other hand, the small size of the data set allowed efficient and profound investigation of the algorithm behaviors.

An extended culture time allows further development of the hPSC-derived neuronal networks and more activity patterns to emerge. In the later stages of development, however, the activity has been shown to switch from bursts to more complex and dynamic activity patterns (Kirwan et al. 2015). Dispersion of bursts in the later cultures was also observed in the hPSC-derived neuronal networks in this work. As the resulting patterns were similar to those of the previously included spike trains (Cat. II and III), no spike trains were included to the data set from the cultures after 30 days on MEA. Due to the complexity of the later activity patterns however, it is not secure to say that the burst detection algorithms would perform similarly on all of these complex patterns. All things considered, the assembled test data set was considered to be representative of the activity patterns identified in the human and rat neuronal networks. Derivation of data from both human and rat networks as well as inclusion of modulated activity patterns were significant strengths of the test data set.

5.4. Comparative analysis of algorithm performances

In the comparative performance analysis, logISI and CMA showed high overall performance whereas MI and PS were not as capable. LogISI and CMA had high performance scores and their sensitivities and specificities were well balanced. Of the two, logISI received a higher performance score mainly because it failed on fewer spike trains than CMA. MI had a very low specificity resulting from its tendency to overestimate the number of spikes included in bursts. This also reflected in its performance score. Contrary to MI, PS had an unacceptably low sensitivity as it shortened bursts and often failed to detect bursts altogether. MI and PS both failed on multiple spike trains. It is notable that all algorithms except PS failed on KA-treated non-bursting high frequency activity (of Cat. II). PS showed satisfactory performance on this spike train. All the aforementioned points remained the same when minSpikes was increased because the increase improved the performances of all algorithms in a more or less identical scale. The effect of minSpikes selection is discussed later. It should be noted that in the majority of the referred studies minSpikes had been set

to 3. As minSpikes was set to 5 in the second run of this work, new information was obtained. Here, the algorithm performances are discussed based on the results using 5 as minSpikes as it provided results that were more in accordance with visual observations.

5.4.1. Performance of logISI method

LogISI performed generally well on all activity patterns. It outperformed other algorithms on non-bursting activity patterns (Cat. I and II). On bursting activity patterns (Cat. III and IV), however, it tended to shorten and split bursts which impaired its performance especially on human bursts. Shortening and splitting of bursts results in underestimated burst durations and proportions of intra-burst spikes. Similar underestimations have been reported earlier (Cotterill et al. 2016). Low intra-burst spike frequency has been shown to be one reason for detection of shortened or split bursts on synthetic data (Cotterill et al. 2016). In the test data of this study, human bursts displayed lower intra-burst spike frequency than rat bursts, which explains why logISI performance was weaker on human bursts than on rat bursts.

On one spike train, logISI extended and merged bursts, which is contrary to the behavior described above. The spike train in question contained well-separated short human bursts. The merging behavior has earlier been reported on synthetic data, which displayed short irregular bursts occurring at a high frequency and no noise (Cotterill et al. 2016). The high frequency of bursts results in lower separation of bursts and could be the reason behind the behavior but there might be other factors in play as well. LogISI had no problem detecting correctly timed bursts in gabazine-treated well-separated rat bursts, which also occurred at high frequency. However, the gabazine-treated rat bursts occurred more regularly, and the intra-burst spike frequency was remarkably higher in these rat bursts in comparison to human short bursts. The differences in regularity and intra-burst spike frequency are visible in the spike plots and the log-adjusted ISI histograms, respectively (Appendix 2, Figure A1). Proportional effects of different factors cannot be determined based on the current test data set alone.

All things considered, logISI displayed highest performance and was nominated as the most promising burst detection algorithm. LogISI was also ranked amongst the two highest-performing algorithms in the comparative study of Cotterill et al. (Cotterill et al. 2016). They reported that logISI showed utmost promise on activity recorded from mouse retinal ganglion cells and from hiPSC-derived neurons. In the study by Kapucu et al. (Kapucu et al. 2012), logISI was praised for its performance on

matured bursting activity on hESC-derived neuronal networks although it was criticized of being unable to detect unstable bursting activity in the developing networks. In this thesis work, the most immature and unstable bursts in hESC-derived cultures were observed in the form of short bursts. Two samples of such bursting activity, recorded after 7 and 14 days on MEA, were included to the test data set and logISI performance was satisfactory on both with sensitivities of 0.92 and 0.71, respectively. The latter was still considered acceptable as the relatively low value was partly due to poor spike detection. When minSpikes was set to 3, as it was by Kapucu et al., the respective sensitivities were 0.99 and 0.88. More immature activity in this study was determined non-bursting during visual observation.

5.4.2. Performance of Cumulative moving average method

CMA performed generally well on bursting activity but had major issues on non-bursting activity patterns. On bursting activity patterns (Cat. III and IV), its only issue was splitting of bursts. This behavior has been previously described on synthetic data (Cotterill et al. 2016). On non-bursting high frequency activity (Cat. II), CMA failed as it could not distinguish between a bursting spike train and a non-bursting high frequency train. The authors of CMA proposed post hoc screening to solve this issue (Kapucu et al. 2012). With thresholding, spike trains with mean burst duration > 5 s or mean number of spikes in a burst > 50, would be determined as non-bursting (Kapucu et al. 2012). Post hoc screening with thresholding would solve the issue on un-treated high frequency activity, but higher thresholds would be needed. When bursts were detected by CMA, the highest mean burst durations were 59.9, 4.3 and 2.9 on un-treated non-bursting high frequency activity, well-separated super bursts, and D-AP5-treated non-bursting low frequency activity, respectively. The highest mean numbers of spikes in burst were 310, 114 and 64 on un-treated non-bursting high frequency activity, well-separated super bursts, and well-separated short rat bursts, respectively. It can be concluded that thresholds for mean duration and number of spikes can be increased. More spike trains displaying non-bursting high frequency activity (Cat. II) and well-separated bursts (Cat. IV) should be analyzed to determine appropriate threshold values. However, it is uncertain whether suitable threshold values could be found. Post hoc screening with thresholding has earlier been applied for hiPSC-derived neuronal networks with the original threshold values and though long false bursts were successfully excluded many true short bursts in the same spike train were missed as the whole spike train was designated non-bursting (Cotterill et al. 2016).

Another problem of CMA was that it detected long bursts even on non-bursting low frequency activity (Cat. I). Because of this, the mean burst duration of D-AP5-treated low frequency activity was third highest in the test data, as mentioned above. The issue was due to the tendency of CMA to detect unusual, or surprising, activity events as bursts, which has also been described earlier on synthetic data (Cotterill et al. 2016). It was reported that CMA detected false bursts especially on non-bursting synthetic spike trains with a nonstationary spike frequency. The spike frequency of the D-AP5-treated spike train was also considered nonstationary based on visual inspection (Appendix 2, Figure A1). The other low frequency spike trains were more stationary than the D-AP5-treated train. The issue of detecting long bursts on nonstationary low frequency spike trains could not be assessed using post hoc screening with thresholding because the mean burst duration and the mean number of spikes were higher on well-separated super bursts than on D-AP5-treated spike train. Instead, it might be possible that an extensive investigation of the skewness of the ISI histograms of different activity patterns and optimization of the skewness thresholds accordingly might improve the performance of the algorithm. Cotterill et al. (Cotterill et al. 2016) also suggested a simpler modification to improve the performance by restricting the allowed values of intra-burst ISI to biologically realistic range. Nevertheless, it is uncertain whether the performance of CMA could take over the performance of logISI. LogISI showed evidently more potential in the initial performance analysis and was even able to overcome the issues related to KA-treated non-bursting high frequency activity during the parameter optimization. In this work, CMA was ranked second right below logISI and above MI. In the earlier study by Cotterill et al. (Cotterill et al. 2016), CMA was ranked below both logISI and MI. In their study, CMA was used to detect only the bursts cores whereas in this thesis also burst-related spikes were detected. Nevertheless, similar to the results of this thesis work, Cotterill et al. reported that the major problem of CMA was the low specificity on non-bursting spike trains resulting from the detection of multiple false bursts. It should be noted that they used 3 as minSpikes. In this work, minSpikes was increased to 5, which decreased the number of false bursts but did not solve the issue completely. It is very probable that the multiple false bursts stem from the fact that CMA was built on developing hESC-derived neuronal networks to detect even primitive and unstable bursting activity (Kapucu et al. 2012). The concept of burst was probably looser in comparison to this work, in which only mature bursts obvious to the human eye were considered as desirable findings.

5.4.3. Performance of MaxInterval method

MI performed well on well-separated bursts (Cat. IV) and on most non-bursting low frequency spike trains (Cat. I). Its major issues were with noisy bursting activity (Cat. III) and non-bursting high frequency activity (Cat. II). This was because MI tended to extend bursts and, more importantly, was unable to differentiate between bursts and a period of mere high frequency. The average specificity of MI on these activity patterns was lower than that of any other algorithm. Previously, it has been reported that on high frequency activity from hiPSC-derived neurons MI detected larger proportion of spikes in bursts in comparison to logISI, CMA (including post hoc screening) and PS (Cotterill et al. 2016). However, no comparison to visually identified bursts was presented for this particular type of activity pattern, so the ground truth is unknown. It is notable that the begISI in that study had been increased from 0.17 s to 0.20 s. Such increase would have resulted in even lower specificity in this study. As the other algorithms in this thesis had generally higher specificity and comparable sensitivity on both bursting (Cat. III and IV) and non-bursting high frequency activity (Cat. II), the performance of MI should not be trusted over the other algorithms on high frequency spike trains. Thus, it is possible that MI extended bursts also on activity derived from hiPSC-derived neurons. Despite the deviating behavior of MI on high frequency activity, the algorithm was nominated as the most promising algorithm in the comparative study by Cotterill et al. (Cotterill et al. 2016). Nevertheless, they highlighted the challenge presented by parameter choice, and suggested that parameters could be altered for the high frequency activity that was observed at a certain time point during the network development. Parameter alteration is acceptable and sometimes required for specific type of data but, unfortunately, it prevents comparison of results.

Admittedly, parameter optimization could highly improve the performance of MI. In this data set, decreasing the value of begISI was recognized as a key optimization point. However, optimization of MI for many distinct types of activity was considered unprofitable. First of all, MI was not suitable for both human and rat cultures because the spike frequencies in human and rat bursts were very different. The human bursts often contained spikes with wider spacing, and the longest burst begISIs were approximately 150 ms. The high frequency activity preceding rat bursts very often included more than five subsequent ISIs < 150 ms. Typical range was observed to be 60-130 ms. Moreover, the ISIs were even shorter in the KA-treated non-bursting high frequency train from human culture. The mean ISI was 88 ms, which is very low considering that the spike train was non-bursting. Finding begISI, which would recognize a beginning of a human burst but ignore mere high frequency activity, would thus be impossible. The restricted applicability of MI-like algorithms using pre-

defined parameters has been discussed in earlier studies (Pasquale et al. 2010; Kapucu et al. 2012). The aim of this thesis was to find a single well-performing algorithm with constant parameter values suitable for hPSC-derived neuronal networks, and preferable also for rat neuronal networks. MI would not be able to meet these criteria even after parameter optimization.

5.4.4. Performance of Poisson surprise method

PS displayed poorest performance of the four algorithms. Its performance was generally better on rat data than on human data. The distinction in performance between the two types of data was not similarly obvious for other algorithms. PS had its major issues on human data. It detected many false bursts on non-bursting low frequency activity (Cat. I). Similar behavior has been described previously on synthetic non-bursting spike trains with nonstationary spike frequency (Cotterill et al. 2016). On the contrary, PS missed many bursts on bursting human data (Cat. III and IV). Additionally, it tended to shorten bursts on both human and rat data. Similarly, the sensitivity of PS has been shown to be low on synthetic spike trains displaying noisy bursting or high frequency bursts without noise (Cotterill et al. 2016). Peculiarly, opposite results have been shown on biological activity. On activity from hiPSC-derived neurons, PS tended to extend and merge bursts that logISI, CMA and MI detected as separate bursts (Cotterill et al. 2016). The threshold for the surprise statistic for the data in question was set to -ln(0.0025) (~6.0) instead of -ln(0.01) (~4.6), which was used in this thesis work. Different thresholds, however, cannot explain the difference in results as the algorithm uses the threshold only to exclude potential bursts that have been detected in the previous step. The distinction in results thus raises a question whether the electrical activity of hESC- and hiPSC-derived neuronal networks differ. All things considered, PS does not provide steady performance across different activity patterns of various sources. Both false positives and false negatives were common with PS. Fixing both of these contrary problems with parameter optimization was deemed unachievable.

5.5. Significance of minimum number of spikes in a burst

The performances of the four algorithms, namely MI, PS, logISI and CMA, were first evaluated using the default parameters. MinSpikes was set to 3, which resulted in multiple extremely short false bursts. This was expected as these extremely short bursts had been considered insignificant findings in the visual identification of bursts. When examining the number of spikes in noisy bursting activity (Cat. III), it was noticed that the median for three algorithms was 5 spikes or less. CMA had a higher

median, but it was also affected by a great number of extremely short bursts. Increasing minSpikes to 5 consequently excluded up to half of the bursts detected by each algorithm.

It has been suggested that the minSpikes required for a burst could be altered according to the activity type of the data (Turnbull et al. 2005) but this would prevent comprehensive comparison and interpretation of the results. Thus, a single value is desirable. Exclusion of the extremely short bursts makes the burst features, which are calculated from the detected bursts, more informative and representative of the activity. This allows recognition of significant events and trends in the developing neuronal networks as well as changes in activity induced by neuromodulators. Although 3 has been shown to be a practical value for example in developing human neuronal networks where bursting activity is primitive and unstable (Kapucu et al. 2012), it is not feasible for the detection and characterization of mature bursting activity. Value 5 but also higher values, e.g. 10, have been considered feasible in earlier studies (Pasquale et al. 2010; Chiappalone et al. 2005). In this work, use of value 5 excluded majority of false bursts but also resulted in a loss of some true bursts, which had been correctly detected in the first run. Therefore, value 5 was proved to be optimal for the data in this work and no further increase was applied. Nevertheless, some of the lost bursts were due to poor spike detection. Enhanced spike detection could allow or even require further increase of minSpikes.

5.6. Significance of spike detection performance

Adequate spike detection performance is crucial for reliable burst detection (Mayer et al. 2018; Quiroga et al. 2004). All burst detection algorithms included in this study utilize ISIs, which are naturally influenced by performance of spike detection. In this study, burst detection was occasionally compromised by poor spike detection performance. Often more spikes were observed within bursts by visual examination than by the spike detection algorithm. The issue was obvious especially for burst-related spikes but few bursts were missed completely. As mentioned earlier, increase of the minSpikes led to loss of some true bursts partly due to poor spike detection. Poor spike detection is also partly to blame for the splitting of bursts, which was a major issue of logISI and CMA. Failure to detect one or more subsequent intra-burst spikes resulted in a long ISI, which could be interpreted as an IBI by the burst detection algorithms. Nevertheless, probably most of the longer ISIs observed within bursts are real biological events. ISIs within a single burst can display great variability (Pasquale et al. 2010; Kapucu et al. 2012).

Despite the poor spike detection, the performances of the algorithms are still comparative as the conditions were same for all of them. Enhancement of spike detection would most likely improve the performance of all burst detection algorithms on most of the spike trains. However, the enhancement could be of different magnitude since the principles of function are different for each of the burst detection algorithms. Burst detection algorithms can compensate for poor spike detection at some level *via* parameter optimization. Especially optimization of maxISI-like parameters can allow improved identification of burst-related spikes and reduce splitting of bursts, as remarked in this study while optimizing maxISI for logISI algorithm.

5.7. Effects of logISI parameter optimization

The selection of minSpikes was discussed above and it was determined crucial for recognition of significant events. The remaining adjustable parameters for logISI included void threshold, cutoff for the intra-burst peak time window, and default maxISI. Of the three, alteration of maxISI had the greatest positive effect. In general, increasing maxISI from the original value of 100 ms reduced splitting of bursts and increased sensitivity, sometimes in the expense of decreased specificity. Using value of 150 ms resulted in the best performance although using 200 ms had its advantages as well. On this test data set, specificity decrease with 200 ms was considered too grave. On developing hESC-derived neuronal networks however, even increase to 200 ms has been considered insufficient (Kapucu et al. 2012) but this was at least partly because the study in question concentrated on detection of more primitive and unstable bursting activity. On hiPSC-derived neuronal networks, 150 ms has been considered optimal as it was in this study (Cotterill et al. 2016). It should be noted that in both studies also cutoff was simultaneously changed to 150 ms. Although it is impossible to absolutely determine the relative effects of the alterations without assessing them separately, it seems more probable that the positive effects are due to increased maxISI. This suggestion arises from the notion that in this thesis work the intra-burst peak was successfully determined for all spike trains with both 75 and 100 ms. Increasing the cutoff cannot increase the probability of finding an ISIth because if ISIth is found for a peak with a longer ISI, it will also be found for the preceding peaks. The ISIth found by the preceding peaks will be either of the same value or smaller. Consequently, increasing the cutoff value may only decrease the probability of finding ISIth. This is disadvantageous since the path that is selected when no ISIth is found (path 3) was shown to display weaker performance in comparison to the other paths. Thus, reverting cutoff to 100 ms or lower but maintaining default maxISI at 150 ms might improve the performance on hiPSC-

derived neuronal networks. If aiming to detect primitive bursting, the increase of cutoff might be advantageous if the majority of intra-burst ISIs are believed to be above 100 ms as mentioned by Kapucu et al. (Kapucu et al. 2012). In this thesis work, such events were considered insignificant findings.

Decrease of cutoff from 100 ms to 75 ms enhanced logISI performance on KA-treated spike train and had no effect on other spike trains. The effect was outstanding since the KA-treated spike train was then recognized as non-bursting. No other algorithm had succeeded in this during the comparative performance analysis and even parameter optimization of the other algorithms was not believed to yield such outstanding results. Further decrease of cutoff was unprofitable. A larger test data set would be needed to determine whether the effect, here observed on a single spike train, was a chance or general behavior. A larger set would be needed also to define an optimal value for the cutoff, but it should be well above 55 ms and below 92 ms.

Decrease of void threshold from the original 0.70 to 0.60 increased the performance of logISI on one spike train and had no significance on other spike trains. The effect was similar to that of increasing maxISI since the splitting was reduced. Due to these facts, the positive effect of decreased void threshold was not very significant when the optimal parameters were combined. Nevertheless, it was believed that the effect of void threshold of 0.60 would become apparent in a larger data set also when combined with 150 ms. Further decrease of void threshold to 0.35 was unprofitable. Again, a larger test data set would be needed to determine the precise optimal threshold value as very few spike trains were affected in this test data set. The results from this experiment are in agreement with the original authors about the approximate value of void threshold (Pasquale et al. 2010). The original threshold has yielded good results in other studies (Cotterill et al. 2016; Kapucu et al. 2012) but it might be beneficial to try a lower threshold for example for hiPSC-derived neuronal networks.

5.8. Future prospects

In this thesis, the enhancement of algorithm performance focused on parameter optimization. Besides parameter optimization, it might be possible to enhance logISI performance by small modifications to the algorithm function. Currently, only path 2 searches for burst-related spikes after burst core detection. It might be advantageous to extend this function to the two other paths. Especially the performance of path 3, which uses the default maxISI to detect burst cores only, was weaker in comparison

to the other paths. Defining a default threshold for burst-related spikes might increase the performance with path 3. Another potential modification could tackle the problem encountered when increasing minSpikes. When the value of minSpikes was increased to 5, some of the erroneously excluded bursts included in fact 5 or more spikes. This was because the algorithm applies minSpikes to the burst cores. If it was applied to the whole burst, the algorithm performance would probably improve.

KA-treated non-bursting high frequency spike train (of Cat. II) proved to be the biggest challenge for many of the algorithms. In comparison to the un-treated non-bursting high frequency spike train, the KA-treated spike train had remarkable higher spike frequency. The spike frequency on un-treated spike train was 5.2 Hz whereas on KA-treated spike train it was 11.3 Hz. The spike frequency of KA-treated spike train was second only to the un-treated spike trains displaying rat bursts (20.4 and 20.6 Hz) or human super bursts (19.1 Hz). The KA-treated activity pattern was a challenge to the burst detection algorithms because of its high but varying spike frequency. Due to the variability, especially self-adapting and surprise-based algorithms tend to detect false bursts within the non-bursting spike train. A solution for the KA-treated spike train was found during the logISI optimization and it was successfully classified as non-bursting. In the future however, it could be beneficial to find a way for logISI to recognize and separately classify this kind of non-bursting spike trains with extremely high spike frequency to a new category instead of simply defining them as non-bursting or bursting. This could possibly be achieved by investigating the log-adjusted histogram properties specific to this activity pattern.

Comprehensive evaluation of algorithm performance requires testing on wide variety of activity patterns. In this study, the test data for algorithm performance analysis was derived from healthy hPSC-derived neuronal networks. In the following studies, it would be interesting to use patient-derived hiPSCs to develop neuronal networks. In diseases such as epilepsy proteins involved in generation of electrical activity are dysfunctional (Weick 2016) and thus patient-derived networks might present activity patterns that are not present in healthy neuronal networks. To obtain multiple different types of data, it would be beneficial to record both spontaneous activity as well as pharmacologically modulated activity as done in this study.

LogISI has previously been shown to be amongst the two highest performing burst detection algorithms for the data obtained from hiPSC-derived neuronal networks as well as mouse retinal ganglion cells (Cotterill et al. 2016). In this thesis, logISI was shown to be the most promising burst detection algorithm for the data recorded from hESC-derived and rat cortical neuronal networks, and parameters of logISI were

optimized for these networks. After parameter optimization, logISI successfully detected bursts in the variety of electrical activity patterns identified from spontaneous and pharmacologically modulated activity of these neuronal networks. Based on its high competence on this variable data, logISI has potential to become a standard burst detection method in the field. Naturally, a larger test data set would be needed to confirm the applicability of the optimal parameter values determined in this work. Furthermore, the optimal parameters need to be tested on a wider range of data derived from different types of cells.

References

Abbott, N.J., Rönnbäck, L. and Hansson, E. Astrocyte–endothelial interactions at the blood–brain barrier. *Nature Reviews Neuroscience.* 2006, **7**(1), 41–53.

Bear, M.F., Connors, B.W. and Paradiso, M.A. 2015. Neuroscience: Exploring the brain. 4th ed. Philadelphia, PA: Lippincott Williams and Wilkins. ISBN 978-1-4511-0954-2.

Biedler, J.L., Roffler-Tarlov, S., Schachner, M. and Freedman, L.S. Multiple neurotransmitter synthesis by human neuroblastoma cell lines and clones. *Cancer research.* 1978, **38**(11), 3751–3757.

Brennand, K.J., Simone, A., Jou, J., Gelboin-Burkhart, C., Tran, N., Sangar, S., Li, Y., Mu, Y., Chen, G., Yu, D., McCarthy, S., Sebat, J. and Gage, F.H. Modelling schizophrenia using human induced pluripotent stem cells. *Nature*. 2011, **473**(7346), 221–225.

Buzsáki, G., Anastassiou, C.A. and Koch, C. The origin of extracellular fields and currents – EEG, ECoG, LFP and spikes. *Nature Reviews Neuroscience*. 2012, **13**(6), 407–420.

Chambers, S.M., Fasano, C.A., Papapetrou, E.P., Tomishima, M., Sadelain, M. and Studer, L. Highly efficient neural conversion of human ES and iPS cells by dual inhibition of SMAD signaling. *Nature Biotechnology*. 2009, **27**(3), 275–280.

Charlesworth, P., Cotterill, E., Morton, A., Grant, S.G.N. and Eglen, S.J. Quantitative differences in developmental profiles of spontaneous activity in cortical and hippocampal cultures. *Neural Development.* 2015, **10**, 1.

Chiappalone, M., Novellino, A., Vajda, I., Vato, A., Martinoia, S. and van Pelt, J. Burst detection algorithms for the analysis of spatio-temporal patterns in cortical networks of neurons. *Neurocomputing.* 2005, **65-66**, 653–662.

Clarke, L.E. and Barres, B.A. Emerging roles of astrocytes in neural circuit development. *Nature Reviews Neuroscience.* 2013, **14**(5), 311–321.

Cotterill, E., Charlesworth, P., Thomas, C.W., Paulsen, O. and Eglen, S.J. A comparison of computational methods for detecting bursts in neuronal spike trains and their application to human stem cell-derived neuronal networks. *Journal of Neurophysiology.* 2016, **116**(2), 306–321.

Cummings, J. Lessons learned from Alzheimer disease: Clinical trials with negative outcomes. *Clinical and Translational Science.* 2018, **11**(2), 147–152.

Di Giorgio, F.P., Boulting, G.L., Bobrowicz, S. and Eggan, K.C. Human embryonic stem cell-derived motor neurons are sensitive to the toxic effect of glial cells carrying an ALS-causing mutation. *Cell Stem Cell.* 2008, **3**(6), 637–648.

Einevoll, G.T., Kayser, C., Logothetis, N.K. and Panzeri, S. Modelling and analysis of local field potentials for studying the function of cortical circuits. *Nature Reviews Neuroscience.* 2013, **14**(11), 770–785.

Eroglu, C. and Barres, B.A. Regulation of synaptic connectivity by glia. *Nature.* 2010, **468**(7321), 223–231.

Fukushima, K., Miura, Y., Sawada, K., Yamazaki, K. and Ito, M. Establishment of a human neuronal network assessment system by using a human neuron/astrocyte co-culture derived from fetal neural stem/progenitor cells. *Journal of Biomolecular Screening.* 2016, **21**(1), 54–64.

Gage, F.H. Mammalian neural stem cells. *Science.* 2000, **287**(5457), 1433–1438.

Gelfman, S., Wang, Q., Lu, Y.-F., Hall, D., Bostick, C., Dhindsa, R., Halvorsen, M., McSweeney, K.M., Cotterill, E., Edinburgh, T., Petrovski, S., Boland, M.J., Allen, A.S., Goldstein, D.B. and Eglen, S.J. meaRtools: An R package for the analysis of neuronal networks recorded on microelectrode arrays. *PLoS Computational Biology.* 2018, **14**(10), e1006506.

Ghane-Motlagh, B. and Sawan, M. Design and implementation challenges of microelectrode arrays: A review. *Materials Sciences and Applications.* 2013, **4**(8), 483–495.

Ginhoux, F., Greter, M., Leboeuf, M., Nandi, S., See, P., Gokhan, S., Mehler, M.F., Conway, S.J., Ng, L.G., Stanley, E.R, Samokhvalov, I.M. and Merad, M. Fate mapping analysis reveals that adult microglia derive from primitive macrophages. *Science.* 2010, **330**(6005), 841–845.

Gourévitch, B. and Eggermont, J.J. A nonparametric approach for detection of bursts in spike trains. *Journal of Neuroscience Methods.* 2007, **160**(2), 349–358.

Hai, A., Dormann, A., Shappir, J., Yitzchaik, S., Bartic, C., Borghs, G., Langedijk, J.P.M. and Spira, M.E. Spine-shaped gold protrusions improve the adherence and electrical

coupling of neurons with the surface of micro-electronic devices. *Journal of The Royal Society Interface.* 2009, **6**(41), 1153–1165.

Heikkilä, T.J., Ylä-Outinen, L., Tanskanen, J.M.A., Lappalainen, R.S., Skottman, H., Suuronen, R., Mikkonen, J.E., Hyttinen, J.A.K. and Narkilahti, S. Human embryonic stem cell-derived neuronal cells form spontaneously active neuronal networks *in vitro*. *Experimental Neurology.* 2009, **218**(1), 109–116.

Hennig, M.H., Grady, J., van Coppenhagen, J. and Sernagor, E. Age-dependent homeostatic plasticity of GABAergic signaling in developing retinal networks. *Journal of Neuroscience.* 2011, **31**(34), 12159–12164.

Hongisto, H., Ilmarinen, T., Vattulainen, M., Mikhailova, A. and Skottman, H. Xeno- and feeder-free differentiation of human pluripotent stem cells to two distinct ocular epithelial cell types using simple modifications of one method. *Stem Cell Research & Therapy.* 2017, **8**, 291.

Kapucu, F.E., Tanskanen, J.M.A., Mikkonen, J.E., Ylä-Outinen, L., Narkilahti, S. and Hyttinen, J.A.K. Burst analysis tool for developing neuronal networks exhibiting highly varying action potential dynamics. *Frontiers in Computational Neuroscience.* 2012, **6**, 38.

Kirwan, P., Turner-Bridger, B., Peter, M., Momoh, A., Arambepola, D., Robinson, H.P.C. and Livesey, F.J. Development and function of human cerebral cortex neural networks from pluripotent stem cells *in vitro*. *Development.* 2015, **142**(18), 3178–3187.

Lappalainen, R.S., Salomäki, M., Ylä-Outinen, L., Heikkilä, T.J., Hyttinen, J.A.K., Pihlajamäki, H., Suuronen, R., Skottman, H. and Narkilahti, S. Similarly derived and cultured hESC lines show variation in their developmental potential towards neuronal cells in long-term culture. *Regenerative Medicine.* 2010, **5**(5), 749–762.

Legendy, C.R. and Salcman, M. Bursts and recurrences of bursts in the spike trains of spontaneously active striate cortex neurons. *Journal of Neurophysiology.* 1985, **53**(4), 926–939.

Mayer, M., Arrizabalaga, O., Lieb, F., Ciba, M., Ritter, S. and Thielemann, C. Electrophysiological investigation of human embryonic stem cell derived neurospheres using a novel spike detection algorithm. *Biosensors and Bioelectronics.* 2018, **100**, 462–468.

Mertens, J., Marchetto, M.C., Bardy, C. and Gage, F.H. Evaluating cell reprogramming, differentiation and conversion technologies in neuroscience. *Nature Reviews Neuroscience.* 2016, **17**(7), 424–437.

Monti, D.A., Zabrecky, G., Kremens, D., Liang, T.-W., Wintering, N.A., Cai, J., Wei, X., Bazzan, A.J., Li, Z., Bowen, B., Intenzo, C.M., Iacovitti, L. and Newberg, A.B. N-acetyl cysteine may support dopamine neurons in Parkinson's disease: Preliminary clinical and cell line data. *PLoS One.* 2016, **11**(6), e0157602.

Muramoto, K., Ichikawa, M., Kawahara, M., Kobayashi, K. and Kuroda, Y. Frequency of synchronous oscillations of neuronal activity increases during development and is correlated to the number of synapses in cultured cortical neuron networks. *Neuroscience Letters.* 1993, **163**(2), 163–165.

Navarrete, E.G., Liang, P., Lan, F., Sanchez-Freire, V., Simmons, C., Gong, T., Sharma, A., Burridge, P.W., Patlolla, B., Lee, A.S., Wu, H., Beygui, R.E., Wu, S.M., Robbins, R.C., Bers, D.M. and Wu, J.C. Screening drug-induced arrhythmia using human induced pluripotent stem cell–derived cardiomyocytes and low-impedance microelectrode arrays. *Circulation.* 2013, **128**(11_suppl_1), S3–S13.

Nex Technologies, 2014. Neuroexplorer Manual. http://www.neuroexplorer.com/downloads/NeuroExplorerManual.pdf. Viewed July 25th 2019.

Obien, M.E.J., Deligkaris, K., Bullmann, T., Bakkum, D.J. and Frey, U. Revealing neuronal function through microelectrode array recordings. *Frontiers in Neuroscience.* 2015, **8**, 423.

Odawara, A., Katoh, H., Matsuda, N. and Suzuki, I. Physiological maturation and drug responses of human induced pluripotent stem cell-derived cortical neuronal networks in long-term culture. *Scientific Reports.* 2016, **6**, 26181.

Pang, Z.P., Yang, N., Vierbuchen, T., Ostermeier, A., Fuentes, D.R., Yang, T.Q., Citri, A., Sebastiano, V., Marro, S., Südhof, T.C. and Wernig, M. Induction of human neuronal cells by defined transcription factors. *Nature.* 2011, **476**(7359), 220–223.

Pasquale, V., Martinoia, S. and Chiappalone, M. A self-adapting approach for the detection of bursts and network bursts in neuronal cultures. *Journal of Computational Neuroscience.* 2010, **29**(1-2), 213–229.

Pine, J. Recording action potentials from cultured neurons with extracellular microcircuit electrodes. *Journal of Neuroscience Methods.* 1980, **2**(1), 19–31.

Quiroga, R.Q., Nadasdy, Z. and Ben-Shaul, Y. Unsupervised spike detection and sorting with wavelets and superparamagnetic clustering. *Neural Computation.* 2004, **16**(8), 1661–1687.

Rajala, K., Hakala, H., Panula, S., Aivio, S., Pihlajamäki, H., Suuronen, R., Hovatta, O. and Skottman, H. Testing of nine different xeno-free culture media for human embryonic stem cell cultures. *Human Reproduction.* 2007, **22**(5), 1231–1238.

Robinson, J.T., Jorgolli, M. and Park, H. Nanowire electrodes for high-density stimulation and measurement of neural circuits. *Frontiers in Neural Circuits.* 2013, **7**, 38.

Homma, R., Baker, B.J., Jin, L., Garaschuk, O., Konnerth, A., Cohen, L.B. and Zecevic, D. Wide-field and two-photon imaging of brain activity with voltage- and calcium-sensitive dyes. *Philosophical Transactions of the Royal Society B: Biological Sciences.* 2009, **364**, 2453–2467.

Ryynänen, T., Kujala, V., Ylä-Outinen, L., Korhonen, I., Tanskanen, J.M.A., Kauppinen, P., Aalto-Setälä, K., Hyttinen, J., Kerkelä, E., Narkilahti, S. and Lekkala, J. All titanium microelectrode array for field potential measurements from neurons and cardiomyocytes—a feasibility study. *Micromachines.* 2011, **2**(4), 394–409.

Sahu, M.P., Nikkilä, O., Lågas, S., Kolehmainen, S. and Castren, E. Culturing primary neurons from rat hippocampus and cortex. *Neuronal Signaling.* 2019, **3**, NS20180207.

Selinger, J.V., Kulagina, N.V., O'Shaughnessy, T.J., Ma, W. and Pancrazio, J.J. Methods for characterizing interspike intervals and identifying bursts in neuronal activity. *Journal of Neuroscience Methods.* 2007, **162**(1-2), 64–71.

Shi, Y., Kirwan, P. and Livesey, F.J. Directed differentiation of human pluripotent stem cells to cerebral cortex neurons and neural networks. *Nature Protocols.* 2012, **7**(10), 1836–1846.

Skottman, H., 2010. Derivation and characterization of three new human embryonic stem cell lines in Finland. *In Vitro Cellular & Developmental Biology: Animal.* 2010, **46**(3/4), 206–209.

Spira, M.E. and Hai, A. Multi-electrode array technologies for neuroscience and cardiology. *Nature Nanotechnology.* 2013, **8**(2), 83–94.

Takahashi, K., Tanabe, K., Ohnuki, M., Narita, M., Ichisaka, T., Tomoda, K. and Yamanaka, S. Induction of pluripotent stem cells from adult human fibroblasts by defined factors. *Cell.* 2007, **131**(5), 861–872.

Takahashi, K. and Yamanaka, S. Induction of pluripotent stem cells from mouse embryonic and adult fibroblast cultures by defined factors. *Cell.* 2006, **126**(4), 663–676.

Thomas Jr., C.A., Springer, P.A., Loeb, G.E., Berwald-Netter, Y. and Okun, L.M. A miniature microelectrode array to monitor the bioelectric activity of cultured cells. *Experimental Cell Research.* 1972, **74**(1), 61–66.

Toivanen, M., Pelkonen, A., Mäkinen, M., Ylä-Outinen, L., Sukki, L., Kallio, P., Ristola, M. and Narkilahti, S. Optimised PDMS tunnel devices on MEAs increase the probability of detecting electrical activity from human stem cell-derived neuronal networks. *Frontiers in Neuroscience.* 2017, **11**, 606.

Tokdar, S., Xi, P., Kelly, R.C. and Kass, R.E. Detection of bursts in extracellular spike trains using hidden semi-Markov point process models. *Journal of Computational Neuroscience.* 2010, **29**(1-2), 203–212.

Turnbull, L., Dian, E. and Gross, G. The string method of burst identification in neuronal spike trains. *Journal of Neuroscience Methods.* 2005, **145**(1-2), 23–35.

Vieira, M.S., Santos, A.K., Vasconcellos, R., Goulart, V.A.M., Parreira, R.C., Kihara, A.H., Ulrich, H. and Resende, R.R. Neural stem cell differentiation to mature neurons: Mechanisms of regulation and biotechnological applications. *Biotechnology Advances.* 2018, **36**(7), 1946–1970.

Vierbuchen, T., Ostermeier, A., Pang, Z.P., Kokubu, Y., Südhof, T.C. and Wernig, M. Direct conversion of fibroblasts to functional neurons by defined factors. *Nature.* 2010, **463**(7284), 1035–1041.

Wagenaar, D.A., Pine, J. and Potter, S.M. An extremely rich repertoire of bursting patterns during the development of cortical cultures. *BMC Neuroscience.* 2006, **7**, 11.

Weick, J.P. Functional properties of human stem cell-derived neurons in health and disease. *Stem Cells International.* 2016, **2016**, 4190438.

Ylä-Outinen, L., Heikkilä, J., Skottman, H., Suuronen, R., Äänismaa, R. and Narkilahti, S. Human cell-based micro electrode array platform for studying neurotoxicity. *Frontiers in Neuroengineering.* 2010, **3**, 111.

Zhang, Y., Pak, C., Han, Y., Ahlenius, H., Zhang, Z., Chanda, S., Marro, S., Patzke, C., Acuna, C., Covy, J., Xu, W., Yang, N., Danko, T., Chen, L., Wernig, M. and Südhof, T.C. Rapid single-step induction of functional neurons from human pluripotent stem cells. *Neuron.* 2013, **78**(5), 785–798.

Appendices

Appendix 1: Additional data on statistical tests

Table A1. Statistical tests for the effects of neuromodulators in human and rat neuronal networks. For each treatment, the number of electrodes included in the analysis (N) is shown in the first column under the network. Median RC_f and lower (Q1) and upper quartiles (Q3) are presented in the second column. The p-value for the tested difference against control is reported in the third column.

	Human			Rat		
Treatment	**N**	**Median RC_f (Q1, Q3) (%)**	**p-value**	**N**	**Median RC_f (Q1, Q3) (%)**	**p-value**
Control	50	102.45 (90.76, 112.52)	-	63	93.12 (76.19, 104.68)	-
Gabazine	46	147.05 (112.41, 190.41)	<0.01	44	105.82 (68.38, 174.49)	0.57
GABA	49	43.73 (25.25, 65.99)	<0.01	68	0.00 (0.00, 0.04)	<0.01
KA	42	38.67 (10.07, 84.43)	<0.01	54	0.86 (0.04, 24.23)	<0.01
CNQX	49	27.97 (6.81., 40.84)	<0.01	64	9.96 (2.48, 49.18)	<0.01
D-AP5	40	27.34 (15.03, 49.53)	<0.01	57	6.02 (1.08, 17.73)	<0.01

Appendix 2: Additional data on test data set

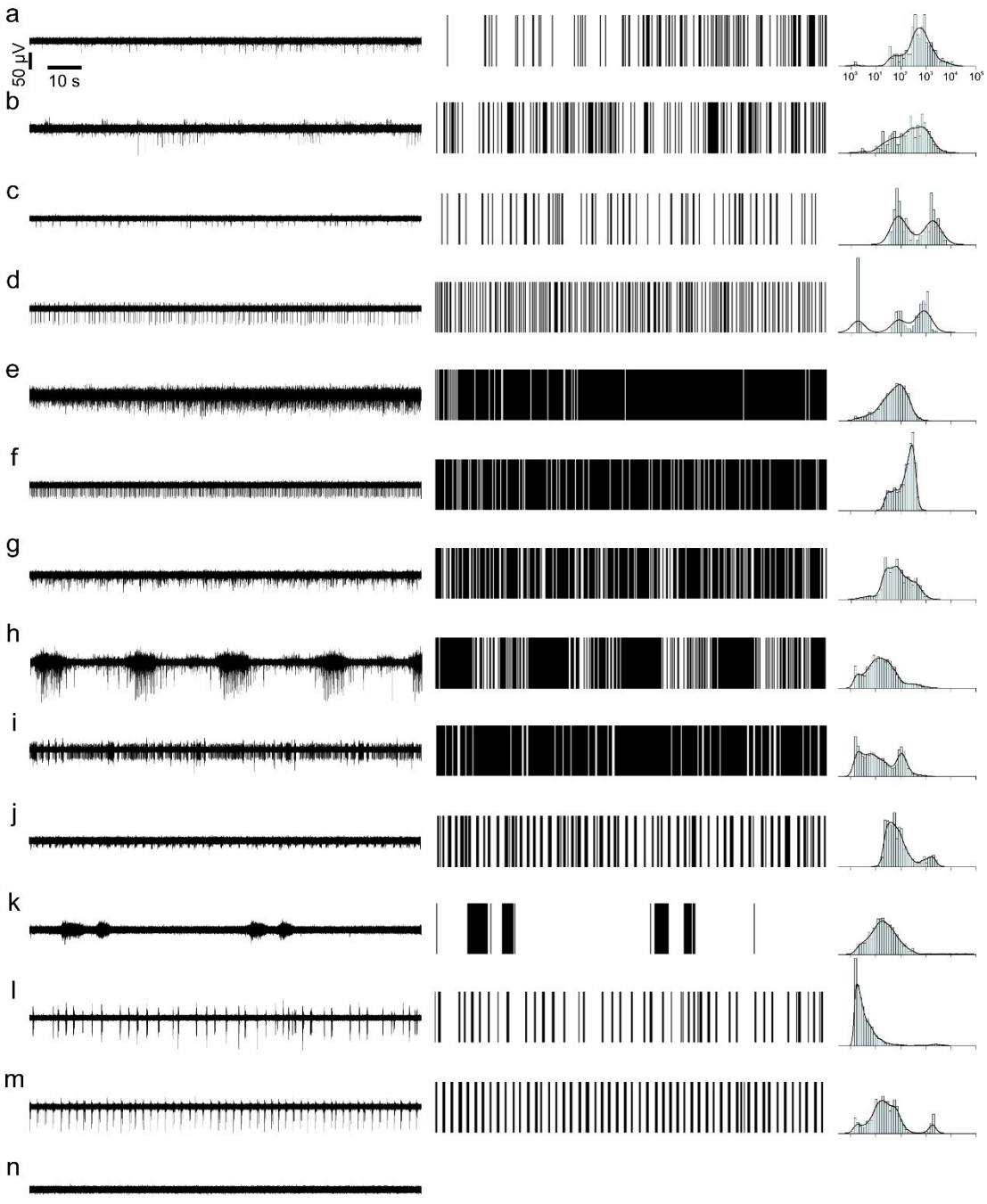

Figure A1. Raw MEA signals, detected spikes, and ISI distributions of the spike trains included in the test data set. Length of the raw signal (left) in the figure is two minutes. Detected spikes (middle) are presented in the same time scale as the raw signal. The ISI distributions (right) are presented as log-adjusted histograms with a Kernel density estimate displayed as a black line on top. The spike trains are a) D-AP5-treated human spike train (I), b) GABA-treated human spike train (I), c) un-treated low frequency rat spike train (I), d) CNQX-treated rat spike train (I), e) un-treated high frequency rat spike train (II), f) KA-treated human spike train (II), g) noisy spike train

with short human bursts (III), h) noisy spike train with human super bursts (III), i) noisy spike train with rat bursts (III), j) well-separated short human bursts (IV), k) gabazine-treated human super bursts (IV), l) well-separated rat bursts (IV), m) gabazine-treated rat bursts (IV), and n) TTX-treated recording without activity. Numbers I-IV in parenthesis represent the category of the spike train.

Appendix 3: Burst detection results on test data set

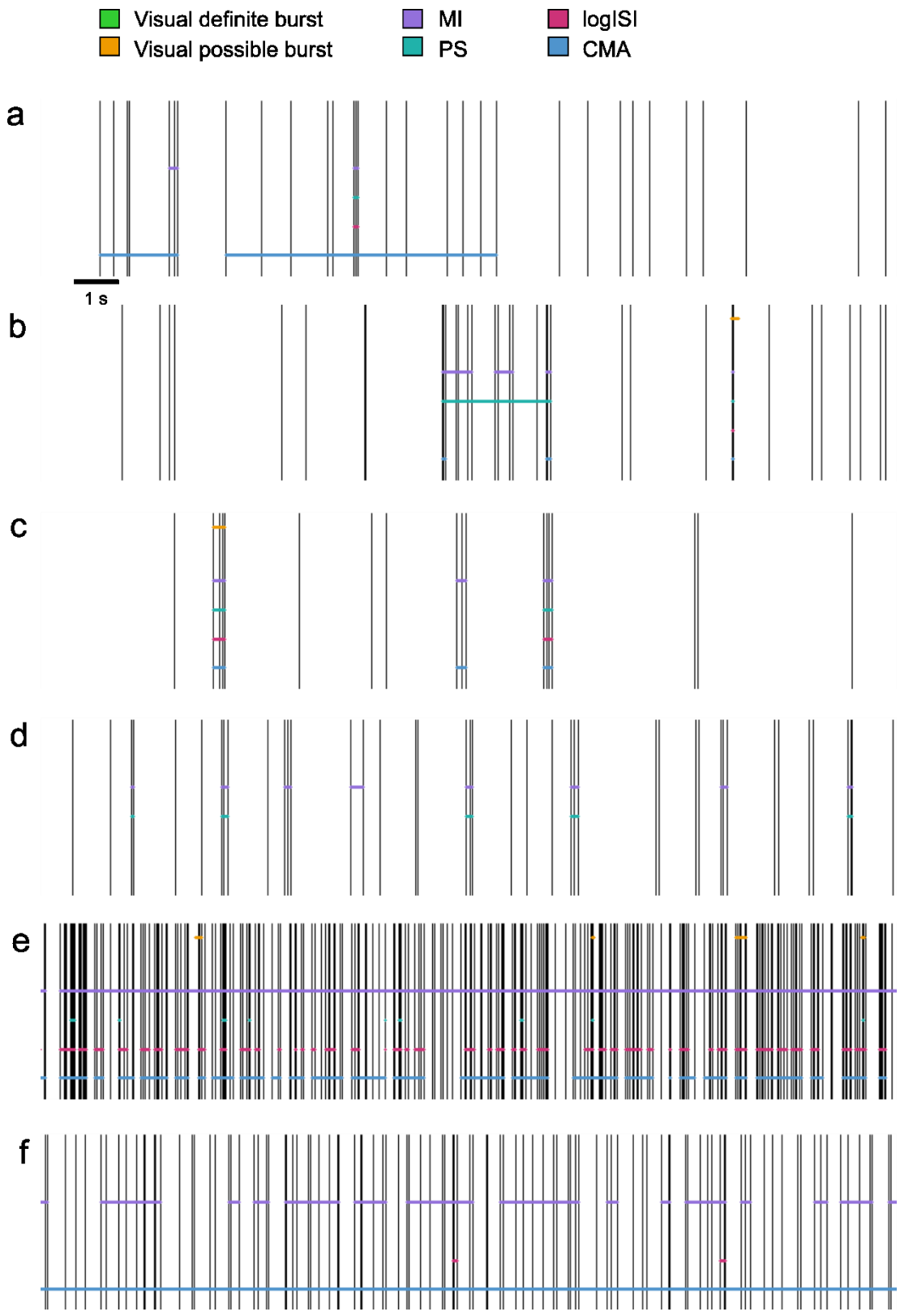

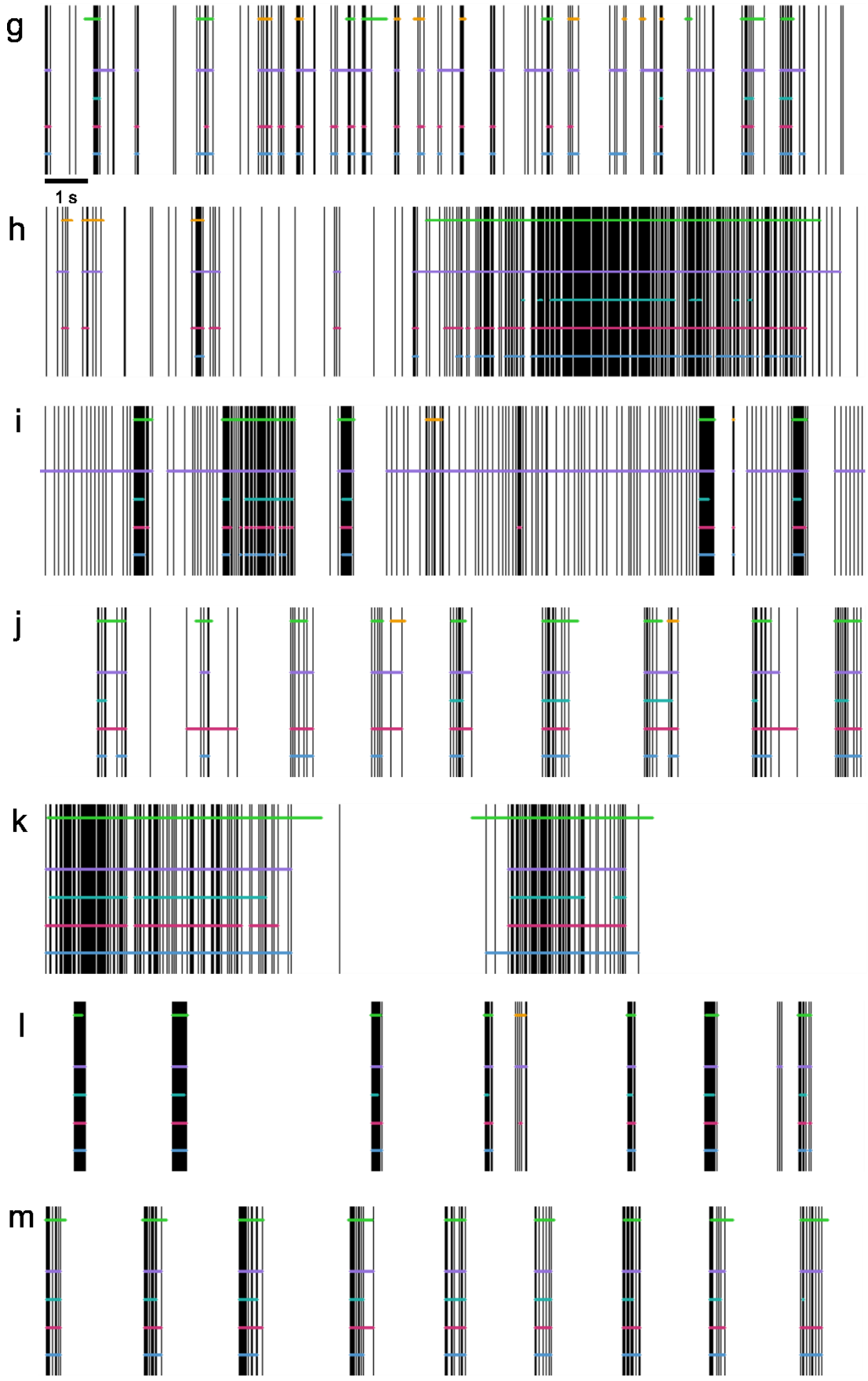
g
1 s
h
i
j
k
l
m

Figure A2. Burst detection results of MI, PS, logISI and CMA algorithms using default parameters. MinSpikes was set to 3. The vertical lines represent spikes. The horizontal lines represent visually identified bursts and algorithm results. Visually identified bursts are drawn at the highest point. The time interval in each image is 20 s. The spike trains are a) D-AP5-treated human spike train (I), b) GABA-treated human spike train (I), c) un-treated low frequency rat spike train (I), d) CNQX-treated rat spike train (I), e) un-treated high frequency rat spike train (II), f) KA-treated human spike train (II), g) noisy spike train with short human bursts (III), h) noisy spike train with human super bursts (III), i) noisy spike train with rat bursts (III), j) well-separated short human bursts (IV), k) gabazine-treated human super bursts (IV), l) well-separated rat bursts (IV), and m) gabazine-treated rat bursts (IV). Numbers I-IV in parenthesis represent the category of the spike train.

Appendix 4: LogISI optimization results on test data set

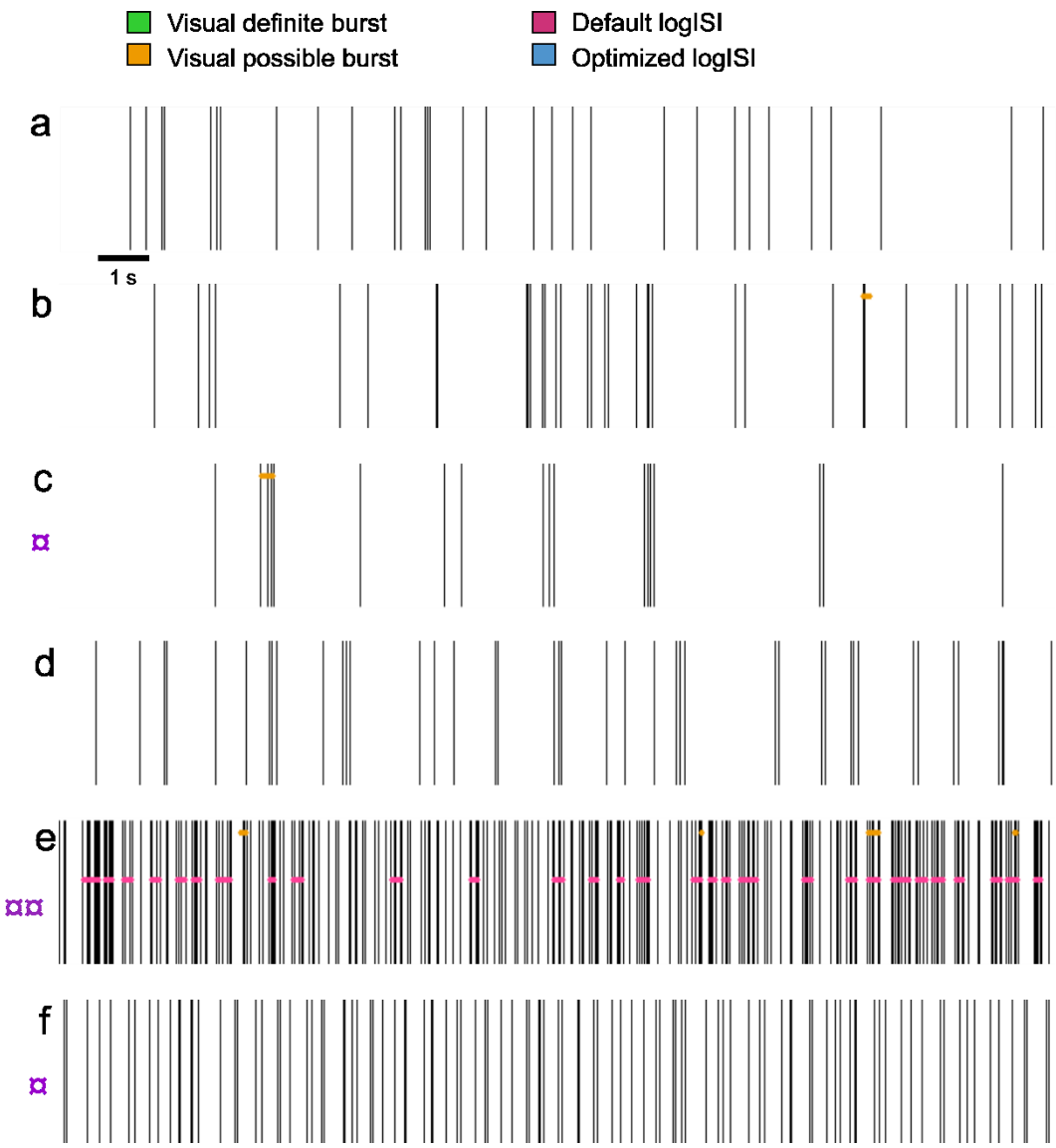

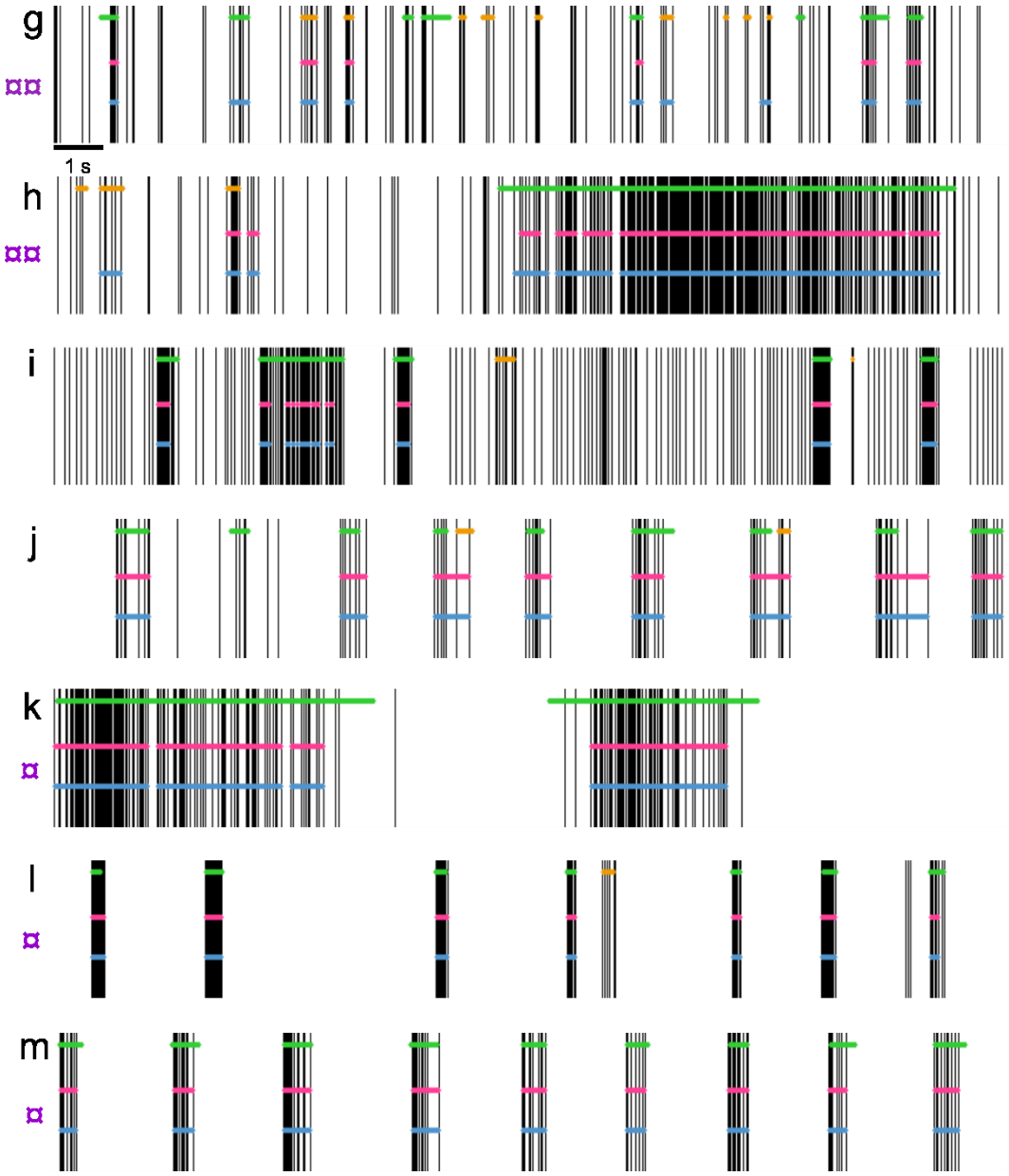

Figure A3. Burst detection results of logISI algorithm using default and optimized parameters. MinSpikes was set to 5 in both runs. In the default run, void threshold was 0.70 and both cutoff for intra-burst peak time window and default maxISI were 100 ms. In the optimized run, void threshold was 0.60, cutoff was 75 ms, and default maxISI was 150 ms. The vertical lines represent spikes. The horizontal lines represent visually identified bursts (top) and algorithm results with default (middle) and optimized (bottom) parameters. Spike trains, which were affected by parameter optimization but on which performance remained unchanged, are marked with ¤. Affected spike trains with altered performance are marked with ¤¤. The time interval is 20 s. The spike trains are a) D-AP5-treated human spike train (I), b) GABA-treated human spike train (I), c) un-treated low frequency rat spike train (I), d) CNQX-treated rat spike train (I), e) un-treated high frequency rat spike train (II), f) KA-treated human spike train (II), g) noisy spike train with short human bursts (III), h) noisy spike train with human super bursts (III), i) noisy spike train with rat bursts (III), j) well-separated short human bursts (IV), k) gabazine-treated human super bursts (IV), l) well-separated rat bursts (IV), and m) gabazine-treated rat bursts (IV). Numbers I-IV in parenthesis represent the category of the spike train.